BOOK OF ABSTRACTS

Photron

UNIVERSITIES FOR NORTH EAST ENGLAND

Durham University

Northumbria University NEWCASTLE

Newcastle University

Table of Contents

ICTW 2025 23rd INTERNATIONAL COUETTE-TAYLOR WORKSHOP 14th-16th JULY DURHAM, UK

Small-scale instabilities in inertia-gravity waves

Abhiram D S*, Manikandan Mathur†, Yohei Onuki‡

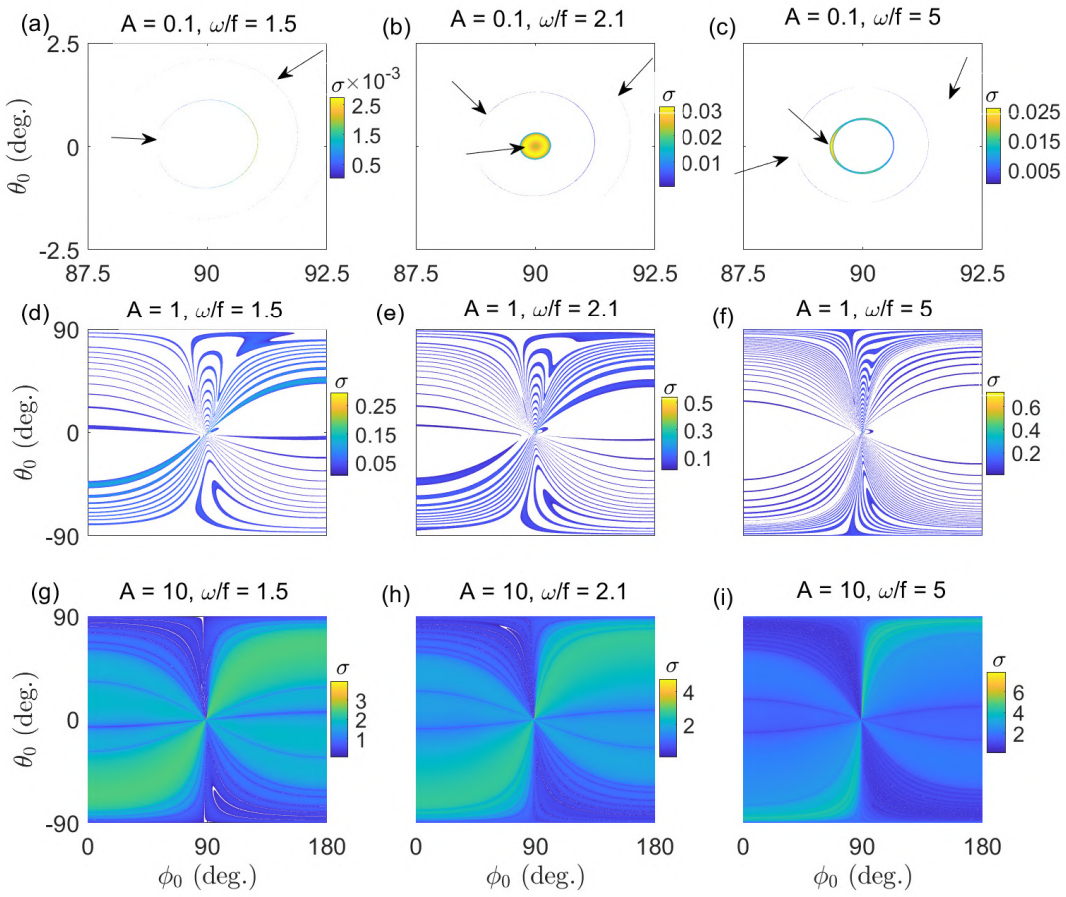

Figure 1: Non-dimensional growth rate (σ) as a function of ϕ_0 (deg.) and θ_0 (deg.) for $\omega/f = 1.5, 2.1, 5$ (column-wise) and $A = 0.1, 1, 10$ (row-wise). All the plots correspond to $\omega/N = 0.025$. In the first row, all growth rates are very negligible everywhere outside the range shown.

Semi-diurnal internal tides are a significant part of internal waves in the ocean. While several dissipation mechanisms have been proposed for internal tides, the relative importance of each of them in the ocean is not fully resolved. Linear instability is one potential pathway towards dissipation for inertia-gravity waves, which are internal waves that are influenced by both stratification and rotation. Here, we perform a linear stability analysis of a finite-amplitude plane inertia-gravity wave by considering the inviscid evolution of three-dimensional (3-D), small-amplitude, short-wavelength perturbations. Characterizing the base flow plane inertia-gravity wave by its non-dimensional amplitude A and the ratio of frequency to background rotation (ω/f), the local stability equations are solved over the entire range of perturbation wave vector orientations, which are denoted by θ_0 (angle made by the perturbation wave vector with the inertia-gravity wave plane) and ϕ_0 (angle made

*Corresponding author: ae20d751@smail.iitm.ac.in
†Geophysical flows lab, Department of Aerospace Engineering, Indian Institute of Technology Madras, Chennai, India, 600036
‡Research Institute for Applied Mechanics, Kyushu University, Kasuga, Fukuoka 816-8580, Japan

by the projection of perturbation wave vector in the inertia-gravity wave plane with the horizontal). To be representative of internal tides in the ocean, ω/N is held fixed at 0.025 for our entire study, where N is the Brunt Väisälä frequency associated with the uniform stratification.

Figure 1 shows the growth rate distribution on the (ϕ_0, θ_0) plane for three different amplitudes ($A = 0.1, 1, 10$) and three choices of Coriolis frequencies ($\omega/f = 1.5, 2.1, 5$. For $A = 0.1$, perturbations are stable in most part of the (ϕ_0, θ_0) plane, except for a small region around $(\phi_0, \theta_0) = (90°, 0°)$, which corresponds to planar (in the plane of the base flow inertia-gravity wave) wave vectors that are aligned with the direction of background rotation. At $A = 1$ (middle row of figure 1), non-zero growth rates are observed over much wider regions on the $\phi_0 - \theta_0$ plane compared to the case of $A = 0.1$. Specifically, several instability bands that span over $(\phi_0, \theta_0) = [0, 180] \times [-90, 90]$, interspersed with stable regions in between, are observed for all three values of ω/f (figures 1 d-f). Finally, upon increasing A to 10, finite growth rates are observed almost entirely over the $\phi_0 - \theta_0$ plane, with significant fractions of the plane showing growth rates comparable to the maximum growth rate. The instabilities at small A are found to be associated with triadic resonance instability of various orders by identifying the frequencies present in the unstable perturbations. For $\omega/f \geq 2$ and $\omega/f < 2$, the dominant instability is two-dimensional (2-D) and its growth rate is proportional to A and A^2, respectively at sufficiently small A, associated with parametric subharmonic instability ($n = 1$ TRI) and $n = 2$ TRI. Above $A \approx 1$, the maximum growth rate at a given A occurs at very large ω/f, suggesting that the internal gravity wave limit of $\omega/f \to \infty$ is most unstable at sufficiently large A. As A is increased, for small $\omega/f \approx 1$, the dominant instability becomes 3-D above $A \approx 10$,whereas for $\omega/f > 6$, the dominant instability becomes 3-D above A 1.3.

To quantify the roles of shear and buoyancy gradient in the evolution of a given perturbation, we perform an energy budget analysis. For large A, shear and static instabilities are the dominant instabilities. The transition from 2-D PSI to static instability is reasonably captured by the threshold amplitude below which the vertical density gradient is statically stable throughout the inertia-gravity wave period. The transition to shear instability is captured by a criterion based on Richardson number.

ICTW 2025 23rd INTERNATIONAL COUETTE-TAYLOR WORKSHOP 14th-16th JULY DURHAM, UK

Suspension Rheology and Routes to Turbulence in Taylor-Couette Flow

Meheboob Alam*†, M. Ghosh†

May 18, 2025

Abstract:

In the first part of my talk, the rheology of particulate suspensions of non-colloidal particles will be briefly reviewed, focussing on the Stokesian regime. This is followed by experimental results on the role of inertial particles on pattern transition routes to turbulence (Taylor, 1923; Coles, 1965; Andereck *et al.*, 1986; Iooss, 1994; Grossmann *et al.*, 2016) in a Taylor-Couette (TC) setup. All experiments have been conducted with neutrally-buoyant suspensions of rigid, non-colloidal particles up-to a particle volume fraction of $\phi = 0.3$. The TC cell, having a radius ratio of $\eta = r_i/r_o \approx 0.89$ and an aspect ratio of $\Gamma = h/(r_o - r_i) \approx 8.5$, is mounted on a Rheometer which is equipped with two independent motors that are connected to the inner and outer cylinders, with the end-caps being allowed to rotate with the outer cylinder. The present setup facilitates the exploration of both co- (Ghosh and Alam, 2024) and counter-rotation (Singh *et al.*, 2022) regimes, thus going beyond recent experiments on inertial suspensions (Majji *et al.*, 2018; Ramesh *et al.*, 2019; Dash *et al.*, 2020; Ramesh & Alam, 2020; Moazzen *et al.*, 2022) that considered pure inner cylinder rotation (i.e., $\omega_i \neq 0$ and $\omega_o = 0$). For each $\phi \geq 0$, the experiments are carried out by increasing/decreasing the angular speeds of two cylinders via quasi-steady ramping protocols at fixed values of the rotation ratio ($\Omega = \omega_o/\omega_i$). The explored range of Ω spans across cyclonic and anti-cyclonic regimes for which the Coriolis/rotation number is negative (i.e. $R_\Omega = \tau_{sh}/\tau_m = (1-\eta)(1+\Omega/\eta)/(1-\Omega) < 0$, the ratio between the shear time scale and the mean rotation time scale (Dubrulle *et al.*, 2005)) and positive ($R_\Omega > 0$, i.e. $\Omega > -\eta$) , respectively. The video images and the measured torque (Alam & Ghosh, 2023) on the inner cylinder have been analysed to gain insights into the spectral routes that run through various transitional flow states, culminating into two distinct turbulent states at large values of the shear Reynolds number $Re_s(\phi, \Omega)$, depending on the value of the rotation ratio Ω and the particle loading ϕ.

It is shown that the laminar flow (i.e. the circular Couette flow, CCF, with axial-boundary-induced Ekman rolls) makes a direct transition to a chaotic state at large enough counter-rotation ($\Omega = -1.5$), and the final bifurcating state represents a featureless turbulent (TUR) state, devoid of large-scale structures. The chaotic state, called NIS (non-propagating interpenetrating spirals), is characterized by a power-law decay $\mathcal{P}(f) \sim f^{-\beta}$ of the power spectra of the scattered light intensity, and the vanishing of its exponent $\beta(Re_s) \to 0$ with increasing shear Reynolds number $Re_s(\phi)$, signifying the broadband nature of $\mathcal{P}(f)$, is tied to the onset of TUR. The origin of TUR is tied to a non-axisymmetric primary bifurcation, leading to spiral vortex flows (SVF, an axially propagating and azimuthally rotating helical mode) at $\Omega = -\eta$ which undergoes a sequence ot bifurcations CCF→SVF→ISV→NIS→TUR, followed by (i) a quasi-periodic state (ISV, interpenetrating spiral vortices), (ii) a chaotic state (NIS) and (iii) a featureless turbulent state (TUR). With further decreasing the rotation ratio $\Omega < -\eta$, the SVF and ISV states disappear progressively, resulting in a direct transition to to chaos and turbulence (CCF→NIS→TUR) at large enough values of $\Omega \ll -\eta$ (Ghosh and Alam, 2025b).

In the anti-cyclonic regime ($R_\Omega > 0$, or, $\Omega > -\eta$), however, the Ruelle-Takens-like (Ruelle & Takens, 1971) bifurcation scenario holds, leading to turbulent Taylor vortices (TTV) which is characterized by large-scale Taylor-like stationary rolls in the background of small-scale structures (Coles, 1965; Andereck *et al.*, 1986). It is shown that the transition pathway at $\Omega > -\eta$, leading to the onset of chaos (i.e. the chaotic wavy vortices, CWV), can be mediated by vortex splitting and merging (VSM) events (Ghosh and Alam, 2025a). The onset of VSM is found to coincide with the transition of a quasi-periodic state (modulated wavy vortices, MWV, characterized by at least one incommensurate frequency) to CWV that finally gives

*Corresponding author: meheboob@jncasr.ac.in
†Engineering Mechanics Unit, Jawaharlal Nehru Centre for Advanced Scientific Research, Jakkur PO, Bengaluru 560064, India

birth to TTV via an intermediary state of turbulent wavy vortices (TWV). The VSM events are shown to be temporally uncorrelated, with a multi-modal skewed probability density function for the inter-event time interval, implying that the VSM-induced chaos is stochastic. The phase diagrams of patterns in $(Re_s(\phi), \Omega)$- and $(Re_s(\phi), R_\Omega)$-planes are compared with their particle-free ($\phi = 0$) counterpart to infer the crucial role of inertial particles (Bagnold , 1954; Ho & Leal , 1974; Baroudi *et al.* , 2020) on transition pathways towards TUR and TTV.

References

Taylor, G.I. (1923) "Stability of a viscous liquid contained between two rotating cylinders", *Phil. Trans. Roy. Soc. A*, **223** 289–343.

Coles, D. (1965) "Transition in circular Couette flow", *J. Fluid Mech.* **21** (3), 385–425.

Andereck, C.D., Liu, S.S. & Swinney, H.L. (1986) "Flow regimes in a circular Couette system with independently rotating cylinders", *J. Fluid Mech.* **164**, 155–183.

Iooss, G. (1994) *The Couette-Taylor problem*, Springer.

Grossmann, S., Lohse, D. & Sun, C. (2016) "High–Reynolds number Taylor–Couette turbulence", *Annu. Rev. Fluid Mech.* **48**, 53–80.

Ghosh, M. & Alam, M. (2024) "Instabilities and particle-induced patterns in co-rotating suspension Taylor–Couette flow", *J. Fluid Mech.* **995**, R4.

Singh, S.P., Ghosh, M. & Alam, M. (2022) "Counter-rotating suspension Taylor–Couette flow: pattern transition, flow multiplicity and the spectral evolution", *J. Fluid Mech.* **944**, A18.

Majji, M.V., Banerjee, S. & Morris, J.F. (2018) "Inertial flow transitions of a suspension in Taylor–Couette geometry", *J. Fluid Mech.* **835**, 936–969.

Ramesh, P., Bharadwaj, S. & Alam, M. (2019) "Suspension Taylor–Couette flow: co-existence of stationary and travelling waves and the characteristics of Taylor vortices and spirals", *J. Fluid Mech.* **870**, 901–940.

Dash, A., Anantharaman, A. & Poelma, C. (2020) "Particle-laden Taylor–Couette flows: higher-order transitions and evidence for azimuthally localized wavy vortices", *J. Fluid Mech.* **903**, A20.

Ramesh, P. & Alam, M. (2020) "Interpenetrating spiral vortices and other co-existing states in suspension Taylor–Couette flow", *Phys. Rev. Fluids* **5**, 042301(R).

Moazzen, M., Lacassagne, T., Thomy, V. & Bahrani, S.A. (2022) "Torque scaling at primary and secondary bifurcations in a Taylor–Couette flow of suspensions", *J. Fluid Mech.* **937**, A2.

Alam, M. & Ghosh, M. (2023) "Unified torque scaling in counter-rotating suspension Taylor–Couette flow", *Phil. Trans. Roy. Soc. A*, **381** (2243) 20220226.

Dubrulle, B., Dauchot, O., Daviaud, F., Longaretti, P.-Y., Richard, D. & Zahn, J.-P. (2005) "Stability and turbulent transport in Taylor–Couette flow from analysis of experimental data", *Phys. Fluids* **17**, 095103.

Ghosh, M., & Alam, M. (2025a) "Routes to turbulent Taylor vortices: vortex splitting and merging in chaotic state and the role of particles", *J. Fluid Mech.*, (in revision).

Ghosh, M., & Alam, M. (2025b) "Direct transition to chaos and turbulence in suspension Taylor-Couette flow", *preprint*.

Ruelle, D. & Takens, F. (1971) "On the nature of turbulence", *Commun. Math. Phys.* **20**, 167–192.

Bagnold, R.A. (1954) "Experiments on a gravity-free dispersion of large solid spheres in a Newtonian fluid under shear", *Proc. R. Soc. Lond.* A **225**, 49–63.

Ho, B.P. & Leal, L.G. (1974) "Inertial migration of rigid spheres in two-dimensional unidirectional flows", *J. Fluid Mech.* **65** (2), 365–400.

Baroudi, L., Majji, M.V., & Morris, J.F. (2020) "Effect of inertial migration of particles on flow transitions of a suspension Taylor–Couette flow", *Phys. Rev. Fluid* **5**, 114303.

ICTW 2025 23rd INTERNATIONAL COUETTE-TAYLOR WORKSHOP 14th-16th JULY DURHAM, UK

Instabilities and Pattern Selection in Inclined Binary Convection

A. Alonso*†, I. Mercader †, O. Batiste †, A. Meseguer †

Abstract:

In this work, we numerically investigate pattern formation in binary fluid convection within slightly inclined cylindrical cells heated from below. Our focus is on the Soret regime for mixtures with a positive Soret coefficient.

We begin by presenting an overview of the stable flow patterns observed in moderately sized cells with aspect ratio around 5 ($\Gamma \approx 5$). The emerging patterns are diverse and dynamically rich, with the observed dynamics showing high sensitive to small variations in Γ. By varying the Rayleigh number and smoothly adjusting its increments, we capture a wide range of spatio-temporal behaviours (see Figure 1 and Figure 2 for an example with a $\Gamma = 5.4$ cell). These include large-scale shear flows (LSF) and several types of superhighway convection (SHC) patterns (oscillatory plumes travelling in adjacent lanes along the direction of inclination). Beyond steady and periodic regimes, we identify modulated SHC patterns, including quasiperiodic and chaotic states. These flows exhibit complex temporal dynamics while preserving the fundamental SHC structure. The associated bifurcation scenarios are intricate and strongly case-dependent (Alonso et al., 2025).

To gain deeper insight into the transition mechanisms and reduce spatio-temporal complexity, we extend our analysis to smaller cells with aspect ratio 3 ($\Gamma = 3.0$). This configuration is expected to yield more structured and robust bifurcation sequences, providing a clearer understanding of the instabilities that govern binary convection in inclined cylindrical geometries.

We employ in-house numerical tools to solve the Navier-Stokes equations for binary mixtures in cylindrical domains. Most results are obtained with a three-dimensional time-stepping spectral code (Mercader et al., 2010) that captures stable patterns. For the smaller aspect ratio cells, we additionally use a Newton-Krylov solver to compute steady solutions and trace the underlying branches of stable and unstable states that may explain the complex dybnics observed in the Soret regime.

Figures and References:

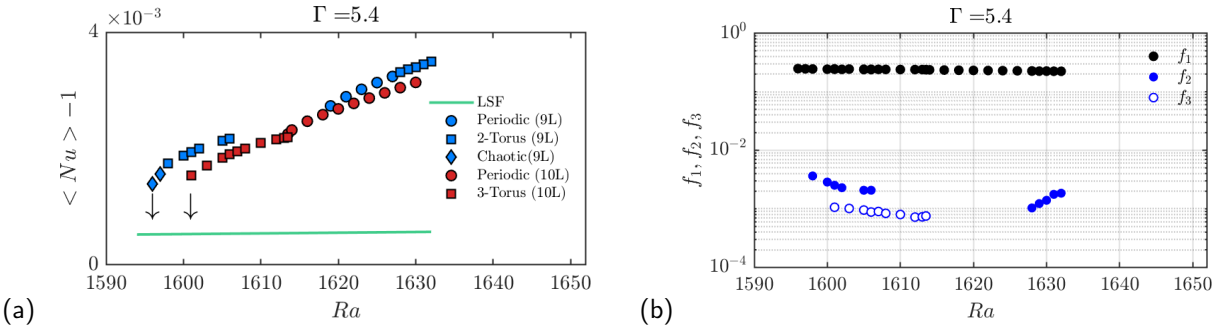

Figure 1: (a) Averaged Nusselt number and (b) temporal frequencies of the patterns as a function of the Rayleigh number Ra for different 9 and 10-lane SHC patterns arising in a $\Gamma = 5.4$ cell.

*Corresponding author: arantxa.alonso@upc.es
†Universitat Politècnica de Catalunya Barcelona Tech, Barcelona, Spain

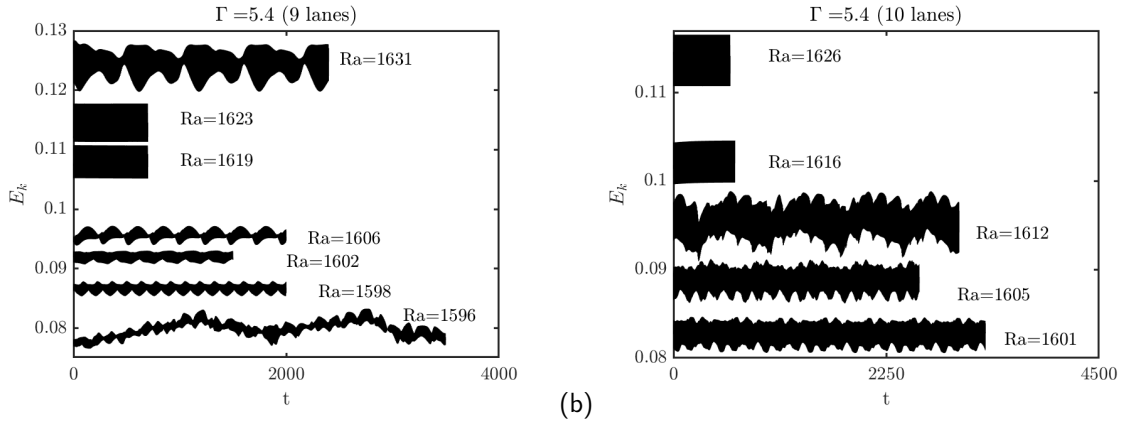

(a) (b)

Figure 2: Kinetic energy as a function of nondimensional time for (a) 9-lane and (b) 10-lane periodic and modulated SHC-like states obtained for different values of Ra in a $\Gamma = 5.4$ cell.

Acknowledgements:

This research is supported by the Ministerio de Ciencia, Innovación y Universidades (Agencia Estatal de Investigación, project nos. PID2020-114043GB-I00 (MCIN/AEI/10.13039/501100011033) and PID2023-150029NB-I00 (MCIN/AEI/10.13039/501100011033/FEDER, UE).

References

Alonso, A., Mercader, I., Batiste, O., Meseguer, A. (2025). "Numerical Simulation of Binary Convection within the Soret Regime in a Tilted Cylinder". *J. Non-Equilib. Thermodyn.*, DOI:10.1515/jnet-2024-0064.

Mercader I., Batiste O., & Alonso A. (2010), "An efficient spectral code for incompressible flows in cylindrical geometries", *Computers & Fluids*, **39**, 215–224.

Forced flow reversal in ferrofluidic Couette flow

Sebastian A. Altmeyer* †

Time-dependent boundary conditions are very common in natural and industrial flows and by far no exception. An example of this is the movement of a magnetic fluid as ferrofluids Rosensweig (1985) forced due to temporal modulations. Using a modified Niklas approximation (Niklas (1987),Altmeyer (2021)), the effect of frequency modulation on non-linear flow dynamics and appearing flow pattern reversal is analyzed. Flow structures of particular interest in the present work are wavy Taylor vortex flows (WVF_2, with dominant azimuthal wavenumber $m = 2$) Wereley and Lueptow (1998); Altmeyer (2024) in the counter-rotating Taylor-Couette system Taylor (1923), which was subjected to a spatially homogeneous magnetic field subject to an alternating modulation ($\mathbf{H} = [H_S + H_M \sin(\Omega_H t)]\mathbf{e}$).

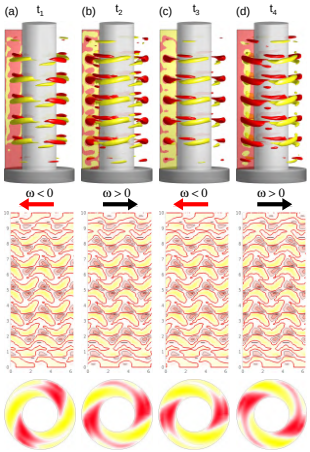

Figure 1: Flow vizualizations of the temporal flow pattern reversal for WVF_2 $(5V, k = 4.21)$ with $s_{z,S} = 0.2 = s_{z,M}$ and $\Omega_H = 5$ for retrograde ($\omega < 0$) and prograde ($\omega > 0$). *Top row*: isosurfaces of azimuthal vorticity $\eta = \pm 200$ [red (yellow) color indicates positive (negative) vorticity]. *Middle row*: radial velocity $u(\theta, z)$ on an unrolled cylindrical surface in the annulus at mid-gap [red (yellow) color indicates in (out) flow]. *Bottom row*: contours of azimuthal velocity component v in the (r, θ) plane at mid-height (viewed from the bottom) [red (yellow) color indicates positive (negative) velocity].

In the absence of a magnetic field, all WVF_2 states move in the opposite direction to the rotation of the inner cylinder, they are retrograde. However, when strength or frequency of the alternating magnetic field increases, the motion direction of the flow pattern changes (Fig. 1). Thus, the alternating field provides a precise and controllable key parameter for triggering the system response and controlling the flow. Aside, we also observed intermittent behavior when one solution became unstable, leading to random transitions in both, the transition time and towards the different final solutions.

We've studied wave propagation reversal for both static and alternating magnetic fields. In the absence of a magnetic field, the WVF_2 moves in a retrograde manner relative to the inner cylinder rotation. However, when we increase the strength of a static or alternating magnetic field, the retrograde wave propagation slows down and eventually becomes zero. At this point, the flow is represented by a *standing wave* and then starts moving in the opposite direction, becoming prograde. The reversal of wave propagation coincides with the stabilization of the basic state due to increasing magnetic field strength, both for static and alternating fields.

The present work indicates the impact of complex fluids under external driving forces. Our findings suggest that, in ferrofluids, flow pattern reversal can be induced by varying a magnetic field in a controlled manner, which may have applications in the development of modern fluid devices in laboratory experiments.

References

Taylor, G.I. "Stability of a Viscous Liquid contained between Two Rotating Cylinders", *Phil. Trans. Roy. Soc. A*, **223** 289–343.

Rosensweig, R. E. "Ferrohydrodynamics". *Cambridge University Press, Cambridge*.

Niklas, M. (1987) "Influence of magnetic fields on Taylor vortex formation in magnetic fluids". *Z. Phys. B* **68**, 493.

Altmeyer, S. (2021) "On the ridge of instability in ferrofluidic Couette flow via alternating magnetic field". *Scientific Reports* **11**, 4705.

Altmeyer, S. (2024) "Forced flow reversal in ferrofluidic Couette Flow via alternating magnetic field" Physics of Fluids **36** 114105

Wereley, S. T. and Lueptow, R. M. (1998)"Spatio-temporal character of non-wavy and wavy Taylor-Couette flow", *J. Fluid Mech.* **364**, 59.

*Corresponding author: sebastian.andreas.altmeyer@upc.edu

†Universitat Politècnica de Catalunya, 08034 Barcelona, Spain

Bifurcations in spherical Couette flow

Ananthu J P*†, Manjul Sharma‡, A. Sameen‡, Vinod Narayanan†

1. **Introduction**

Spherical Couette flow, the motion of fluid in the annular space between two concentric spheres with one or both rotating, serves as a fundamental model in fluid dynamics, offering insights into geophysical and astrophysical phenomena (1). This study focuses on a narrow gap ratio ($\beta = 0.24$) with only the inner sphere rotating, examining how initial conditions influence flow bifurcations(4). Previous research has highlighted the role of gap ratio (β) and Reynolds number (Re) in driving flow transitions, often involving Taylor vortices, spiral instabilities, and chaotic states (2). Here, we use numerical simulations to map bifurcation branches, analyze flow topologies, and explore phase space dynamics, providing a comprehensive understanding of flow behavior in this regime.

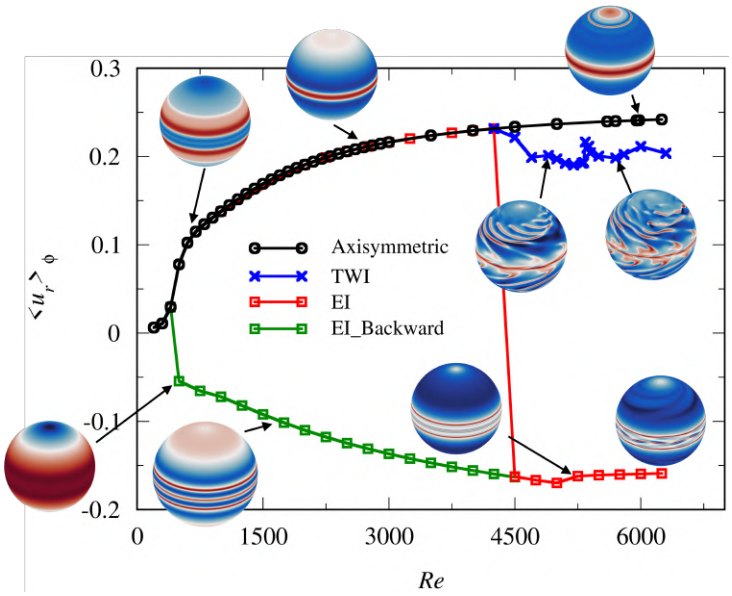

Figure 1: Bifurcation diagram showing the three branches (Axisymmetric, TWI, EI) and hysteresis in the $\langle u_r \rangle_\phi$-Re plane.

2. **Methodology**

The incompressible Navier-Stokes equations in spherical coordinates are solved using the Dedalus framework, a Python-based pseudo-spectral method employing Chebyshev polynomials in the radial direction and Jacobi polynomials for spherical bases (3). The Reynolds number is defined as $\mathrm{Re} = R_i^2\omega_i/\nu$, where R_i is the inner sphere radius, ω_i is its angular velocity, and ν is the kinematic viscosity. The gap ratio is fixed at $\beta = (R_o - R_i)/R_i = 0.24$. Simulations are conducted over $\mathrm{Re} = 400$–6300, with three sets of initial conditions to capture different bifurcation branches: The **Axisymmetric Branch** is initialized with the velocity field from the previous lower Re simulation, the **Traveling Wave Instability (TWI) Branch** starts with zero initial field and perturbation, and the **Equatorial Instability (EI) Branch** is initiated with an artificial perturbation. A grid independence study ensures numerical accuracy, and results are validated against experimental and numerical studies, confirming the reliability of the method.

*Corresponding author: ananthu.jp@iitgn.ac.in
†Indian Institute of Technology, Gandhinagar
‡Indian Institute of Technology, Madras

3. **Results and Discussion**
   The bifurcation diagram, plotted in the $\langle u_r \rangle_\phi$-Re plane (see Figure 1), reveals three distinct branches:

   1. **Axisymmetric Branch** : This branch remains steady and axisymmetric up to Re $= 6250$, with a sub-critical base flow featuring circular cells in each hemisphere at low Re. Pinching at the equator occurs at Re ≈ 430, consistent with theoretical predictions. At Re $= 6250$, the flow becomes weakly periodic, exhibiting a limit-cycle in phase space, with a dominant equatorial jet and slow-moving polar jets at high Re.

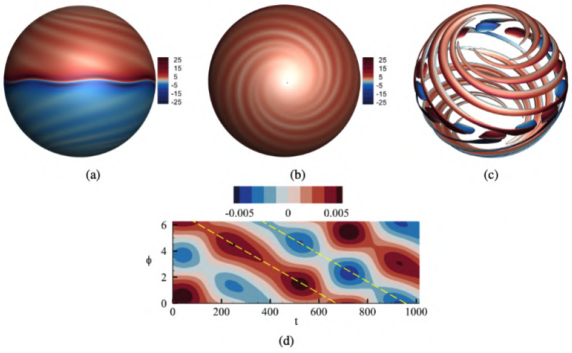

(a) Contours of azimuthal vorticity showing spiral wavy flow at $Re = 4500$ on branch II. (a) Side view, (b) top view, and (c) iso-surface of $u_\phi = -0.0289$. (d) Contours of Azimuthal vorticity $\xi(\phi, t)$ at $r = (R_i + R_o)/2$, $\theta \approx 0$ is plotted along ϕ at $Re = 4500$. Yellow dashed lines show the direction of propagation of the wave.

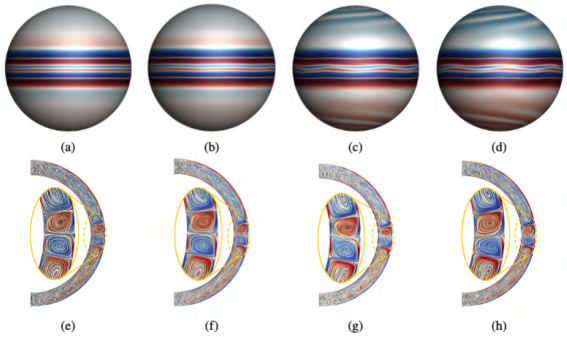

(b) Two-cell flow on the EI branch shown by contours of azimuthal vorticity from (a) to (d) for Reynolds numbers $4500, 4750, 5750$, and 6250 respectively. Figures (e) to (h) show vortex lines in an $r - -\theta$ plane for the respective Reynolds numbers.

   2. **Traveling Wave Instability (TWI) Branch** : Emerging at Re ≈ 4500, this branch is characterized by spiral instabilities near the poles (wavenumber $k = 7$) and equatorial instabilities(see Figure 2a). A notable direction-reversing bifurcation occurs between Re $= 4700$ and 5340, with the spiral wave propagation direction reversing. At higher Re, multiple wavenumbers appear in the equatorial instability, leading to chaotic flow, as evidenced by filled phase space trajectories.
   3. **Equatorial Instability (EI) Branch** : Also branching at Re ≈ 4500, this branch features a two-vortex structure near the equator, driven by twin jet streams. These jets become unstable at Re > 4750, supporting an azimuthal instability ($k = 7$) but no chaotic behavior within the studied Re range. Hysteresis is observed, with the EI branch extending backward to Re $= 400$ before reverting to the axisymmetric branch (see Figure 2b).

4. **Conclusions**
   This study explains the complex bifurcation behavior in narrow gap spherical Couette flow, highlighting the sensitivity to initial conditions and the emergence of distinct flow regimes. The axisymmetric branch transitions to periodicity, the TWI branch exhibits spiral and equatorial instabilities leading to chaos, and the EI branch features unstable twin jets with hysteresis. These findings enhance our understanding of rotational instabilities and flow transitions, with potential applications in rotating machinery and geophysical modeling. Future work should explore larger gap ratios to generalize these observations.

References

[1] M. Wimmer, "Experiments on a viscous fluid flow between concentric rotating spheres," *J. Fluid Mech.*, vol. 78, no. 2, pp. 317–335, 1976.

[2] K. Nakabayashi and T. Yoichi, "Spectral study of the laminar-turbulent transition in spherical couette flow," *J. Fluid Mech.*, vol. 194, pp. 101–132, 1988.

[3] K. J. Burns, G. M. Vasil, J. S. Oishi, D. Lecoanet, and B. P. Brown, "Dedalus: A flexible framework for numerical simulations with spectral methods," *Phys. Rev. Res.*, vol. 2, no. 2, p. 023068, 2020.

[4] J. P. Ananthu, Sharma. M, A. Sameen, Narayanan. V, Bifurcations in narrow gap spherical Couette flow, *J. Fluid Mech.*, 2025 [accepted]

Emergence of Intermittency and hibernation in elastoinertia TC flows

T. Boulafentis *, T. Lacassagne †, N. Cagney‡, S. Balabani¶

Intermittency is a common feature in viscoelastic turbulent flows, occurring in both negligible (Jun , 2017; Singh , 2024) and high (Xi , 2012; Rosti , 2023) inertia regimes but has received comparatively less attention in Taylor-Couette flows.

We report experimental evidence of intermittency in viscoelastic Taylor Couette flows at an intermediate Re = 120 (below the onset of inertia turbulence, corresponding to laminar Taylor Vortex Flow-TVF in Newtonian cases) and high Wi. By performing PIV velocity measurements with solutions of polyacrylamide (PAAM) in water-glycerol spanning a wide range of elasticity values (El=0-0.64, Wi=0-76.4), we show that viscoelasticity initially destabilises the base flow, gradually leading to elastoinertia turbulence (EIT) through a series of flow transitions, and suppresses it at higher values of elasticity (Wi>63.7). The turbulence suppression is accompanied by a promotion of flow intermittency for increasing Wi, characterised by periods of extreme turbulent events (active turbulence) and periods where turbulence is almost fully suppressed (hibernating turbulence).

Active turbulence consists of weakly chaotic solitary pairs of vortices which gradually become scarcer and weaker for increasing Wi due to elastic dissipation. The hibernating state involves weak fluctuations, which are independent of Wi but remain above the laminar case, consistent with the picture of marginal turbulence.

The study highlights the dual effect of viscoelasticity, destabilising and stabilising TC flows even at moderate inertia (Re = 120).

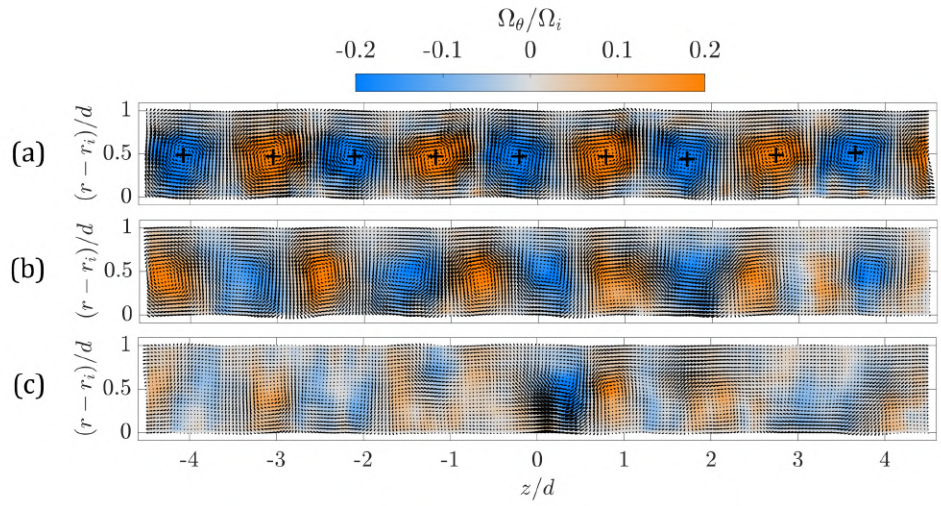

Figure 1: Velocity vectors with azimuthal vorticity contours, normalised by the rotational speed of the inner cylinder, Ω_θ/Ω_i, for fixed Reynolds number, Re=120 and (a) Wi=0 (0 ppm),(b) Wi=8.3 (10 ppm), and (c) Wi=76.4 (700 ppm).

*FLUME, Department of Mechanical Engineering, University College London (UCL), London WC1E 7JE, UK
†IMT Nord Europe, Institut Mines-Télécom, Univ. Lille, Centre for Energy and Environment, Lille F-59000, France
‡School of Engineering and Materials Science, Queen Mary University of London, London E1 4NS, UK
§FLUME, Department of Mechanical Engineering, University College London (UCL), London WC1E 7JE, UK
¶Corresponding author: s.balabani@ucl.ac.uk

References

Y. Jun and V. Steinberg, "Polymer concentration and properties of elastic turbulence in a von Karman swirling flow", Phys. Rev. Fluids 2, 103301 (2017).

R. K. Singh, P. Perlekar, D. Mitra, and M. E. Rosti, "Intermittency in the not-so-smooth elastic turbulence", Nat. Commun. 15, 4070 (2024).

L. Xi and M. D. Graham, "Dynamics on the laminar-turbulent boundary and the origin of the maximum drag reduction asymptote", Phys. Rev. Lett. 108, 028301 (2012).

M. E. Rosti, P. Perlekar, and D. Mitra, "Large is different: Nonmonotonic behavior of elastic range scaling in polymeric turbulence at large Reynolds and Deborah numbers", Sci. Adv. 9 (2023).

Spin-up and Spin-down Flow Instabilities in Cylinders

Ellen Bartle[*†], Cédric Beaume[†], Nik Kapur[†], Greg de Boer [†]

Several areas of academia and industry, ranging from projectile dynamics (Wedemeyer, 1964) to food processing (Goto, 2023), seek to deepen their understanding of fluid behaviour within bounded rotating systems. Despite their practical relevance, the transient flows that emerge in such configurations remain poorly understood, due in part to a lack of targeted studies examining the onset and development of instabilities.

The present study focuses on the impulsive spin-up and spin-down flows, of a Newtonian fluid, in bounded cylinders. In the impulsive spin-up case, a stationary cylinder filled with a fluid, initially at rest, is suddenly set into rotation, while in the impulsive spin-down case, a rotating cylinder containing a fluid in solid-body rotation is abruptly stopped. While geometrically simple, these setups generate complex flow structures driven by viscous boundary layer dynamics, redistribution of angular momentum, and the onset of instabilities (Greenspan, 1968; Benton, 1974). Analytical techniques are employed alongside high-order numerical simulations to investigate the criteria for the development of these instabilities. Starting from the Navier–Stokes equations expressed in cylindrical coordinates under the assumption of axisymmetry, expressions for the azimuthal velocity are derived in unbounded cylinders and in cylinders bounded by rigid walls. A parametric study involving the aspect ratio is conducted to explore the influence of the geometry and show how bounded system flows asymptotically approach the behaviour of unbounded systems as the aspect ratio increases. The investigation is then extended to three-dimensional simulations using spectral methods tailored for cylindrical geometries (Borońki & Tuckerman, 2007a, 2007b). This methodology enables a detailed examination of boundary layer evolution of intricate flow structures and of the onset of instabilities. This combination of analytical and numerical approaches allows the identification of the spatial structure of the vortical modes developing near the side and the end walls, thereby providing the criteria for instability in impulsive spin-up and spin-down flows within rotating cylinders.

References

Wedemeyer, E. H. (1964). The unsteady flow within a spinning cylinder. *Journal of Fluid Mechanics, 20*(3), 383–399. https://doi.org/10.1017/S002211206400129X

Goto, S., Horimoto, Y., Kaneko, T., Oya, K., Sugitani, Y., Aritsu, S., Yoshida, M., Ohyama, H., Eguchi, K., Kukimoto, S., Matsuyama, K., Nishimura, T., Fukuda, K., & Onoda, K. (2023). Precessing cylinder as high-shear-rate mixer: Application to emulsification. *Physics of Fluids, 35*(3), 035139. https://doi.org/10.1063/5.0139991

Greenspan, H. P. (1968). *The theory of rotating fluids*. Cambridge University Press.

Benton, E. R., & Clark, A., Jr. (1974). Spin-up. *Annual Review of Fluid Mechanics, 6*, 257–280. https://doi.org/10.1146/annurev.fl.06.010174.001353

[*] Corresponding author: sceab@leeds.ac.uk
[†] University of Leeds, Leeds, UK

Boroński, P., & Tuckerman, L. S. (2007a). Poloidal-toroidal decomposition in a finite cylinder. I. Influence matrices for the magnetohydrodynamic equations. *Journal of Computational Physics, 227*, 1523-1543. https://doi.org/10.1016/j.jcp.2007.08.023.

Boroński, P., & Tuckerman, L. S. (2007b). Poloidal-toroidal decomposition in a finite cylinder. II. Discretization, regularization and validation. *Journal of Computational Physics, 227*, 1544-1566 https://doi.org/10.1016/j.jcp.2007.08.035.

Near onset dynamics in natural doubly diffusive convection

C. Beaume*†, J. Tumelty†, A. Rucklidge†,
A. Bergeon‡, E. Knobloch§

Doubly diffusive convection may occur when a fluid is subject to thermal and compositional variations that affect the fluid density and diffuse at different rates. In natural doubly diffusive convection, the gradients of temperature and salinity are horizontal and point in the same direction. This configuration has been studied in the balanced case where the buoyancy ratio $N = -1$, i.e., when thermal and solutal variations within the fluid yield forces of equal strengths but opposite directions. This configuration admits a conduction state, where the fluid is stationary and the temperature and concentration profiles are linear. Natural doubly diffusive convection possesses a rich bifurcation structure (Beaume, Rucklidge & Tumelty , 2022) and most of the attention has focused on the subcritical case, where the primary instability from the conduction state generates families of subcritical steady convection states.

In vertically extended domains with rigid top and bottom end-walls and a square horizontal cross-section, the primary bifurcation leads to the formation of spatially localized convection rolls known as convectons. These steady states are organized in a pair of intertwined solution branches within a well-defined range of Rayleigh numbers. This behavior is known as snaking. Secondary instabilities along the primary branches of convectons are found to yield twisted convectons and secondary snaking (Beaume, Bergeon & Knobloch , 2013). The twist instability destabilizes the primary convectons and is responsible for the absence of stable steady states, localized or otherwise (Beaume, Bergeon & Knobloch , 2018). As a result, for Rayleigh numbers beyond the threshold for primary instability, the system undergoes an abrupt transition to large amplitude spatio-temporal chaos (Beaume , 2020).

In this talk, I will describe the aforementioned dynamical phenomena. I will also present the computation of doubly diffusive convectons in the supercritical regime, a scenario that was thought to be impossible about a decade ago (Tumelty, Beaume & Rucklidge , 2023), and describe what happens to convectons when thermal and solutal variations do no longer yield forces of equal strengths, i.e., in the unbalanced, $N \neq -1$, case (Tumelty, Beaume & Rucklidge , 2025).

References

Beaume, C., Bergeon, A. & Knobloch, E. "Convectons and secondary snaking in three-dimensional natural doubly diffusive convection", *Phys. Fluids*, **25** 024105 (2013).

Beaume, C., Bergeon, A. & Knobloch, E. "Three-dimensional doubly diffusive convectons: instability and transition to complex dynamics", *J. Fluid Mech.*, **840** 74–105 (2018).

Beaume, C. "Transition to doubly diffusive chaos", *Phys. Rev. Fluids*, **5** 103903 (2020).

Beaume, C., Rucklidge, A.M. & Tumelty, J. "Near-onset dynamics in natural doubly diffusive convection", *J. Fluid Mech.*, **934** A42 (2022).

Tumelty, J., Beaume, C. & Rucklidge, A.M. "Toward convectons in the supercritical regime: Homoclinic snaking in natural doubly diffusive convection", *SIAM J. Appl. Dyn. Sys.*, **22** 1710–1742 (2023).

Tumelty, J., Beaume, C. & Rucklidge, A.M. "Convectons in unbalanced natural doubly diffusive convection", *Phys. Rev. Fluids*, accepted (2025).

*Corresponding author: c.m.l.beaume@leeds.ac.uk
†University of Leeds, Leeds, UK
‡Université de Toulouse, Toulouse, France
§University of California, Berkeley, USA

Finite amplitude analysis of Poiseuille flow in fluid overlying porous domain

P. Bera*†, A. Aleria*

A weakly nonlinear stability analysis of isothermal Poiseuille flow in a fluid overlying porous domain (see Fig. 1) is proposed and investigated in this article (aleria (2024)). The flow is characterized by Navier-Stokes equations in the fluid domain and by Darcy's law in the porous domain.

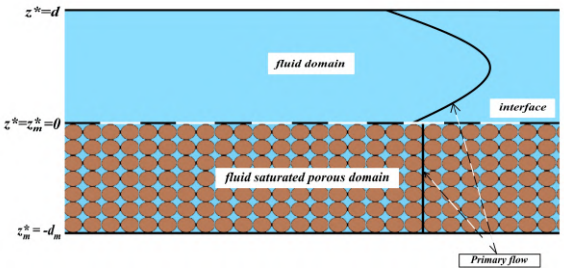

Figure 1: Schematic of the physical problem.

The nonlinear interactions are studied by imposing finite amplitude disturbances to the classical model deliberated in chang (2006). The order parameter theory (stuart (1960)) is used to ascertain the cubic Landau equation:

$$\text{In fluid domain:} \quad \frac{d|A|^2}{dt} = 2ac_i|A|^2 + 2a_{1r}|A|^4. \tag{1}$$

$$\text{In porous domain:} \quad \frac{d|A_m|^2}{dt_m} = 2a_m c_{mi}|A_m|^2. \tag{2}$$

The amplitude $(|A|, |A_m|) = (0, 0)$ is stable for $Re < Re_c$ and unstable for $Re > Re_c$. Here Re_c stands for the critical value of Reynolds number, whereas, a and c_i denote the wave number in stream-wise direction and imaginary part of complex wave-speed, respectively. Consequently, from equation 1-2, the bifurcations depend on only real part of Landau constant (a_{1r}). Now, the non-zero finite amplitude solution exists when ac_i and a_{1r} are of opposite signs. This raises two such possible combinations: first, $ac_i > 0$ and $a_{1r} < 0$; second, $ac_i < 0$ and $a_{1r} > 0$. The former leads to the supercritical bifurcation and the latter leads to the subcritical bifurcation (rogers (1993),sharma (2018)).

The well-established controlling parameters viz. the depth ratio ($\hat{d}$ = depth of fluid domain/depth of porous domain), Beavers-Joseph constant (α) and the Darcy number (δ) are inquired upon for the bifurcation phenomena. The imposed finite amplitude disturbances are viewed for bifurcations along the neutral stability curves and away from the critical point as a function of the Reynolds number (Re). Linear stability analysis predicts three different modes of instability: porous (for relatively smaller values of a), even-fluid-layer (for moderate value of a), and odd-fluid-layer (for relatively large value of a). For large value of $(\hat{d})$ even-fluid-layer mode dominates instability (see figure 2(b)). The even-fluid-layer (porous) mode along the neutral stability curves correlates to the subcritical (supercritical) bifurcation phenomena (see figure 2(c)-(d)). On perceiving the bifurcations as a function of Re by moving away from the bifurcation/critical point, subcritical bifurcation is observed for increasing $\hat{d}, \alpha$ and decreasing δ. In contrast to only fluid flow through a channel, it is found that the inclusion of porous domain aids in the early appearance of subcritical bifurcation when

*Corresponding author: pberafma@iitr.ac.in
†Indian Institute of technology Roorkee, Roorkee, India

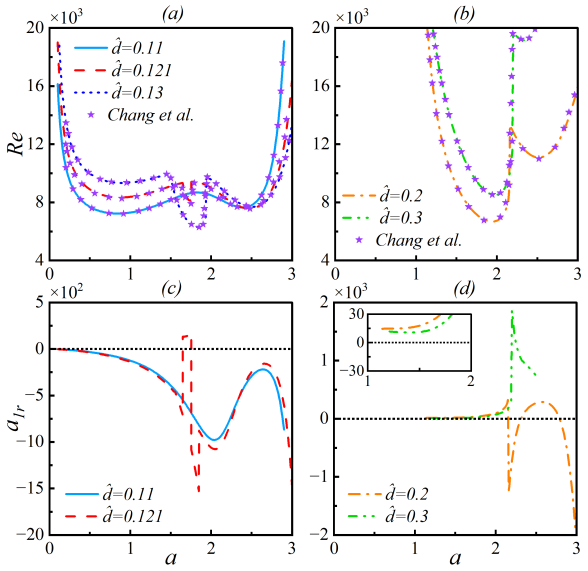

Figure 2: (a, b) Neutral stability curves obtained by linear theory for different values of $\hat{d}$, (c, d) Variation of Landau constant (a_{1r}) obtained by weakly nonlinear theory along the neutral stability curves for different values of $\hat{d}$ $(\alpha = 0.1, \delta = 0.001)$.

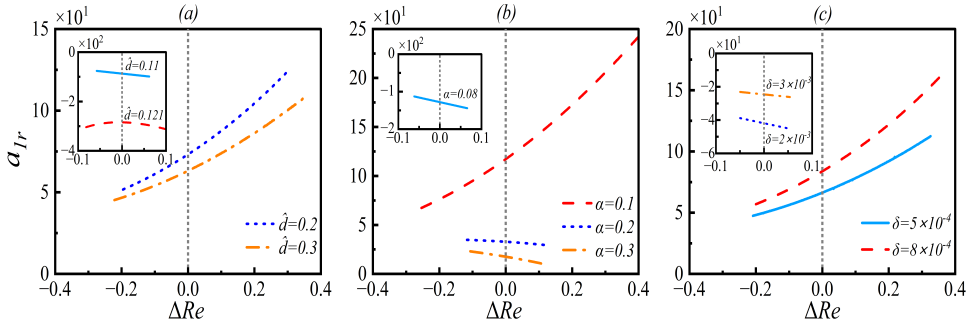

Figure 3: Variation of a_{1r} with ΔRe for different values of (a) $\hat{d}$ $(\alpha = 0.1, \delta = 0.001)$, (b) α $(\hat{d} = 0.13, \delta = 0.001)$ and (c) δ $(\hat{d} = 0.13, \alpha = 0.1)$.

$\alpha = 0.2, \hat{d} = 0.13, \delta = 0.001$. A considerable difference between the computed skin friction coefficient for the base and the distorted state is observed for small (large) values of $\hat{d}$ (α). In addition, an intrinsic relation amongst the mode of instability, bifurcation phenomena and secondary flow pattern is also observed.

References

Aleria, A. and Khan, A. and Bera, P. "Finite amplitude analysis of poiseuille flow in fluid overlying porous domain", *SIAM J. Appl. Math.*, **84** 433–463.

Chang, M. H. and Chen, F. and Straughan, B. (2006), "Instability of Poiseuille flow in a fluid overlying a porous layer", *J. Fluid Mech.*, **564** 287–303.

Rogers, B. B., Moulic, S. Ghosh, & Yao, L. S. (1993). "Finite-amplitude instability of mixed convection", *J. Fluid Mech.*, **254** 229–250.

Sharma, A. K., Khandelwal, M. K., & Bera, P. (2018), "Finite amplitude analysis of non-isothermal parallel flow in a vertical channel filled with a highly permeable porous medium", *J. Fluid Mech.*, **857** 469–507.

Stuart, J. T. (1960), "On the non-linear mechanics of wave disturbances in stable and unstable parallel flows Part 1. The basic behaviour in plane Poiseuille flow", *J. Fluid Mech.*, **9** 353–370.

Stochastic excitation of acoustic waves by turbulent convection: influence of rotation and magnetic fields

L. Bessila[1] [2], S. Mathis[2]

Abstract Format:

Acoustic waves can be stochastically excited by the motion of a turbulent flow (Samadi & Goupil 2001). This phenomenon has many applications in astrophysics: acoustic waves are generated in the convective regions of stars and gas giant planets (Aerts 2010, Gaulme 2015), providing valuable information about their internal structure. However, most theoretical models of stochastic excitation neglect the effects of magnetic fields and rotation, despite their significant impact on convective dynamics (Stevenson 1979, Ecke et al 2023). Notably, observations from the *Kepler* space mission have notably revealed the absence of acoustic mode signals in a substantial fraction of rapidly rotating and highly magnetised stars (Mathur et al. 2019). Since these waves are essential for characterizing stars and their planetary systems, it is crucial to incorporate rotation and magnetic effects into existing theoretical models.

We present a theoretical framework to model stochastic excitation, applicable to all types of waves in spherical geometry. We include the influence of a magnetic field and of rotation on the dynamics of excitation by turbulent convection. We demonstrate that rotation systematically reduces the efficiency of mode excitation. Moreover, we identify two distinct magnetic regimes: while a moderate magnetic field can enhance the excitation of acoustic waves, a strong magnetic field suppresses their generation. We discuss the implications of these findings for a star similar to the Sun.

References

Aerts, C., Christensen-Dalsgaard, J., Kurtz D. W. (2010) “Asteroseismology”, Springer

Ecke, R.E., Shishkina, O. (2023) “Turbulent Rotating Rayleigh–Bénard Convection”, Annual Review of Fluid Mechanics, 53, 603-638

Gaulme, P., Mosser, B., Schmider, F.-X., Guillot, T., Jackiewicz, J. (2015), “Seismology of Giant Planets”, Extraterrestrial Seismology , Cambridge University Press, 189-202

[1] Corresponding author: leila.bessila@cea.fr
[2] CEA IRFU, Astrophysics Department

Mathur, S., García, R. A., Bugnet, L., Santos, A. R. G., Santiago, N., Beck, P. G. (2019), "Revisiting the impact of stellar magnetic activity on the detectability of solar-like oscillations by Kepler", Frontiers in Astronomy and Space Sciences, 6, 46

Samadi, R & Goupil, M.-J. (2001) "Excitation of stellar p-modes by turbulent convection: I. Theoretical formulation", Astronomy & Astrophysics, 370, 136-146

Stevenson, D.J. (1979), "Turbulent thermal convection in the presence of rotation and a magnetic field: A heuristic theory", Geophysical & Astrophysical Fluid Dynamics, 12, 139-169

Angular momentum transport in Quasi-Keplerian flow with radial convection.

A. Bhadra[†], J. Wicht[†], X. Zhu[*†]

Protoplanetary disks are expected to be turbulent based on observational data. However, because their gas orbits at nearly Keplerian speed—a Rayleigh-stable configuration—the physical origin of this turbulence remains a mystery. Radial thermal convection may drive turbulence in the weakly-ionized regions of protoplanetary disks (Teed and Latter, 2021; Lesur et al., 2022). To explore this mechanism, we perform direct numerical simulations of thermal convection in a Taylor–Couette flow setup in the quasi-Keplerian regime with radius ratio $\eta = 0.2$ subject to a centrally directed gravitational field. The inner cylinder is held at a higher temperature than the outer cylinder, and we vary the Taylor number over the range $10^7 \leq Ta \leq 10^9$. To mimic disk-relevant buoyancy-to-shear ratios, we fix the Richardson number $Ri = Ra\,Pr/Ta = 0.1$, where Ra and Pr are the Rayleigh and Prandtl numbers, respectively. Pr is fixed at 1. Our results show that, as Ta increases, the thermal Nusselt number Nu_t grows—signifying enhanced outward heat transport—while the angular velocity Nusselt number Nu_ω decreases and, across most of the parameter range, becomes negative. The latter indicates a net inward transport of angular velocity, which we attribute to Reynolds stresses generated by convective motions. These findings not only shed light on the potential role of radial convection in astrophysical disks but also guide the design and interpretation of future laboratory experiments aimed at reproducing quasi-Keplerian turbulence.

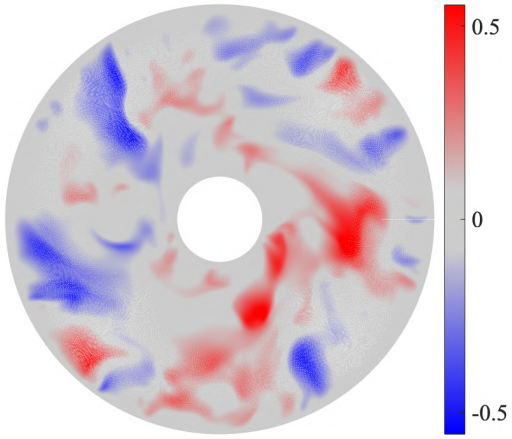

Figure 1: Radial velocity profile along the $r - \theta$ plane at mid-height for $Ta = 10^8$ and $Ri = 0.1$.

References

Teed, R.J. and H.N. Latter, "Axisymmetric simulations of the convective overstability in protoplanetary discs," *Monthly Notices of the Royal Astronomical Society*, **507**(4), 5523–5541.

Lesur, G., B. Ercolano, M. Flock, M.-K. Lin, C.-C. Yang, J. A. Barranco, P. Benitez-Llambay, J. Goodman, A. Johansen, H. Klahr, G. Laibe, W. Lyra, P. Marcus, R. P. Nelson, J. Squire, J. B. Simon, N. Turner, O. M. Umurhan, and A. N. Youdin,
"Hydro-, Magnetohydro-, and Dust-Gas Dynamics of Protoplanetary Disks," *arXiv preprint* arXiv:2203.09821 (2022).

*Corresponding author: zhux@mps.mpg.de
[†]Max Planck Institute for Solar System Research, 37077 Göttingen, Germany

Theory and simulation of internal wave spectra in the ocean

O. Bühler, M. Shavit*†

One hundred years ago the atmosphere and oceans were believed to be in turbulent motion based on their enormous Reynolds numbers. This slowly gave way to the realization that density stratification and Coriolis forces strongly inhibit three-dimensional turbulence, making it the exception rather than the rule in geophysical fluid dynamics. This poses long-standing problems, especially for deep ocean dynamics, where turbulent vertical mixing is crucial but stems from hard-to-predict rare pockets of turbulence caused by breaking internal gravity waves. Much effort has therefore been spent in trying to understand the creation and maintenance of internal wave energy cascades in the ocean. In this talk I will show recent results based on kinetic wave theory for internal waves that treats both stratification and Coriolis forces on equal footing. This leads to a simpler kinetic equation for the wave dynamics, albeit currently only in a two-dimensional setting. Theoretical and numerical results are shown for wave energy spectra and cascades in this system and compared to observations.

*Corresponding author: obuhler@cims.nyu.edu
†Courant Institute of Mathematical Sciences, New York University, NY, U.S.A.

Revision of the linear stability paradox for known bounded shear flows

S. Chefranov[1,2], A. Chefranov[3]

The well-known paradox of linear stability for the Hagen-Poiseuille (HP) and Plane Couette (PC) flows is not solved up to now and is bypassed on the basis of the non-linear mechanisms consideration. We prove that it is arising only due to an idealized assumption of an exact space periodicity for the small hydrodynamic perturbations. When finite non-zero viscosity is taken into account only quasi-periodic in space perturbations can be considered in the frame of linear stability theory. For the quasi-periodic in longitudinal direction disturbances the linear instability of the HP flow, Plane Poiseuille flow (PP) and PC flow at the finite Reynolds numbers, is obtained. The generalization of Landau's critical velocity for the vortexes arising in the laminar HP, PP and PC flows of classical fluids also stated.

References

Taylor, G.I. (1923) "Stability of a Viscous Liquid contained between Two Rotating Cylinders", *Phil. Trans. Roy. Soc. A,* 223 289-343. https://doi.org/10.1098/rsta.1923.0008

Egbers, C., & Pfister, G. (Eds.). (2008). "Physics of Rotating Fluids: Selected Topics of the 11th International Couette-Taylor Workshop Held at Bremen, Germany, 20-23 July 1999 (Vol. 549)." Springer.

Chefranov, S.G., & Chefranov, A.G. (2014) "Hagen-Poiseuille Flow Linear Stability Paradox Resolving and Viscous Dissipative Mechanism of the Turbulence Emergence in the Boundary Layer", *arXiv: 1007.1097v1 [physics.flu-dyn] 7 Jul 2010*

Chefranov, S.G., & Chefranov, A.G. (2014) "Solution to the Paradox of the Linear Stability of the Hagen-Poiseuille Flow and the Viscous Dissipative Mechanism of the Emergence of Turbulence in a Boundary Layer", *JETP, 119,* 331-340. https://doi.org/10.1134/S1063776114070127

Chefranov, S.G., & Chefranov, A.G. (2015) The Hagen-Poiseuille Linear Flow Instability, *Dokl. Phys., 60*, 327-332; https://doi.org/10.1134/S1028335815070083

Chefranov, S.G., & Chefranov, A.G. (2016) Linear Instability of Plane Couette and Poiseuille Flows, *J. Exp. Theor. Phys. (JETP), 122*, 925-931 ;https://doi.org/10.1134/S1063776116050034

[1] Corresponding author: schefranov@mail.ru
[2] A. M. Obukhov Institute of Atmospheric Physics, Moscow, Russia
[3] Eastern Mediterranean University, Famagusta, Northern Cyprus

Accessing the dipole-multipole transition in rapidly rotating spherical shell dynamos

A. T. Clarke*† C. J. Davies† S. Naskar† S. J. Mason†

Earth's magnetic field has exhibited erratic polarity reversals over much of its history; however, the processes that cause polarity transitions are still poorly understood. Dipole reversals have been found in many numerical dynamo simulations and often occur close to the transition between dipole-dominated and multipolar dynamo regimes. However, the physical conditions used in reversing simulations are necessarily far from those in Earth's liquid iron core because of the long runtimes needed to capture polarity transitions and because a systematic exploration of parameter space is needed to find the dipole-multipole transition.

We develop a unidimensional path theory in an attempt to simplify the search for the dipole-multipole transition at increasingly realistic physical conditions. We consider three paths that are all built from the requirements of a constant magnetic Reynolds number Rm; one path further attempts to impose balance between Magnetic, Coriolis, and Archimedean forces (a MAC balance) while the other two seek to constrain solutions to an inertia-MAC, or IMAC, balance. The presence of inertia, although not geophysically realistic, allows us to build paths that more closely follow the conditions where simulated reversals have been found to date.

Numerical simulations show reasonable agreement with the expected physical conditions along the paths within the accessible parameter space, but also deviate from predicted behaviour for certain diagnostic quantities, particularly the magnetic field strength and the magnetic/kinetic energy ratio. Furthermore, the paths do not follow the dipole-multipole transition; starting from reversing conditions, simulations move into the dipolar non-reversing regime as they are advanced along the path. By increasing the Rayleigh number, a measure of the buoyancy driving convection, above the values predicted by the path theory, we are able to access the dipole-multipole transition down to an Ekman number $E \sim 10^{-6}$, comparable to the most extreme conditions reported to date.

Our results, therefore, demonstrate that the path approach is an efficient method for seeking the dipole-multipole transition in rapidly rotating dynamos. However, the conditions under which we access the dipole-multipole transition become increasingly hard to access numerically and also increasingly unrealistic because Rm rises beyond plausible bounds inferred from geophysical observations. Future work combining path theory with variations in the core buoyancy distribution, as suggested by recent studies, appears a promising approach to accessing the dipole-multiple transition at extreme physical conditions.

*Corresponding author: a.t.clarke@leeds.ac.uk
†University of Leeds, Leeds, UK

Exploring Bifurcation Structures in the Regularized Four-Sided Lid-Driven Cavity Flow

M. Reborido[*], J. Curbelo[†‡], A. Alonso[†], A. Meseguer[†]

The four-sided lid-driven cavity flow problem is of high interest for two main reasons: it is a benchmark in computational fluid mechanics for validating different numerical solvers of the Navier-Stokes equation, and it acts as a test bed for studying particular physical effects.

In this study, we provide an overview of the bifurcation analysis for this problem and carry out some explorations for new possible emerging branches of the bifurcation diagram. In order to avoid corner singularities caused by the discontinuities of the velocity at the boundary, we consider a regularized version of the problem by setting the wall speed to follow a double exponential distribution. This allows for exponential convergence in spectral discretization schemes, such as the Newton-Krylov method, which we use alongside a continuation algorithm for computing steady solutions with different Reynolds numbers.

Additionally, we present four different explorations on the bifurcation diagram based on introducing a small perturbation in the velocity of one (or more) of the lids . We then study the nature of the resulting branches, calculated with the previously mentioned continuation algorithm; and whether the original bifurcation points are conserved or not.

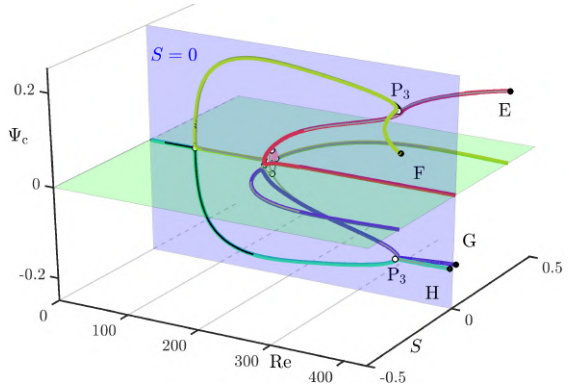

Figure 1: Bifurcation diagram visualized after breaking both rotational and reflection symmetries in the boundary conditions.

Acknowledgments:

We acknowledge the support of PID2020114043GB-I00, RYC2018-025169,CNS2023-144555 funded by MICIU/AEI/10.13039/501100011033 and by the European Union NextGenerationEU/PRTR.

References

Meseguer, A., Alonso, A., Batiste, O., An, B., & Mellibovsky, F. (2024). "Bifurcation analysis in the regularized four-sided cavity flow: Equilibrium states in a D 2-symmetric fluid system". *Physics of Fluids*, **36**(6).

Reborido Fuentes, M. (2024). Homotopic D2-symmetry breaking of bifurcation scenarios of the four-sided lid driven cavity flow problem (Master's thesis, Universitat Politècnica de Catalunya).

[*]Universidad de Santiago de Compostela
[†]Corresponding author: jezabel.curbelo@upc.edu
[‡]Universitat Politècnica de Catalunya- BarcelonaTech

Role of Elasticity and Inertia in Particle Migration: A Theoretical and Experimental Study in Complex Taylor Vortices

M. Davoodi[1] [2], A. Clarke[2]

The flow between concentric cylinders, driven by wall motion, is widely studied in fluid mechanics due to the ability to create diverse flow conditions. These range from simple shear flows to complex steady state and to time-dependent behaviours characterised by Taylor vortices. While often considered in academic research, this geometry is also found in practical applications, such as in the oil and gas industry, where drilling fluids are used to transport cuttings along an annulus to the surface (Davoodi and Clarke, 2024). Understanding the behaviour of these fluids, especially when they exhibit non-Newtonian and viscoelastic properties, is crucial for practical purposes; that is, improving particle transport and well-bore cleaning efficacy.

In this study we aim to clarify the roles of different physical forces, particularly elasticity and inertia, in particle migration within annular flow with center-body rotation. We develop a comprehensive approach that combines theoretical analysis, numerical simulations, and experimental observations (Clarke and Davoodi, 2025). Our Eulerian-Eulerian model solves separate momentum equations for both the fluid and particle phases, allowing us to determine distinct velocity fields for each. This approach highlights the relative motion between the particles and fluid, framing the problem as a "resistance" rather than a "mobility" issue.

By examining how inertial and elastic forces influence the drag and lift on particles, we demonstrate their combined effects on particle migration. Our results reveal that inertia causes particles to move outward within the vortices, forming ring-like structures, while elasticity tends to pull them toward the vortex center. The interplay between these forces is captured effectively by our model and aligns well with experimental observations, offering new insights into suspension flow dynamics in complex conditions.

References

Davoodi M, Clarke A. Sedimenting-particle redistribution in a horizontal Couette. Journal of Fluid Mechanics. 2024 Jan;979:A37.

Clarke A, Davoodi M. The movement of particles in Taylor–Couette flow of complex fluids. Journal of Non-Newtonian Fluid Mechanics. 2025 Jan 1;335:105354.

[1] Corresponding author: mdavoodi@slb.com

[2] Schlumberger Cambridge Research, Cambridge, UK

Instability in centrifugally stable shear flows

K. Deguchi*†, M. Dong‡

We investigate the linear instability of flows that are stable according to Rayleigh's criterion for rotating fluids. Using Taylor-Couette flow as a primary test case, we develop large Reynolds number matched asymptotic expansion theories. Our theoretical results not only aid in detecting instabilities previously reported by Deguchi (2017) across a wide parameter range but also clarify the physical mechanisms behind this counterintuitive phenomenon. Instability arises from the interaction between large-scale inviscid vortices and the viscous flow structure near the wall, which is analogous to Tollmien-Schlichting waves. Furthermore, our asymptotic theories and numerical computations reveal that similar instability mechanisms occur in boundary layer flows over convex walls.

References

Deguchi, K. "The rapid-rotation limit of the neutral curve for Taylor-Couette flow", *J. Phys. Rev. E*, **95**, 021102(R).

Deguchi, K. & Dong, M. "Instability in centrifugally stable shear flows", *J. Fluid Mech.*, **1006** A13.

*Corresponding author: kengo.deguchi@monash.edu
†Monash University, VIC 3800, Australia
‡Chinese Academy of Sciences, PR China

Axisymmetric rolls in rotor-stator flow

Y. Duguet*†, A. Gesla ,2*‡, L. Martin Witkowski ‡§, P. Le Quéré *

Rotor-stator flows exhibit instabilities in the form of circular and spiral rolls. The origin of the spirals is known as a standard supercritical bifurcation, however the dynamical origin of the circular rolls is still unclear. In the present work we propose an explanation for the circular rolls as a linear response of the system to external forcing. We consider two types of axisymmetric forcing: bulk forcing (based on the resolvent analysis) and boundary forcing (based on direct numerical simulation). Using the singular value decomposition of the resolvent operator the optimal response is computed and takes the form of circular rolls. The optimal energy gain is found to grow exponentially with the Reynolds number (based on the rotation rate and interdisc spacing H), in connection with huge levels of non-normality. The results for both types of forcing are compared with former experiments (Schouveiler , 2001). The linear response is also compared with the fully nonlinear self-sustained periodic and quasiperiodic solutions found for the unforced problem. Our findings suggest that at low Reynolds number typical of experimental observations, the circular rolls observed experimentally are the combined effect of the high forcing gain and the roll-like form (cf. fig. 1) of the leading response of the linearised operator. At slightly higher Reynolds number, nonlinear receptivity can also lead to the nonlinear oscillatory states identified in the unforced problem (Gesla , 2024).

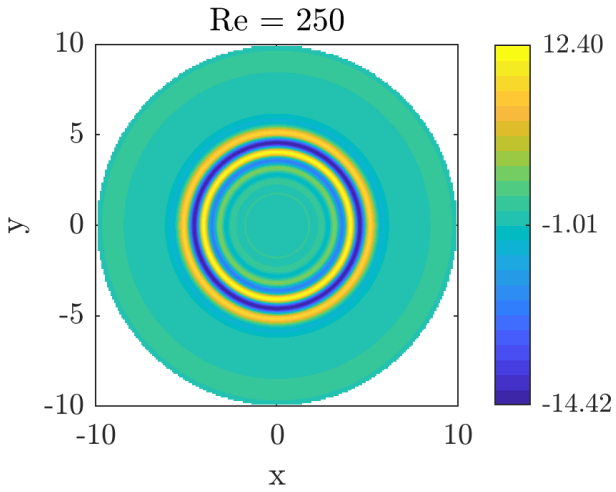

Figure 1: Vorticity of axisymmetric rolls forced externally at $Re = 250$.

References

A. Gesla *et al.* "On the origin of circular rolls in rotor-stator flow", *J. Fluid Mech.*, **1000** A47.

L. Schouveiler *et al.* "Instabilities of the flow between a rotating and a stationary disk", *J. Fluid Mech.*, **443** 329-350.

*Corresponding author: duguet@lisn.fr
†LISN, Université Paris-Saclay, France
‡EPFL, Lausanne, Switzerland
§LMFA, Univ. Lyon 1, France

Recent activities in experimental research on liquid metal Rayleigh-Bénard convection at HZDR

T. Vogt[1], F. Schindler[1], N. Kim[1], S. Su[2], M. Sieger[1]
T. Wondrak[1], S.Eckert[1,3]

Abstract

For about 10 years, the Department of Magnetohydrodynamics at the HZDR has been increasingly involved in the experimental investigation of Rayleigh-Bénard convection in liquid metals at very low Prandtl numbers, $Pr \sim 10^{-2}$ - 10^{-3}, which is of great interest for geo- and astrophysics. The thermally driven convective flow dynamics of liquid metals are very different from moderate-*Pr* fluids, such as water. Owing to the large discrepancies in the diffusion of heat and momentum, significant differences between velocity and temperature fields occur. The large-scale convection (LSC) in liquid metals exhibits a significantly more pronounced intermittent behavior and higher turbulence at comparable Rayleigh numbers, *Ra*. Here, the thermal boundary layer (BL) thickness exceeds that of the viscous BL, exposing it to direct interaction with the turbulent flow. It is well-known that the intermittent behavior of the viscous and thermal BL's increase significantly at small *Pr*. The viscous BL in a liquid metal becomes turbulent at smaller Ra than comparable convection in gases or water. Thus, a stronger influence of the LSC on the thermal BL thickness and, furthermore, on the local properties of the heat transport is likely.

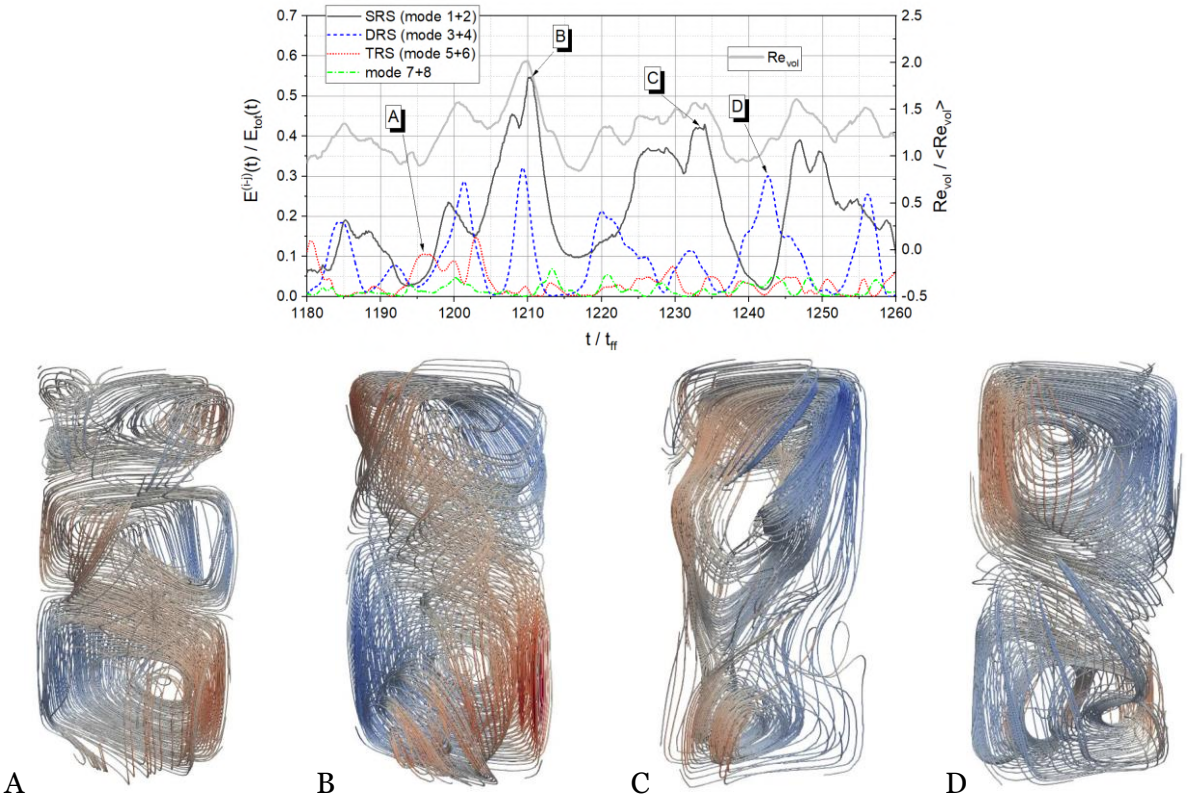

Figure 1: Time series of the energy contributions of the main POD modes and the volume-averaged Reynolds number with snapshots of the 3D flow pattern (streamlines) at $Ra = 6\times10^8$, $Pr = 0.025$, aspect ratio 0.5

[1] Helmholtz-Zentrum Dresden-Rossendorf (HZDR), Dresden, Germany
[2] Universitė Rouen Normandie, Rouen, France
[3] Corresponding author

Here, we present investigations in cylindrical convection cells of aspect ratio 1 and 0.5 as well as in a rectangular cell with a square base area of 1 m^2 and an aspect ratio of 25. Our flow measurements demonstrate that the reduction of the aspect ratio in the cylindrical cells increases the volatility of the LSC, one can even describe this as a collapse of the coherent LSC (Schindler et al., 2022). Figure 1 shows, how the single-roll structure of the LSC alternates in short succession with double-roll and triple-roll structures in time periods smaller than the turn-over time (Wondrak et al., 2023). Temperature measurements within the thermal BL reveal strong fluctuations of the BL thickness and increasing deviation from the Prandtl–Blasius–Pohlhausen profile with increasing Ra (Kim et al., 2024). Furthermore, we will show measurements of the temperature and velocity fields in the shallow convection cell. These experiments focus on the search for so-called turbulent superstructures with their special characteristics in low-Pr fluids. Figure 2 shows an example of flow measurements by means of the ultrasound Doppler velocimetry (UDV).

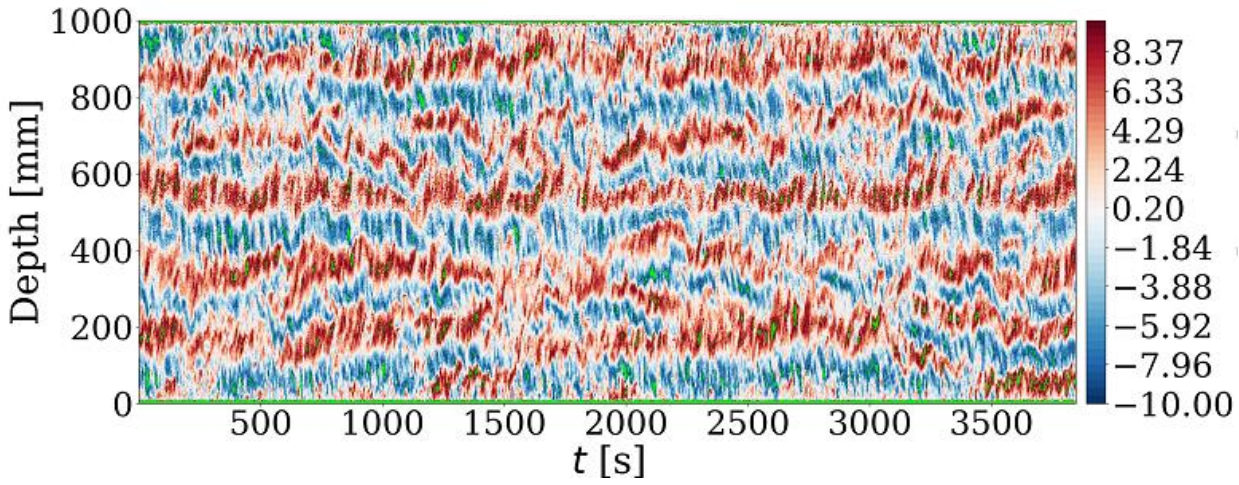

Figure 2: Spatio-temporal flow pattern recorded by UDV in a rectangular convection cell of aspect ratio 25, $Ra = 1.8 \times 10^5$, $Pr = 0.025$

References

Schindler, F., Eckert, S., Zürner, T., Schumacher, J., Vogt, T. (2022) "Collapse of Coherent Large Scale Flow in Strongly Turbulent Liquid Metal Convection ", *Phys. Rev. Lett.,* 128, 164501.

Wondrak, T., Sieger, M., Mitra, R., Schindler, F., Stefani, F., Vogt, T., Eckert, S. (2023). "Three-dimensional flow structures in turbulent Rayleigh–Bénard convection at low Prandtl number Pr = 0.03" *J. Fluid Mech.,* 974, A48.

Kim, N., Schindler, Vogt, T., Eckert, S. (2024). "Thermal boundary layer dynamics in low-Prandtl-number Rayleigh–Bénard convection" *J. Fluid Mech.,* 994, A4.

ICTW 2025 23rd INTERNATIONAL COUETTE-TAYLOR WORKSHOP 14th-16th JULY DURHAM, UK

Wall modes in rotating Rayleigh-Bénard convection: robustness and breakdown

B. Favier*†, L. Terrien†, E. Knobloch‡

Heat transport by rapidly-rotating Rayleigh-Bénard convection is of fundamental importance to many geophysical and astrophysical flows. However, laboratory measurements in tall, narrow cylinders (Cheng , 2018) are often compromised by the emergence of robust wall modes that develop along vertical boundaries (Favier & Knobloch , 2020). These modes can significantly enhance the overall heat flux (de Wit , 2020; Zhang , 2020), complicating efforts to isolate and measure the contribution from bulk convection.

Using Direct Numerical Simulations, we demonstrate the surprising persistence of wall modes, even far beyond their linear onset and despite substantial changes to domain geometry. Finally, we show that adding narrow horizontal fins along the vertical walls effectively suppresses these modes, reducing their contribution to the total heat flux to negligible levels in the geostrophic regime (Terrien , 2023). This method could be experimentally feasible and may open the door to more accurate studies of rotating convection in the geophysically relevant regime.

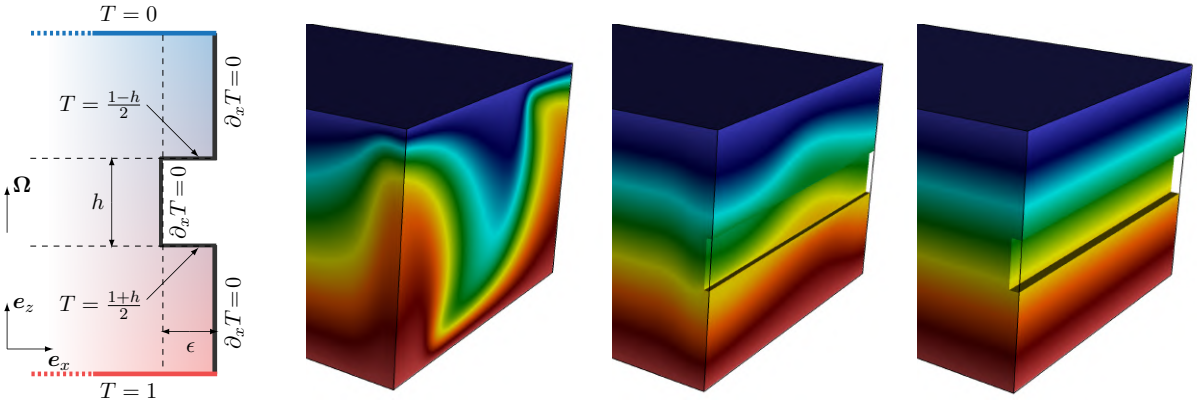

Figure 1: Left: Transverse section focusing on one side of the Cartesian domain. All boundaries are no-slip with periodic boundary conditions in the direction normal to the plane. The obstacle has a height h and width ϵ. All vertical boundaries are thermally insulating while we impose a temperature equal to that of the linear equilibrium background on all horizontal boundaries (including the barrier). Right: Visualizations of the temperature field for a fixed barrier height and increasing barrier width from left to right. The wall mode attached to the boundary is clearly visible on the left while it has completely disappeared on the right.

References

Cheng et al. (2018) *Geophys. & Astrophys. Fluid Dyn.* **112**.

Favier and Knobloch (2020) *J. Fluid Mech.* **895**.

de Wit et al. (2020) *Phys. Rev. Fluids* **5**.

Zhang et al. (2020) *Phys. Rev. Lett.* **124**.

Terrien et al. (2023) *Phys. Rev. Lett.* **130**.

*Corresponding author: benjamin.favier@univ-amu.fr
†Aix Marseille Univ, CNRS, Centrale Marseille, IRPHE, Marseille, France
‡Department of Physics, University of California at Berkeley, Berkeley, California 94720, USA

Influence of Surface Tension and Gravity Force on Compressible Kelvin-Helmholtz Instability

Y. Fukumoto*†, R. Zou‡, K. Matsuura§, N. Taniguchi¶

For an incompressible fluid, an interface of tangential-velocity discontinuity suffers from the Kelvin-Helmholtz instability (KHI), with growth rate proportional to velocity discontinuity. Compressibility acts to stabilize KHI and, if limited to two dimensions, suppresses KHI for the Mach number larger than $\sqrt{8}$ (Landau, 1944). We extend this analysis to include surface tension and the gravity effect, with allowance made for density discontinuity. In case a light gas lies over a heavy gas, the gravity force as well as the surface tension acts as restoring forces. We find that these restoring forces cause instability of the interface, otherwise being stabilized by compressibility effect at high Mach numbers.

Compressible Kelvin-Helmholtz Instability

Let us take, as the basic flow, $\boldsymbol{U} = (U, 0, 0)$ $(z > 0)$, $\boldsymbol{U} = \boldsymbol{0}$ $(z < 0)$, in Cartesian coordinates with z directed vertically upward. We superpose irrotational disturbances to this basic flow, with the interface $z = 0$ being disturbed in the form $\exp[i(kx + ly - \omega t)]$. The disturbed pressure field is governed by a wave equation derived from the compressible linear Euler equation. Requiring that the pressure is continuously connected at the interface, we gain the dispersion relation (Landau 1944, Landau and Lifshitz 1987).

$$\omega = \frac{1}{2}kU \pm \widetilde{k}\sqrt{\frac{1}{4}U^2\cos^2\phi + c^2 \pm c\sqrt{c^2 + U^2\cos^2\phi}}, \tag{1}$$

where c is the speed of sound and $(k, l) = (\widetilde{k}\cos\phi, \widetilde{k}\sin\phi)$ with $\widetilde{k} = \sqrt{k^2 + l^2}$ and ϕ being the angle of the wave vector measured from the x-axis. As the velocity difference $|U|$ increases, the quantity with $-$ sign under the root symbol increases from a negative value and turns into positive values when $M > \sqrt{8}/|\cos\phi|$ with $M = |U|/c$ being the Mach number. Restricting to two-dimensional disturbances ($\phi = 0$), the critical

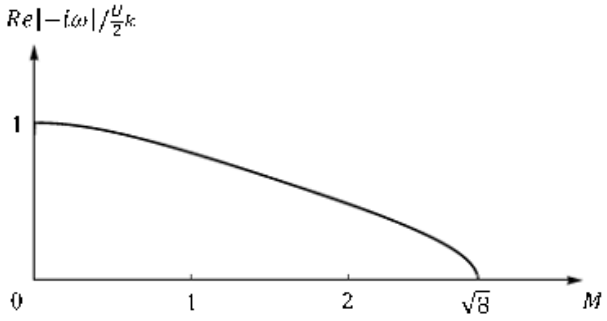

Figure 1: Amplification factor of compressible Kelvin-Helmholtz instability, relative to the incompressible KHI, for two-dimensional perturbations ($\phi = 0$).

Mach number for stabilization is $M_c = \sqrt{8} \approx 2.828$. Fig. 1 shows the amplification factor, relative to the incompressible KH instability, of the growth rate. For 3D disturbances, M_c increases and the amplification factor decreases with ϕ.

*Corresponding author: yasuhide@imi.kyushu-u.ac.jp
†Kyushu University, Fukuoka and Osaka Central Advanced Research Institute, Osaka, Japan
‡Hawaii Pacific University, Honolulu, USA
§Matsuyama University, Matsuyama, Japan
¶Tohoku University, Sendai, Japan

There is a mathematical analogy between the shallow water and a compressible gas flow. A discontinuous surface in tangential velocity of an incompressible shallow-water flow of depth H is stabilized when the discontinuous velocity is greater than $\sqrt{8gH}$ (Jin, Le and Fukumoto 2019, Le, Fukumoto and Koch 2024).

Compressible Rayleigh-Taylor Instability

When the density is discontinuous across the interface, a question naturally arises of how the gravity force influences KHI. When a heavy gas lies below, internal gravity waves propagate along the interface, but, when a heavy gas lies above, the Rayleigh-Taylor instability (RTI) is invited. Knowledge of the effect of compressibility on RTI has been accumulated over a half century since 1970's (Gauthier and Creurer, 2010).

We take the motionless state $\boldsymbol{U} = \boldsymbol{0}$ as the basic flow, and consider the isothermal process. The pressure p and the density ρ is connected through $p = \rho c^2$. Here c is the isothermal sound speed. In the presence of the gravity force, the density of the basic state varies with the height z as $\rho(z) = \rho(0)\exp(-gz/c^2)$. We refer to the upper ($z > 0$) and the lower ($z < 0$) fluids by using the subscripts 1 and 2. By enforcing continuity of the normal velocity and the pressure at the disturbed interface, we are led to the dispersion relation (Mathews and Blumenthal 1977).

$$\omega^2(\rho_2 Q_2 - \rho_1 Q_1) - k^2(\rho_2 - \rho_1)g = 0, \tag{2}$$

where Q_i is the z component of the wavenumber vector,

$$Q_1 = \frac{g}{2c_1^2}\left\{1 - \sqrt{1 + \frac{4c_1^4}{g^2}\left(k^2 - \frac{\omega^2}{c_1^2}\right)}\right\}, \quad Q_2 = \frac{g}{2c_2^2}\left\{1 + \sqrt{1 + \frac{4c_2^4}{g^2}\left(k^2 - \frac{\omega^2}{c_2^2}\right)}\right\}. \tag{3}$$

An analysis of (2) tells that, for small values of $g/(c_1^2 k)$ and $g/(c_2^2 k)$, compressibility has a tendency of decreasing the growth rate from the incompressible limit $\sqrt{gk(\rho_1 - \rho_2)/(\rho_1 - \rho_2)}$.

Influence of surface tension and gravity force on compressible KHI

A natural question is raised as regards the interaction between KHI and RHI of a compressible gas. Here we highlight the influence of surface tension and gravity force on KHI. In case a light gas lies over a heavy gas, the gravity force as well as the surface tension acts as restoring forces. We find that the both restoring forces cause instability of the interface, otherwise being stabilized by compressibility effect at high Mach numbers. To resolve this puzzling result, we are requested to clarify the role not only of the vorticity, but also of the dilatation $\nabla \cdot \boldsymbol{u}$. The mechanism for predominance of 3D disturbances, over 2D ones, is also to be clarified.

A mixing layer is thought of as a model that desingularizes the jump in tangential velocity discontinuity. A highly complex vortical structures are created, as the Reynolds number is increased, by going through successive instabilities. We conduct numerical simulations of a compressible mixing layer based on the Naiver-Stokes equations. By applying the hierarchical eddy clustering method Matsuura and Fukumoto (2022) to the numerical data, which automatically extracts and tracks locally connected vortical structures, we identify and classify fine vortical structures, and thereby draw a possible scenario for transition to turbulence.

References

Landau, L.D. "On the stability of tangential gaps in contracted fluid", *Dokl. Akad. Nauk SSSR*, **44** 151, 1944

Landau, L.D., & Lifshitz, E.M. (1987). "Fluid Mechanics, 2nd ed." Pergamon Press, New York.

Jin, L., Le, T.T., & Fukumoto, Y. "Frictional effect on stability of discontinuity interface in tangential velocity of a shallow-water flow", *Phys. Lett. A*, **383** 125839, 2019.

Le, T.T., Fukumoto, Y., & Koch, T. "Linear stability of a simple shear layer between two parallel streams in a shallow water flow", *Phys. Lett. A*, **493** 129264, 2024.

Gauthier, S., & Creurer, B.L. "Compressibility effects in Rayleigh-Taylor instability-induced flows", *Phil. Trans. R. Soc. A*, **368** 1681–1704, 2010.

Mathews, W.G., & Blumenthal G.R. "Rayleigh-Taylor stability of compressible and incompressible radiation-supported surfaces and slabs: Application to QSO clouds", *AstroPhys. J.*, **214** 10–20, 1977.

Matsuura, K., & Fukumoto, Y. "Hierarchical clustering method of volumetric vortical regions with application to the late-stage of laminar-turbulent transition", *Phys. Rev. Fluids*, **7** 054703, 2022.

Dielectrophoretic-driven convection in spherical Taylor-Couette flow

Y. Gaillard *†, P.S.B. Szabo*, C. Egbers*

The AtmoFlow experiment is a laboratory model designed to investigate idealized large-scale atmospheric flow fields, scheduled to operate aboard the International Space Station (ISS) by 2026. The setup consists of two concentric, independently rotating spherical shells, simulating planetary rotation. Thermal gradients are imposed by equatorial heating and polar cooling, replicating the temperature differences driven by solar radiation. An electric field is applied to the dielectric fluid confined between the shells, generating a dielectrophoretic force that acts as an artificial gravity, inducing buoyant convection. The resulting central force field is governed by Gauss's law, producing a thermal flow analogous to Rayleigh-Bénard convection. By employing the continuity, momentum, and energy equations, a forcing parameter analogous to the Rayleigh number is given by

$$Ra_{\mathsf{E}} = \frac{\epsilon_0 \epsilon_{\mathsf{r}} \gamma_e V_0^2}{2\rho_0 \nu \kappa} \in \left[1.83 \times 10^5, 2.07 \times 10^7\right], \qquad \text{with} \quad \gamma_e = e\Delta T \tag{1}$$

where ϵ_0 is the vacuum electric permittivity, ϵ_{r} the relative electric permittivity, γ_{e} the thermoelectric parameter, V_0 the applied electric tension, ρ_0 the reference density, ν the kinematic viscosity, κ the thermal diffusivity, γ_e the thermoelectric parameter, e the expansion coefficient of the electric permittivity and ΔT the applied temperature difference between the shells.

While the spherical shell experiment cannot only rotated in solid body configuration, it is also capable of rotating the spherical shells independently resulting in spherical Taylor-Couette flow which is the subject of this study. By utilising the rotating framework of reference at the outer cylinder Ω_2 via the Taylor number, Ta. The relative rotation difference is governed by the Rossby number, Ro, and applied at the inner shell via Ω_1. T

$$Ta \frac{4\Omega_2^2 d^4}{\nu^2} \in \left[1.10 \times 10^2, 6.37 \times 10^5\right], \quad Ro = \frac{\Omega_1 - \Omega_2}{\Omega_2} \in \left[4.29 \times 10^{-1}, 1.14\right] \tag{2}$$

where d is the characteristic length defined by the spherical gap-width.

A combination of momentum flux due to rotation and buoyancy gives rise to distinct flow patterns, which depend on the magnitude of the forcing parameter. Previous studies have shown that the dielectrophoretic force generates plume-like patterns in the radial direction Futterer (2008, 2013), while differential rotation create circulating flows between the Equator and Poles Haberman (1962); Munson (1971). The present study theses combined interactions of both transport mechanisms and explores the resulting flow structures. The numerical simulations are conducted by utilising the OpenFOAM ecosystem, an open-source finite volume solver, to model the AtmoFlow experiment. The simulations show emerging convective regimes in the spherical gap and classifies the observed patterns into distinct regimes, illustrating the transition between different convective states. Additionally, the heat flux through the system is analysed in relation to the forcing strength, providing an estimate of the heat transported across the spherical shell gap. Variations in thermal transport are correlated with kinetic energy, revealing the interplay between convective patterns and energy transfer. This investigation provides a better understanding of thermal and momentum transport and their interaction with one another.

Acknowledgement

The AtmoFlow project is supported by the BMWi via the German Space Administration (Deutsches Zentrum für Luft- und Raumfahrt) under Grant No. 50WP1709, 50WM1841, 50WM2141 and 50WM2441 and via the National High Performance Computing centre NHR with Grant No. bbi00021.

References

*Department of Aerodynamics and Fluid Mechanics, Brandenburg University of Technology Cottbus-Senftenberg, Siemens-Halske-Ring 15a, 03046 Cottbus, Germany

†Corresponding author: gaillard@b-tu.de

Futterer, B., Hollerbach, R., & Egbers, C. (2008, November). "GeoFlow: 3D numerical simulation of supercritical thermal convective states", *In Journal of Physics: Conference Series*, **137**, No. 1, p. 012026. IOP Publishing.

Futterer, B., Krebs, A., Plesa, A. C., Zaussinger, F., Hollerbach, R., Breuer, D., & Egbers, C. (2013). "TSheet-like and plume-like thermal flow in a spherical convection experiment performed under microgravity", *Journal of Fluid Mechanics*, **735**, 647-683.

Haberman, W. L. (1962). Secondary flow about a sphere rotating in a viscous liquid inside a coaxially rotating spherical container. *The Physics of Fluids*, **5**(5), 625-626.

Munson, B. R., & Joseph, D. D. (1971). Viscous incompressible flow between concentric rotating spheres. Part 1. Basic flow. *Journal of Fluid Mechanics*, **49**(2), 289-303.

ICTW 2025 23rd INTERNATIONAL COUETTE-TAYLOR WORKSHOP 14th-16th JULY DURHAM, UK

A shear-flow instability induced by a localised field in ideal MHD

S. P. Myers[†] S. D. Griffiths[*†] S. M. Tobias[†]

The dynamics of an electronically conducting fluid and a magnetic field, coupled through the Lorentz force and the induction equation, are important for understanding many astrophysical processes. When the effects of density stratification may be neglected (e.g., where the flow is constrained to be horizontal, perhaps by background rotation), and for large-scale flows with both Reynolds number $\mathrm{Re} \gg 1$ and magnetic Reynolds number $\mathrm{Rm} \gg 1$, many processes may be modelled by the equations of ideal two-dimensional magnetohydrodynamics (2DMHD). This limit is often used to model the interaction of a toroidal field with the zonal flows that dominate many planets, stars, and accretion discs.

Within 2DMHD, an important paradigm problem is the linear stability of a parallel shear flow with an aligned magnetic field, which is often studied using normal modes for which the growth rate is sought as a function of along-stream wavenumber (e.g., Michael, 1955; Chandrasekhar, 1961; Kent, 1968; Chen and Morrison, 1991; Hughes and Tobias, 2001). A key result of such theory is that a magnetic field that is everywhere sufficiently strong will stabilise a flow that is unstable in the absence of a magnetic field, as first demonstrated by Kent (1968) for a non-rotating flow in Cartesian geometry. However, magnetic fields can be destabilising. This is most evident via a so-called joint instability (Stern, 1963), in which the flow is stable in the absence of a magnetic field, but adding a magnetic field with a carefully chosen strength and cross-stream profile can lead to instability. In the case of the Sun, for which the differential rotation profile is thought to be hydrodynamically stable (Charbonneau et al., 1999), it has been demonstrated that a joint instability is possible when various potentially realistic magnetic field profiles are imposed (Gilman and Fox, 1997; Dikpati and Gilman, 1999).

Here we analyse what is believed to be a novel joint instability in ideal 2DMHD. It arises from the interaction of a localised magnetic field with a shear layer, without background rotation. The instability will be analysed in Cartesian (x, y) geometry for a flow $U(y)\hat{\boldsymbol{x}}$ with aligned field $B(y)\hat{\boldsymbol{x}}$, and for perturbations $\propto \exp(i(kx - \omega t))$. The key ideas can be demonstrated – with all quantities nondimensional – for the shear layer $U(y) = \tanh y$. In the hydrodynamic limit, this flow is known to be unstable for $0 < k < 1$, with a most unstable wavenumber $k_{\max} \approx 0.44$ (Michalke, 1964); this is illustrated by the numerical results show in Figure 1(a). However, when a narrow magnetic field is added around $y = 0$, a second tongue of instability – with a larger growth rate – can appear at higher k. This is shown in Figure 1(a) for $B(y) = 0.15\,\mathrm{sech}^2(25y)$, for which $k_{\max} \approx 4.2$, and for $B(y) = 0.15/(1 + (25y)^2)$, for which $k_{\max} \approx 3.5$. We call this higher wavenumber mode the SaM (shear and magnetic) instability.

Figure 1(a) suggests that the SaM instability is rather insensitive to the lateral profile of $B(y)$. Further, unlike the purely hydrodynamic instability with $k \lesssim 1$, the SaM instability is also rather insensitive to the lateral profile of $U(y)$, provided there is a region of approximately uniform shear where the magnetic field is non-trivial, close to $y = 0$. This is illustrated in Figure 1(b), where the field is fixed as $B(y) = 0.15/(1 + (25y)^2)$, but now three different shear flows are taken. For $U(y) = \tanh y$, the purely hydrodynamic mode is again evident for $k \lesssim 1$ and the SaM instability has $k_{\max} \approx 3.5$. For $U(y) = \tanh y\,\mathrm{sech}\, y$, the purely hydrodynamic mode appears to have $k_{\max} \approx 1$ and the SaM instability has $k_{\max} \approx 3.3$. For $U(y) = y$, there is no hydrodynamic instability, but the SaM instability still appears, now with $k_{\max} \approx 3.6$. In all cases, again note that the SaM instability is the most unstable mode in the system.

Here this SaM instability is investigated both analytically and numerically, in the linear regime. Given the apparent insensitivity to the choice of $U(y)$ and $B(y)$, we specialise to the case with $U(y) = \Lambda y$ and $B(y) = B_0/(1 + (y/L)^2)$, now using dimensional quantities. We will show that this combination permits a matched-asymptotic solution to be developed when $\varepsilon = \Lambda^2 L^2/B_0^2 \ll 1$, which corresponds to the limit of high magnetic energy relative to the kinetic energy over the narrow region of magnetic field. The asymptotic expansion also relies upon a small wavenumber limit, relative to the lengthscale L of the magnetic field;

*Corresponding author: s.d.griffiths@leeds.ac.uk
[†]Department of Applied Maths, University of Leeds, Leeds, UK

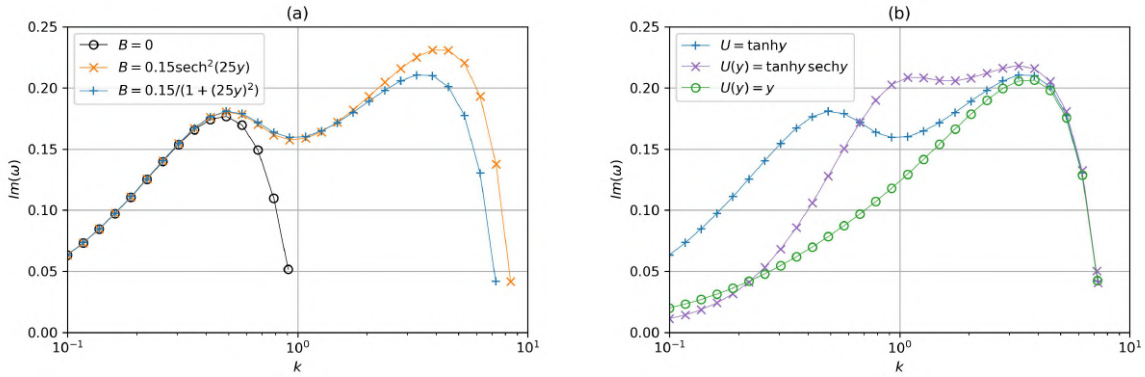

Figure 1: Numerically-determined growth rates as a function of wavenumber k for various flow and field configurations. (a) Instability of $U(y) = \tanh y$, with three different magnetic fields. (b) Instability of $B(y) = 0.15/(1 + (25y)^2)$ with three different flow fields.

for example, in Figure 1, we have $k_{\max} \approx 4$ and $L = 1/25$, so that $k_{\max} L \approx 0.16 \ll 1$. Despite the apparent simplicity of the flow configuration, the asymptotic analysis turns out to be rather complicated, with matching required across *four* regions in y, and unexpected fractional scalings in ε for the different parts of the eigenfunction. However, the outcome is an explicit analytical prediction for the nondimensional growth rate, which scales like $\varepsilon^{1/3}$, and the most unstable wavenumber, which scales like $\varepsilon^{8/9}$ as $\varepsilon \to 0$, both of which are shown to agree with numerical results.

References

Chandrasekhar, S. (1961). *Hydrodynamic and hydromagnetic stability*. Oxford.

Charbonneau, P., Dikpati, M., and Gilman, P. A. (1999). Stability of the solar latitudinal differential rotation inferred from helioseismic data. *Astrophys. J.*, 526:523.

Chen, X. L. and Morrison, P. J. (1991). A sufficient condition for the ideal instability of shear flow with parallel magnetic field. *Phys. Fluids B*, 3:863–865.

Dikpati, M. and Gilman, P. A. (1999). Joint instability of latitudinal differential rotation and concentrated toroidal fields below the solar convection zone. *Astrophys. J.*, 512:417–441.

Gilman, P. A. and Fox, P. A. (1997). Joint instability of latitudinal differential rotation and toroidal magnetic fields below the solar convection zone. *Astrophys. J.*, 484:439–454.

Hughes, D. W. and Tobias, S. M. (2001). On the instability of magnetohydrodynamic shear flows. *Proc. Roy. Soc. Lond.*, A 457:1365–1384.

Kent, A. (1968). Stability of laminar magnetofluid flow along a parallel magnetic field. *J. Plasma Phys.*, 2:543–556.

Michael, D. H. (1955). The stability of a combined current and vortex sheet in a perfectly conducting fluid. *Math. Proc. Cam. Phil. Soc.*, 51:528–532.

Michalke, A. (1964). On the inviscid instability of the hyperbolic-tangent velocity profile. *J. Fluid Mech.*, 19:543–556.

Stern, M. E. (1963). Joint instability of hydromagnetic fields which are separately stable. *Phys. Fluids*, 6:636–642.

Magnetic fields in protostars: generation mechanisms and stability

A. Guseva*†, L. Manchon†, L. Petitdemange†, C. Pinçon‡

Abstract

Recent spectropolarimetric observations of low-mass stars show that large-scale components of their magnetic fields can exhibit cyclic variations or reversals (Jeffers *et al.*, 2023). This magnetic activity affects detection of exoplanets and estimation of their masses, and so its modelling is particularly important. In convective stellar envelopes, magnetic fields are created through dynamo action - systematic stretching and twisting of magnetic field lines by helical convective vortices. It is yet however unclear how low-mass stars, with their strong convective turbulence and relatively slow rotation, are able to maintain coherent large-scale magnetic activity. In this work, we study the physical mechanisms that allow magnetic flux to accumulate at large scales in both turbulent and strongly stratified models of stellar convection. In such models, a highly turbulent convective layer is formed at the surface while the deep flow interiors remain rotationally constrained. Using direct numerical simulations with 3D MHD code MagIC (Gastine and Wicht, 2012), we found that small-scale magnetic flux, generated by small-scale turbulence in the outer flow regions with low density, is systematically transported into more quiescent inner regions by global magnetic pumping mechanism. Consequently, the dipolarity of the field at the surface of the domain increases both with enhancement of turbulence and stratification. These dipoles interact dynamically with zonal flows, resulting in aperiodic transitions between solar- and anti-solar rotation through nonlinear feedback of the Lorentz force, and in dipole reversals and periods of multi-polarity. Finally, we investigate the impact of surface conditions, such as differential rotation and heat flux distribution, that may arise through contraction of the protostar and the interaction with its accretion disc, on destabilization of initially dipole fields. With identified mechanisms of such destabilization, competition of local shear and convection-generated helicity, we derive criteria for dipole stability based on the ratio of shear and convective Rossby number, and assess the approaches to incorporate it in stellar evolution code CESAM (Morel and Lebreton, 2008).

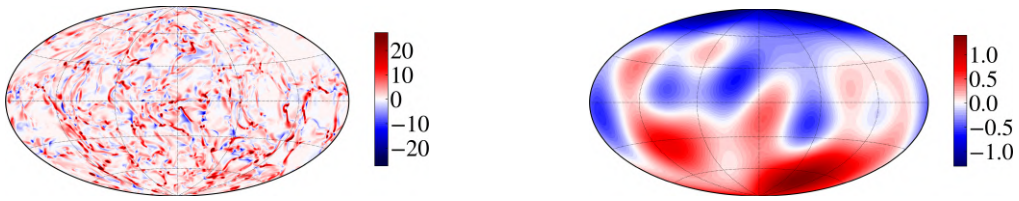

Figure 1: Illustration of the surface topology of magnetic field obtained in DNS. On the left: radial magnetic field component at the surface at a moment in time. On the right: same field but filtered with a large-scale spectral filter.

References

Jeffers, S. V., Kiefer, R., & Metcalfe, T. S. (2023). Stellar activity cycles. Space Science Reviews, 219(7), 54.

Gastine, T., & Wicht, J. (2012). Effects of compressibility on driving zonal flow in gas giants. Icarus, 219(1), 428-442.

Morel, P., & Lebreton, Y. (2008) CESAM: a free code for stellar evolution calculations. Astrophysics and Space Science, 316, 61-73.

*Corresponding author: anna.guseva@obspm.fr
†L'Observatoire de Paris, Paris, France
‡Institut d'Astrophysique Spatiale (IAS), Orsay, France

Dielectrophoretic force induced convection within a cylindrical annulus in various configurations.

M.H. Hamede*†, J. Roller‡, A. Meyer§, V. Heuveline‡, Ch. Egbers†

Research into enhancing heat transfer rates in different systems continues apace due to its necessity in a variety of technical fields. A number of methodologies have been employed to achieve this objective, including the utilization of dielectrophoretic (DEP) force, which, has the capacity to induce thermoelectric convection. The application of an electric field to a dielectric fluid results in the polarization of fluid particles and the subsequent occurrence of electrohydrodynamic (EHD) force. A high-frequency electric field, larger than the inverse of the charge relaxation time of the fluid, prevents free charge accumulation, thereby leading the DEP force to predominate over the Coulomb force. The DEP force can be conceptualized as an effect akin to electric gravity, proportional to the gradient of the electrostatic energy stored per unit volume of the dielectric fluid (Yoshikawa et al. , 2013). In this study, we experimentally investigated the artificially induced convection by applying the dielectrophoretic force (DEP) in different flow configurations. In the initial configuration, two static, concentric cylinders were aligned horizontally. The results demonstrated that the application of the DEP force enhanced the existing natural convection cells in this configuration. At a certain threshold, the flow tended to become unstable. It is evident that the enforcement of the existing convective cells leads to a significant enhancement in the heat transfer rates. (Hamede et al. , 2024). In the second part of the research, the experiment is set in the vertical orientation and we rotate the inner cylinder. Figure 1 shows the effect of rotation on the flow instability for $\Delta T = 10K$ ($Ra = \frac{\alpha g \Delta T d^3}{\nu \kappa} = 1.89 \times 10^5$) and $V_p = 12kV$ ($V_E = \frac{V_0}{\sqrt{\rho \nu \kappa / \varepsilon}} = 2.186 \times 10^3$), with kinematic viscosity ν, thermal diffusivity κ, density ρ and electrical permittivity ε. In the absence of rotation, when Taylor number Ta $= Re\sqrt{d/R_1} = 0$, with Re the Reynolds number and R_1 the radius of the inner cylinder, the natural convective cell is observed, indicating that the flow remains stable even in the presence of an applied electric field. However, when the inner cylinder is set to rotate, an axial flow mode emerges in the flow. It is noteworthy that this effect of rotation was not observed in the cases involving lower applied electric fields. Consequently, it can be concluded that, for specific critical values, rotation facilitates the emergence of thermo-electrohydrodynamic instability.

References

Yoshikawa, H. N., & Crumeyrolle, O., & Mutabazi, I. (2012). "Dielectrophoretic force-driven thermal convection in annular geometry", *Phys. Fluids*, **25** 024106.

Hamede, M. H., & Roller, J., & Meyer, A., & Heuveline, V., & Egbers, Ch.(2024). "Dielectrophoretic force-enhanced thermal convection within a horizontal cylindrical annulus", *Phys. of Fluids*, **36** 124106.

*Corresponding author: Hamede@b-tu.de
†Department of Aerodynamics and Fluid Mechanics, BTU Cottbus-Senftenberg, Cottbus, (Germany)
‡Engineering Mathematics and Computing Lab, Heidelberg University, Heidelberg (Germany)
§LOMC, UMR6294, CNRS-Universite´ Le Havre Normandie, Le Havre (France)

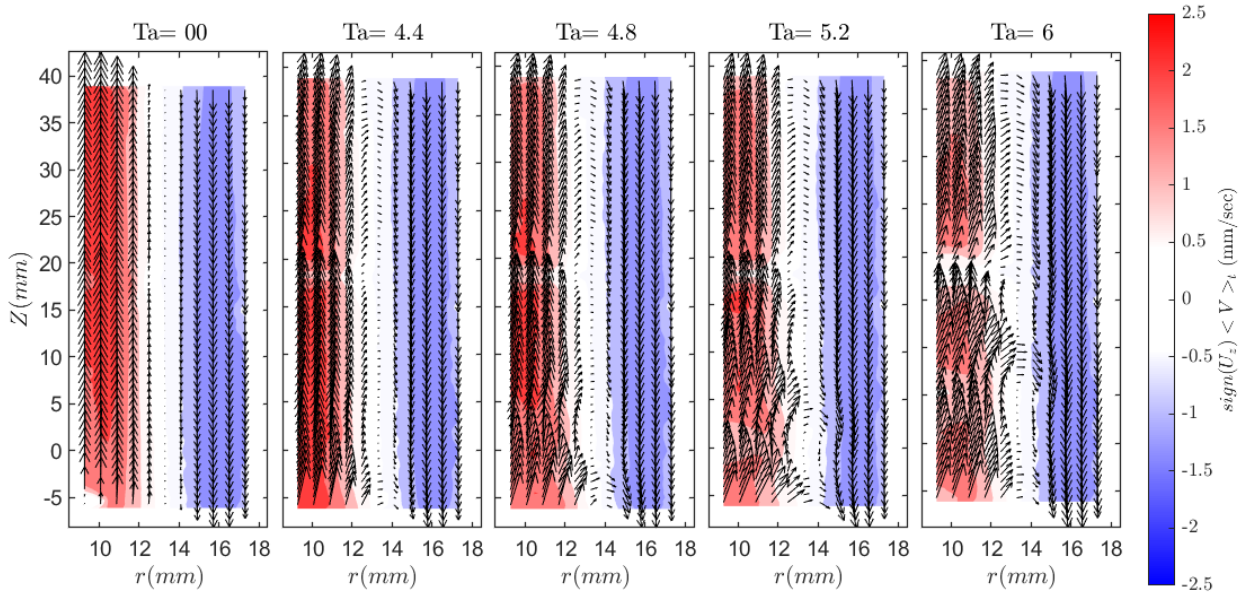

Figure 1: Flow velocity field evaluated by PIV measurements at the radial-axial plane $\Delta T = 10K$ ($Ra = 1.89 \times 10^5$) and $V_p = 12kV$ ($V_E = 2.186 \times 10^3$). The velocity field was evaluated for different cases with different Taylor number (Ta). The plots present the temporal averaged velocity magnitude multiplied by the sign of the temporal averaged axial velocity component. The superimposed arrows indicate the direction of the flow and its magnitude.

Meridional heat flux derived from the Eady model and a rotating annulus experiment: a comparison

U. Harlander*†, A. M. Mancho‡, G. Meletti§

The Eady model is an elegant and simple tool to describe the fundamental aspects of baroclinic instability (Eady, 1949). By this model, the linear dynamics of atmospheric cyclogenesis are captured qualitatively, i.e. the development or strengthening of low-pressure regions in the atmosphere. Eady waves form weather fronts that, later in the baroclinic life-cycle, occlude due to nonlinear processes. We show by comparison that the correspondence with the Eady model is very close for the differentially heated rotating annulus, a common laboratory experiment of baroclinic instability that has a broad range of applications concerning planetary atmospheres (see e.g., Agaoglou et al. (2024), Harlander et al. (2024), Meletti et al. (2025)). Using temperature and flow measurements at the surface, we focus on the radial heat flux since this flux is depth-independent according to the Eady model. First, we consider the nonlinear saturation of the flux using the spatial part of the Eady model streamfunction. Subsequently, we compare this flux with the experimental one. We discuss in detail the role of the phase shift between surface temperature and flow. Finally, we speculate about the possibility of estimating the 3D structure of oceanic vortices from surface temperature measurements alone.

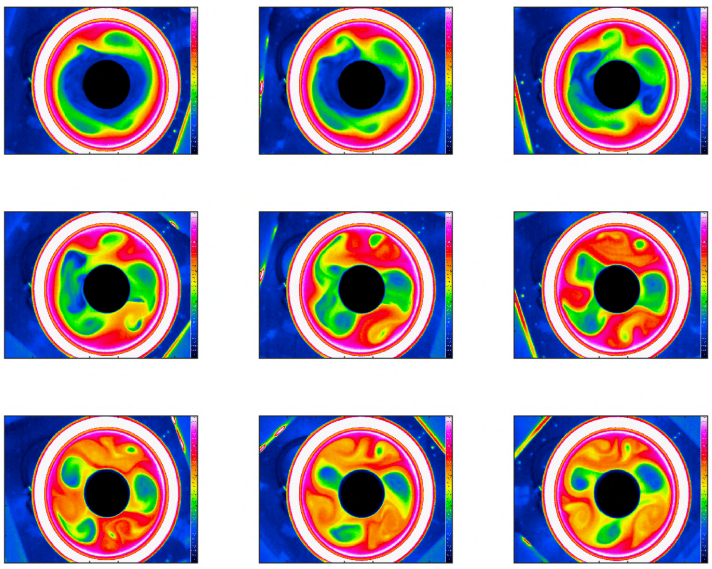

Figure 1: Original infrared image of the exponentially growing wave. Upper left: surface temperature 5.0 minutes after turning on the rotation. Bottom right: surface temperature 9.4 minutes after turning on the rotation. Each picture is 33.3 seconds apart.

*Corresponding author: haruwe@b-tu.de
†BTU Cottbus-Senftenberg, Cottbus, Germany
‡ICMAT, Consejo Superior de Investigaciones Científicas, Madrid, Spain
§Universitat Politècnica de Catalunya, Barcelona, Spain

References

Eady E. T. (1949) "Long Waves and Cyclone Waves", *Tellus*, **1** 33-52.

Agaoglou M., García-Garrido V. J., Harlander U., and Mancho A. M. (2024) "Building transport models from baroclinic wave experimental data", *Physics of Fluids*, **36** 016611.

Harlander U., Kurgansky M.V., Speer K., and Vincze M. (2024) "Baroclinic instability from an experimental perspective", *Comptes Rendus. Physique*, Online first 2024, 1-48.

Meletti G., Abide S., Harlander U., Raspo I., and Viazzo S. (2025) "On the influence of the heat transfer at the free surface of a thermally driven rotating annulus", *Physics of Fluids*, **37** 034101.

ICTW 2025 23rd INTERNATIONAL COUETTE-TAYLOR WORKSHOP 14th-16th JULY DURHAM, UK

Insights into the shear dynamics of the ice shelf ocean interface from laboratory-scale simulations

S. Hartharn-Evans*†, C. Lloyd‡, M. Carr§, A. Jenkins†

Background

The melting of Antarctic ice shelves into the ocean is a major contributor to and key uncertainty of sea level rise projections. Under Antarctic ice shelves, fresh meltwater moves upslope along the underside of the ice shelf, setting up a stratified shear flow with the warmer ocean beneath, reducing the transfer of heat between ice and the ambient ocean (figure 1 *a*). Such features are incredibly difficult to access in situ, and so most research into the transfer of heat and salt from the ocean to the ice itself has focussed on the use of larger scale numerical modelling, laboratory experiments and analytical models to understand these processes, each of which with their own assumptions, advantages and limitations.

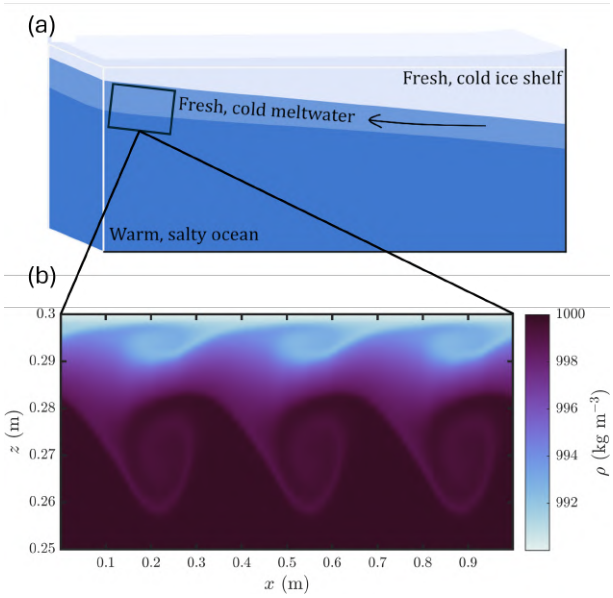

Figure 1: Schematic of (*a*) the ice shelf-ocean boundary layer, where a fresh, cold meltwater layer is formed from mixing of the warm, salty ocean and fresh, cold ice shelf. The plume propagates along the ice underside upslope. (*b*) Snapshot of the shear instability in it's fully developed overturning state, visualised as density.

This work

We present some of the first direct numerical simulations (using the spectral parallel incompressible Navier-Stokes solver, SPINS) of a small-scale idealised version of this flow where a tilted domain is forced with fixed

*Corresponding author: sam.hartharn-evans@northumbria.ac.uk
†Northumbria University, Newcastle upon Tyne, UK
‡Loughborough University, Loughborough, UK
§Newcastle University, Newcastle upon Tyne, UK

densities at the upper and lower boundary to induce such a buoyant boundary shear current. In conjunction with linear stability analysis of the profiles we identify a previously unreported mixed mode shear instability consisting of paired Kelvin Helmholtz-like instabilities above the velocity maximum and Holmboe-like instabilities (figure 1*b*) which arises due to the interaction between a stratified layer and a strong, asymmetric plane Poiseuille (channel) type shear profile (figure 2).

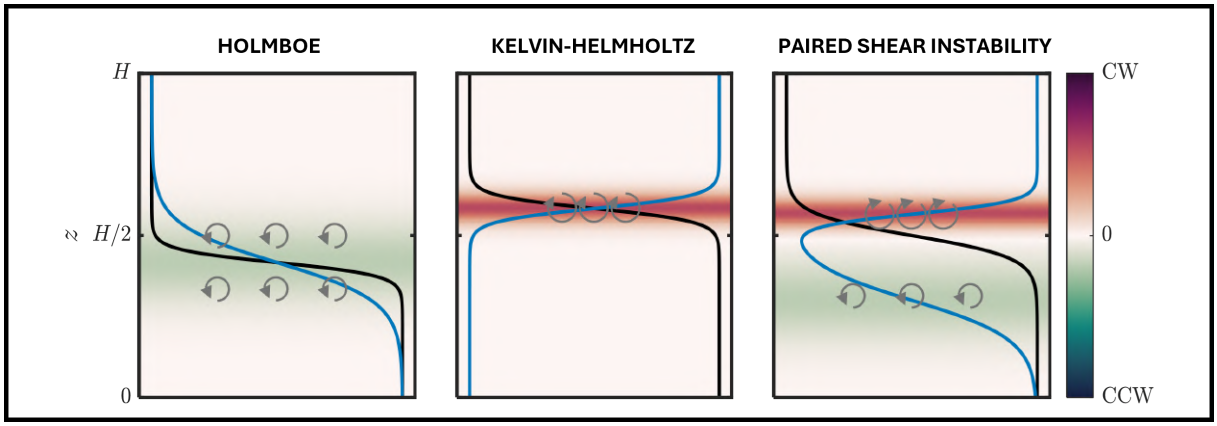

Figure 2: Schematic representation of the paired mode shear instability (*c*) that results from a combination of the Holmboe instability beneath the velocity maximum, and a Kelvin-Helmholtz instability above it. Black lines indicate idealised density profiles and blue lines indicate streamwise velocity, with vorticity shown in the background, and the resulting sense of vortex rotation indicated.

The transition to turbulence (and mixing) is characterised by both the scouring wisp features of Holmboe instability, and the overturning and secondary instability features of Kelvin-Helmholtz instability. It is unclear how well this unusual route to turbulent mixing is represented in current models, highlighting the need for further investigation into their impact on turbulent heat transfer and ice shelf melting. The restoring effect of the boundary forcing indicates a flow subject to a cyclical instability. It is unclear how well this unusual route to turbulent mixing is represented in current models, highlighting the need for further investigation into their impact on turbulent heat transfer and ice shelf melting.

Simulating Large-Scale Vortices in Low Prandtl, Rapidly Rotating Convections

R. Hinz[1] [2], C. Guervilly[2], P. Bushby [2]

Back in 2016, the magnificent cyclonic structures were discovered at the polar regions of Jupiter by NASA's Juno spacecraft. While much is known about the zonal jets of Jupiter, the origin of these polar cyclones have largely remained a mystery, despite how prominent these features are. They are vast in size, long-lived, and beautifully arranged in clusters of five and eight circumpolar vortices around a larger polar vortex. This number has not changed, aside from a small, fluctuating circumpolar vortex appearing and dissipating occasionally (Figure 2).

The goal of our study is to explain the formation and structure of these Large-Scale Vortices (LSVs), and how these interact with the convective layer of Jupiter's atmosphere. It is believed that the Jovian atmosphere has a Prandtl number (ratio of momentum diffusivity to thermal diffusivity) of around 0.01-0.1. At this value, convective flows become oscillatory, and so part of the study is to determine whether the LSVs formed are also oscillatory.

We perform 3D, periodic local box simulations to produce rapidly rotating (fixed, high Taylor number of 1e10), incompressible, low Prandtl Rayleigh-Bénard convective flows for various values of the Rayleigh number (range of 10^5-10^8), and have currently observed four regimes: stationary flows; multiple, small, "bursting" vortices; dipolar vortices; and LSVs. It is our hope to eventually introduce a magnetic friction term, designed to mimic the Lorentz force without performing a full MHD model.

We have also discovered a new regime, dubbed "bursting", which we are currently trying to ascertain the conditions when this occurs. We have found only one case so far at Pr = 0.25, Ra = 8e5, and Ta = 1e10, but work is being done to see if this effect occurs at other values (Figure 1). We believe that by pursuing this, we will discover the process behind the oscillating vortex on the south pole.

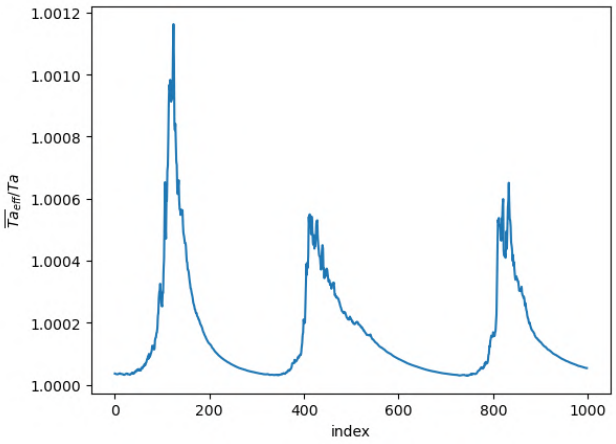

Figure 1: Time series of the mean effective Taylor number (normalised by the set Taylor number) for the oscillatory case of Pr = 0.025, Ra = 8e5, and Ta = 1e10.

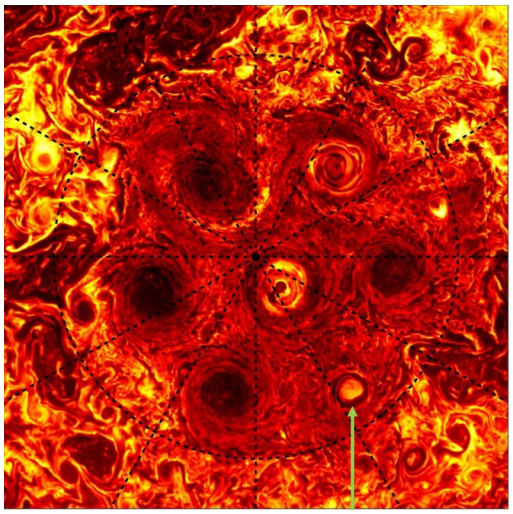

Figure 2: IR image of the southern pole of Jupiter,captured by NASA's Juno spacecraft. The green arrow points out the oscillating vortex. (Mura 2021, 2022)

[1] Corresponding author: b8063820@newcastle.ac.uk
[2] Newcastle University

References

A. Mura, A. Adriani, A. Bracco, et al. Oscillations and stability of the Jupiter polar cyclones. Geophys. Res. Lett., 48, 2021

A. Mura, P. Scarica, D. Grassi, et al. Five years of observations of the circumpolar cyclones of Jupiter. JGR Planets, 127, 2022

Melting of a vertical cylinder including salinity

Sander G. Huisman*†, Simen T. Bootsma†, Dehao Xu†, Detlef Lohse†

The accelerated melting of glaciers and ice sheets becomes an increasing concern as global warming persists. Rapid melting can lead to a weakening of global ocean currents, an increase of sea level rise, and a decrease of albedo which further amplifies global warming. Still, the physical mechanisms that govern the melting of ice are not well understood on a fundamental level (Cenedese and Straneo, 2023). Here, we perform controlled laboratory experiments in a cold room facility to enhance our understanding of the interaction between the melting dynamics of ice in saline water and the resulting natural convective flow. Specifically, we investigate the morphology evolution and melt rate of a vertical ice cylinder with varying ambient salinity (S_∞), while keeping the ambient temperature fixed at $T_\infty = 2\ ^\circ\mathrm{C}$. Due to the density anomaly of water, there exist several flow regimes for a melting vertical ice surface in water, depending on the ambient temperature and salinity (Carey and Gebhart, 1982; Josberger and Martin, 1981). For $T_\infty = 2\ ^\circ\mathrm{C}$, water is below the maximum density temperature for low ambient salinity, such that both thermal and saline buoyancy drive an upward flow. However, for $S_\infty > 10\ \mathrm{g/kg}$, thermal buoyancy acts downwards, resulting in a competition between thermal and saline buoyancy. This leads to a complex bidirectional flow that can affect the melting of an ice object in a non-trivial way (Figure 1). Overall, understanding the physics of melting in such small-scale experiments at relevant ambient conditions serves as a step toward improving predictions of future melt rates of glaciers and ice sheets.

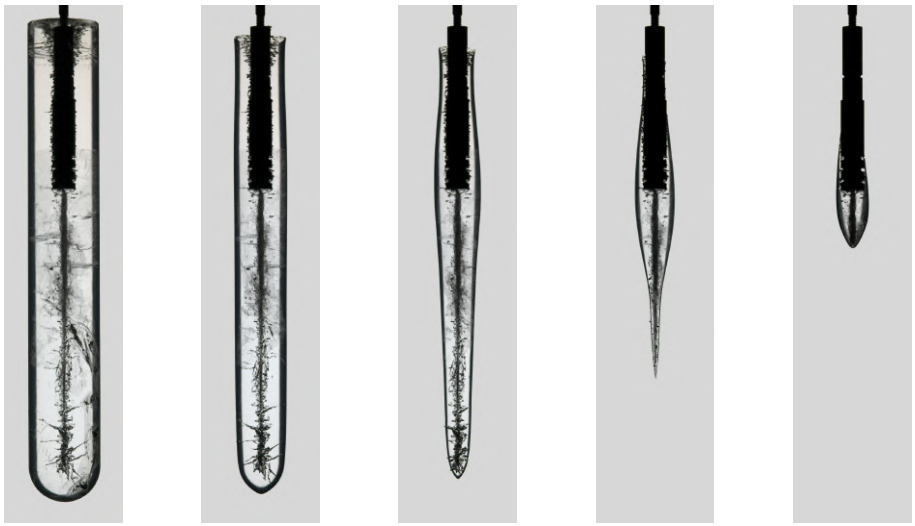

(a) $t = 0$ h (b) $t = 2$ h (c) $t = 4$ h (d) $t = 6$ h (e) $t = 8$ h

Figure 1: Evolution of a melting ice cylinder suspended vertically from a holder. The ambient temperature and salinity are $T_\infty = 2\ ^\circ\mathrm{C}$ and $S_\infty = 15\ \mathrm{g/kg}$, respectively. The initial diameter of the cylinder is $5\ \mathrm{cm}$.

References

Cenedese and Straneo, "Icebergs melting", *Annu. Rev. Fluid Mech.*, **55** 377–402.

Carey and Gebhart, "Transport near a vertical ice surface melting in saline water: experiments at low salinities", *J. Fluid Mech.*, **223** 403–423.

Josberger, "A laboratory and theoretical study of the boundary layer adjacent to a vertical melting ice wall in salt water", *J. Fluid Mech.*, **111** 439–473.

*Corresponding author: s.g.huisman@utwente.nl

†University of Twente, Enschede, Netherlands

Exact solutions and instability for geophysical waves at arbitrary latitude

D. Ionescu-Kruse*

We survey some exact solutions in the Lagrangian framework, representing waves at arbitrary latitude that propagate eastward or westward above a flow which accommodates a constant underlying background current, waves that can be both in the direction of the current and in the opposite direction. These waves are linearly unstable to short-wavelength perturbations, if their steepness exceeds a specific threshold. This threshold depends on the latitude and the strength of the underlying current.

References

[1] J. Chu, D. Ionescu-Kruse, Y. Yang, Exact solution and instability for geophysical waves at arbitrary latitude, Disc. Cont. Dyn. Syst. 39 (2019), 4399–4414.

[2] J. Chu, D. Ionescu-Kruse, Y. Yang, Exact solution and instability for geophysical waves with centripetal forces at arbitrary latitude, J. Math. Fluid Mech. 21 (2019), Art. No.: UNSP 19.

[3] D. Ionescu-Kruse, Instability of Pollard's exact solution for geophysical ocean flows, Phys. Fluids 28 (2016), 086601.

[4] D. Ionescu-Kruse, On the short-wavelength stabilities of some geophysical flows, Philos. Trans. Roy. Soc. Lond. A 376 (2018), no. 2111, 20170090, 21 pp.

*Simion Stoilow Institute of Mathematics of the Romanian Academy, Research Unit No. 6, P.O. Box 1-764, RO-014700, Bucharest, Romania; e-mail: Delia.Ionescu@imar.ro

ICTW 2025 23rd INTERNATIONAL COUETTE-TAYLOR WORKSHOP 14th-16th JULY DURHAM, UK

Supercritical Nature of Helical Magnetorotational Instability in Taylor–Couette Flow

M. Ishaq †, J. Priede*†

Abstract

The magnetorotational instability (MRI) is a mechanism by which the magnetic field can destabilize a hydrodynamically stable flow of a conducting fluid without altering its velocity distribution. This instability was first discovered theoretically in cylindrical Taylor-Couette (TC) flow of perfectly conducting fluid subject to an axial magnetic field. Extensively investigated as a feasible instability mechanism of Keplerian velocity distribution in accretion disks, the MRI is thought to be behind the formation of stars and entire galaxies on the observed timescales. This hypothesis has motivated not only numerous theoretical studies but also several attempts to reproduce the MRI in the laboratory. A major challenge to such experiments is posed by the parameter known as the magnetic Reynolds number Rm, which is required to be at least ~ 10 for the MRI to set in. For a typical liquid metal, characterized by a small magnetic Prandtl number $Pm \sim 10^{-5} - 10^{-6}$, this translates into a large hydrodynamic Reynolds number $Re = Rm/Pm \sim 10^6 - 10^7$. At such large Reynolds numbers, the flow on which the MRI is expected to develop may become turbulent due to purely hydrodynamic instabilities. A solution to this problem was suggested by Hollerbach and Rüdiger (PRL 95, 124501, 2005), who discovered that a magnetorotational-type instability can take place in cylindrical TC flow at $\mathrm{Re} \sim 10^3$ when the imposed magnetic field is helical rather than purely axial as for the standard MRI (SMRI).

So far HMRI has been studied mostly in the linear regime which is limited to sufficiently small amplitude disurbances. Not so much is known about the non-linear evolution of HMRI which in contrast to the SMRI is an inherently resistive instability. It means that HMRI is dominated by the magnetic diffusion and thus fully captured by the so-called inductionless (low-Rm) approximation which formally corresponds to $Pm = 0$. As a result, HMRI unlike SMRI affects only a limited range of hydrodynamic Reynolds numbers. Namely, besides the lower Re_c above which HMRI sets in, there is also an upper critical Reynolds number above which the flow re-stabilizes. This is due to the quadratically nonlinear inertia which starts to dominate over the linear Lorentz force in the $Pm \to 0$ limit. Besides being limited to relatively small hydrodynamic Reynolds numbers, the HMRI can destabilise only flows with sufficiently steep radial rotation profiles which, however, do not reach up the astrophysically relevant Keplerian velocity distribution.

Astrophysical relevance of HMRI critically depends on its ability to extend to subcritical parameter range. We address this question in the present study by carrying out a weakly non-linear stability analysis of HMRI. The Landau constants, which we compute using a highly accurate and efficient algorithm based on the Chebyshev collocation method, indicate that HMRI is a supercritical instability. We also compute strongly non-linear traveling-wave states which confirm the predictions of weakly non-linear analysis.

References

Hollerbach, R., & Rüdiger, G. (2005). "New Type of Magnetorotational Instability in Cylindrical Taylor–Couette Flow", *Phys. Rev. Lett.*, **95**, 124501.

*Corresponding author: aa2371@coventry.ac.uk
†Fluid and Complex Systems Research Centre, Coventry University, Coventry, UK

Interaction of Inertial Waves with Vortices in Rotating Stratified Flows

H. Kafiabad* †, J. Vanneste ‡, W. R. Young §

Anticyclonic vortices in the ocean interact with near-inertial waves, leading to modifications in both wave and vortex dynamics. On the wave side, near-inertial wave energy becomes focused and trapped within anticyclones, elevating energy levels in the vortex core (see figure 1). This process is partly explained by the presence of trapped near-inertial eigenmodes, which are readily excited by an initial wave with a horizontal scale much larger than the vortex radius. We investigate this mechanism using a reduced model of near-inertial dynamics and validate its theoretical predictions against high-resolution numerical simulations of the three-dimensional Boussinesq equations. In the linear approximation, the model predicts eigenmode frequencies, spatial structures, and a near-inertial wave energy signature characterized by an approximately time-periodic, azimuthally invariant pattern (Kafiabad et al, JPO , 2021). On the vortex side, the anticyclone undergoes modifications governed by wave-averaged geostrophic balance, where wave-induced feedback alters potential vorticity through a contribution proportional to the Laplacian of the kinetic energy density of the waves. Using direct numerical simulations of the Boussinesq equations, we quantitatively assess the ability of wave-averaged geostrophic balance theory to describe the modified vortex dynamics (Kafiabad et al, JFM , 2021).

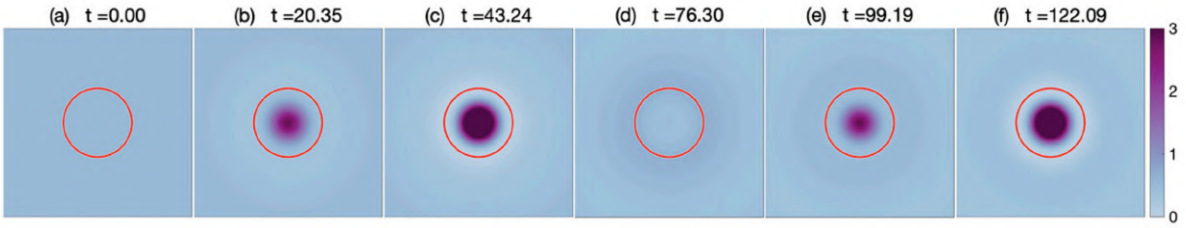

Figure 1: Horizontal slices of wave kinetic energy for a high-resolution Boussinesq simulation initialised by an inertial wave and a Gaussian vortex.

References

Kafiabad, H. A., Vanneste, J., & Young, W. R. (2021) "Interaction of near-inertial waves with an anticyclonic vortex", *Journal of Physical Oceanography*, **51.6** 2035-2048.

Kafiabad, H. A., Vanneste, J., & Young, W. R. (2021) "Wave-averaged balance: a simple example", *Journal of Fluid Mechanics*, **911** R1.

*Corresponding author: hossein.amini-kafiabad@durham.ac.uk
†Durham University, Durham, UK
‡University of Edinburgh, Durham, UK
§University of California San Diego, San Diego, US

Numerical Study of Thermomagnetic Convection in a Ferrofluid inside a Differentially Heated Taylor-Couette System

C. Kang[1 2], I. Mutabazi[3], A. Meyer[3]

Abstract

The flow stability of a ferrofluid with a radial temperature gradient and a magnetic field is investigated by a direct numerical simulation. The inner cylinder is rotating while the outer one is fixed. The inhomogeneous magnetic field created by a stack of magnets inserted inside the inner cylinder interacts with the magnetization of the ferrofluid and produces the Kelvin force. The latter contains, besides a conservative term, a nonconservative part which can be seen as a magnetic buoyancy with a corresponding magnetic gravity. The magnetic buoyancy generates a thermomagnetic convection in the cylindrical annulus at a critical value of the temperature difference. The flow is controlled by the Taylor number *Ta* that measures the intensity of the centrifugal force and the magnetic Rayleigh number Ra_m that indicates the intensity of the magnetic force. For each value of Ra_m, the instability threshold (Ta_c) is determined and compared with that predicted by the linear stability analysis (Meyer et al., 2022). Nonlinear coefficients of the Landau equation are computed to reveal the nature of the transition (supercritical or subcritical bifurcations). The momentum and heat transfer coefficients are obtained to evaluate the efficiency of the flow induced by the magnetic force in the momentum and energy transfer.

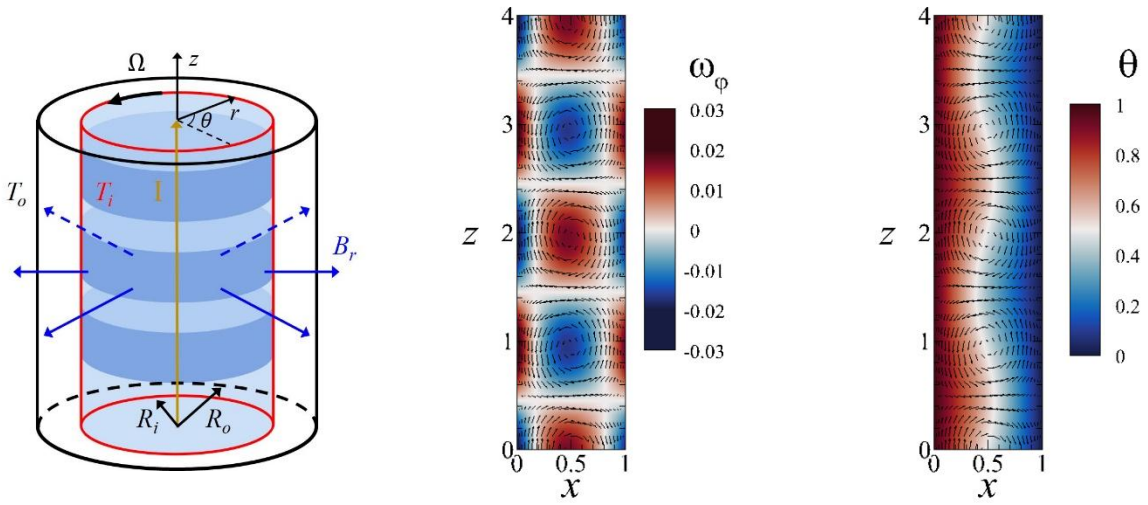

(a) (b) (c)

Figure 1: (a) Schematic representation and contours of (b) azimuthal vorticity and (c) temperature with velocity vectors on a r-z plane for *Ta* = 32 and Ra_m=1000 with *Pr* = 15.

References

Meyer, A., Hiremath, A., & Mutabazi, I. "Thermomagnetic instability of a ferrofluid in a differentially heated Taylor-Couette system", *Phys. Rev. Fluids,* 7 023901.

[1] Corresponding author: changwoo.kang@jbnu.ac.kr
[2] Jeonbuk National University, Jeonju, Republic of Korea
[3] Normandie Université, Le Havre, France

A theory to explain tropical cyclone kinetic energy spectra

Boris Galperin[*], Alexander K. Nickerson[*], Gregory P. King[†‡], Jun A. Zhang[§]

Kinetic energy spectra calculated from winds measured by research aircraft flying through tropical cyclones (TC) were found to vary with storm region and intensity Vonich and Hakim (2018). We have developed a theory to explain these variations and validated them with an observational analysis of our own.

According to the theory, the TC vortex can be thought of as a system undergoing a superposition of planetary and cyclostrophic rotations represented by an effective Coriolis parameter, $\tilde{f} = \hat{f} + f$, where $\hat{f} = 2U_{max}/R_{mw}$, R_{mw} is the radius of maximum wind, and U_{max} is the azimuthal wind speed at that radius. $\hat{f}$ far exceeds its planetary counterpart for all storms and its impact increases with storm intensity. Furthermore, for sufficiently intense storms a cyclostrophic β-effect ($\hat{\beta}$) develops in the inner core that sustains vortex Rossby waves. Horizontal turbulence in such system can be quantified by a two-dimensional anisotropic spectrum that shows a coexistence of three ranges: Kolmogorov at small scales, while at large scales spectral amplitudes are proportional to $\tilde{f}^2$ (classified as *peristrophic*), and a transverse spectrum amplitude proportional to $\hat{\beta}^2$ (classified as zonostrophic).

Our observational analysis shows that for low intensity storms, spectral amplitudes are purely peristrophic. With increasing storm intensity, the spectra change to mixed peristrophic-zonostrophic, and then to predominantly zonostrophic. The latter is akin to the flow regime harboring zonal jets on fast rotating giant planets.

References

P. T. Vonich and G. J. Hakim. Hurricane kinetic energy spectra from in situ aircraft observations. 75:2523–2532, 2018.)

*College of Marine Science, University of South Florida, 140 7th Ave S, St. Petersburg, Florida, USA 33701
†Corresponding author: gkinglisboa@gmail.com
‡Independent Scholar, 5 Kilncroft, Selkirk TD7 5AQ, Scottish Borders, UK
§National Oceanic and Atmospheric Administration, Atlantic Oceanographic and Meteorological Laboratory, Hurricane Research Division, 4301 Rickenbacker Causeway, Miami, Florida, USA 33149

Local monotonic and oscillatory instabilities in differentially heated visco-diffusive swirling flows

O.N. Kirillov*†, I. Mutabazi‡

Hydrodynamic modeling describes swirling flows as arising from the combined effects of rotation and shear in two orthogonal directions. The base state of these flows consists of azimuthal and axial velocity components, occurring in either confined geometries (common in engineering applications) or open geometries (typical of natural phenomena), see Figure 1. The stability of swirling flows and their transition to turbulence pose a significant scientific challenge, especially when factors like temperature gradients, stratification, or electromagnetic fields are involved. In this talk, based on the works (Kirillov, 2025; Kirillov & Mutabazi, 2025, 2024, 2017), we focus on the instabilities of swirling flows with a radial temperature gradient, crucial in industrial processes like combustion (Candel et al, 2014) and natural phenomena like tropical cyclones (Emanuel, 2018), tornadoes, and astrophysical flows (Tziotziou et al., 2023).

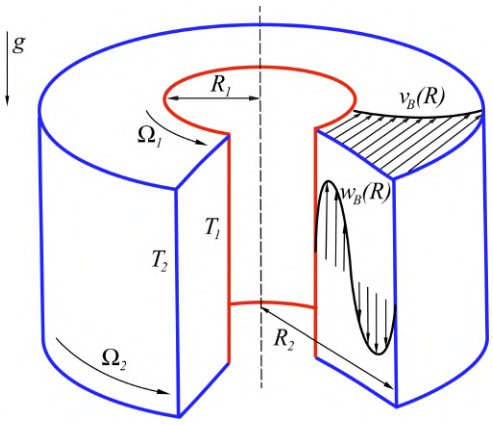

Figure 1: The helical base state (Baroclinic Couette Flow, BCF) as a superposition of the circular Couette flow $v_B(R)$ and an axial annular flow $w_B(R)$ in a differentially heated cylindrical annulus.

Adapting local geometrical optics stability analysis (Kirillov, 2025) to visco-thermodiffusive swirling flows with a radial temperature gradient, we found both monotonic instability—combining the Ludwieg-Eckhoff-Leibovich-Stewartson (LELS) (Leibovich and Stewartson, 1983) and Goldreich-Schubert-Fricke (GSF) instabilities (Kirillov & Mutabazi, 2024)—and a visco-thermodiffusive oscillatory instability (Kirillov & Mutabazi, 2025), Figure 2. The latter extends the McIntyre instability (McIntyre, 1970), previously known only in purely azimuthal rotating flows, to swirling flows. We derived a novel analytical instability criterion for non-isothermal visco-thermodiffusive swirling flows, unifying the LELS and GSF criteria, and developed an algorithm to predict whether oscillatory or stationary instability dominates, depending on parameters like the Prandtl number (Pr), axial Grashof number (Gr), and azimuthal Reynolds number (Re). The theory is applied to the helical base flow of an incompressible visco-thermodiffusive fluid in a differentially rotating vertical cylindrical annulus with radial temperature gradient and natural gravity—Baroclinic Couette Flow, Figures 1 and 2.

References

Kirillov, O.N. (2025) "Geometrical optics stability analysis of rotating visco-diffusive flows", *Mathematics*, **13** 382.

Kirillov, O.N. & Mutabazi, I. (2025) "Instabilities in visco-thermodiffusive swirling flows", *J. Fluid Mech.*, **subm**, arXiv:2502.00773v1.

*Corresponding author: oleg.kirillov@northumbria.ac.uk
†Department of Mathematics, Physics, and Electrical Engineering, Northumbria University, Newcastle upon Tyne, UK
‡LOMC UMR-6294 CNRS, Université Le Havre Normandie, Normandie Université, Le Havre, France

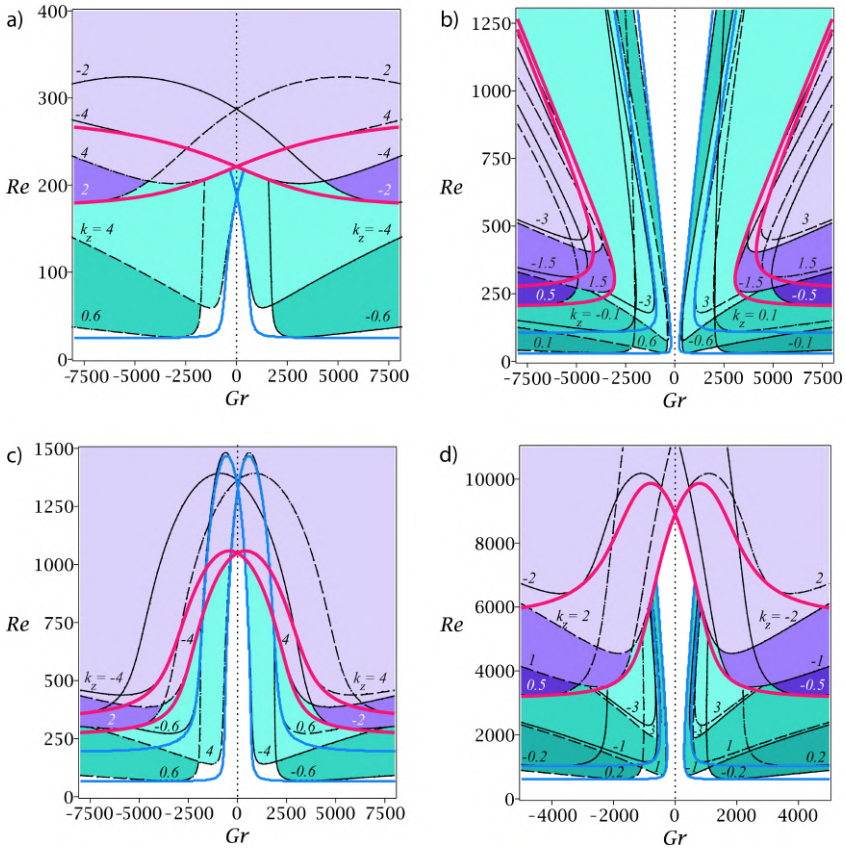

Figure 2: Green-shaded regions represent stationary (LELS-GSF) instability domains touching the thick blue envelope, while purple-shaded regions above them correspond to oscillatory (McIntyre) instability domains touching the thick red envelope. Dashed black lines indicate neutral stability curves for axial wavenumbers $k_z > 0$, and solid black lines indicate neutral stability curves for $k_z < 0$. (a) Rayleigh-unstable BCF ($\eta = 0.8$, $\mu = 0$) with radial wavenumber $k_r = 4\sqrt{2}$, Prandtl number $Pr = 5.5$, outward heating ($\gamma = 0.0004$), and $k_z = \pm 0.6, \pm 2, \pm 4$; (b) Rayleigh-stable BCF ($\eta = 0.8$, $\mu = 0.8$) with $k_r = 3\sqrt{2}$, $Pr = 5.5$, $\gamma = 0.01$, and $k_z = \pm 0.1, \pm 0.5, \pm 0.6, \pm 1.5, \pm 3$; (c) Rayleigh-unstable BCF ($\eta = 0.8$, $\mu = 0.62$) with $k_r = 4\sqrt{2}$, $Pr = 4$, $\gamma = 0.01$, and $k_z = \pm 0.6, \pm 2, \pm 4$; (d) Rayleigh-stable BCF with a quasi-Keplerian azimuthal velocity profile ($\eta = 0.99$, $\mu = \eta^{3/2}$), $k_r = 2\sqrt{2}$, $Pr = 0.5$, inward heating ($\gamma = -0.01$), and $k_z = \pm 0.2, \pm 0.5, \pm 1, \pm 2, \pm 3$. Here $\gamma = \alpha(T_1 - T_2)$, where α is the thermal expansion coefficient, T_1 and T_2 are the temperatures of the inner and outer cylinders, $\eta = \frac{R_1}{R_2}$, and $\mu = \frac{\Omega_2}{\Omega_1}$, where R_1, Ω_1 and R_2, Ω_2 are the radius and the angular velocity of the inner and outer cylinder, respectively (Kirillov & Mutabazi, 2025).

Kirillov, O.N. & Mutabazi, I. (2024) "Unification theory of instabilities of visco-diffusive swirling flows", *Phys. Rev. Fluids*, **9** 124802.

Kirillov, O.N. & Mutabazi, I. (2017) "Short wavelength local instabilities of a circular Couette flow with radial temperature gradient", *J. Fluid Mech.*, **818** 319–343.

Candel, S., Durox, D., Schuller, T., Bourgouin, J.-F., Moeck, J.P. (2014) "Dynamics of swirling flames", *Ann. Rev. Fluid Mech.*, **46** 147–173.

Emanuel, K.A. (2018) "100 Years of Progress in Tropical Cyclone Research", *Meteorological Monographs* **59**, pp. 15.1–15.68 American Meteorological Society.

Tziotziou, K., Scullion, E., Shelyag, S. et al. (2023) "Vortex motions in the solar atmosphere", *Space Sci. Rev.* **219** 1.

Leibovich, S. & Stewartson, K. (1983) "A sufficient condition for the instability of columnar vortices", *J. Fluid Mech.* **126** 335–356.

McIntyre, M.E. (1970) "Diffusive destabilisation of the baroclinic circular vortex", *Geophys. Fluid Dyn.*, **1**(1–2) 19–57.

Emergence of triplet streaks near the inner wall in MHD turbulent Taylor-Couette flow with end walls

H. Kobayashi[1 2], T. Hasebe[3], K. Namba[3], T. Fujino[3], H. Takana[4],

Abstract:

We numerically investigate the influence of magnetohydrodynamic (MHD) interaction on near-wall turbulence in Taylor-Couette (TC) flow. A liquid metal is assumed as a working fluid and is confined in a container covered by the inner, outer, top, and bottom walls. This configuration has been examined for the MHD control of rotational speed of wind turbine shaft (Takana and Tanida 2017, Hasebe et al. 2023). The rotating shaft is connected to the inner cylinder, and the liquid metal surrounds the inner cylinder. The inner cylinder wall rotates, and the other walls are at rest. The magnetic field is applied in the axial direction. The Lorenz force acts against the flow and suppresses the turbulence (Kobayashi et al. 2021). The Hartmann number is defined by the ratio of the Lorentz force to the viscous force and expresses the strength of the MHD interaction.

Incompressible MHD flows are considered. The governing equations consist of the continuity equation, the Navier-Stokes equations with Lorentz force, the Maxwell equations at low magnetic Reynolds number, and the generalized Ohm's law. The second-order Adams-Bashforth method and a second-order central finite difference method are used for time matching and spatial discretization, respectively. The SMAC scheme is utilized for coupling between velocity and pressure. The Poisson equations for pressure and electric potential are solved by using a Bi-CGSTAB method. We conduct a large-eddy simulation, and the subgrid-scale stress tensor is modeled by the coherent structure model (Kobayashi 2005), which can predict the laminarization by the Lorentz force and is suitable for the MHD flows. The computational domain in the azimuthal direction is set to 2π. The aspect ratio in the *r*-*z* cross-section is set to 1.0, and the radius ratio η is set to 0.5. The Hartmann number Ha is proportional to the magnetic flux density. The periodic boundary condition is used in the azimuthal direction, and no-slip boundary conditions are applied to the top, bottom, inner, and outer walls. All walls are assumed to the insulating walls.

Figure 1 shows the instantaneous azimuthal and radial velocity distributions for Reynolds number Re=8000 at Ha=0, 70, and 100 near the inner wall. High- and low-speed streaks are seen in Fig. 1(a), left, and are produced by a pair of vortices with inflow and outflow as shown in Fig. 1(a), right. At Ha=70, fine streaks near the top and bottom walls are suppressed by the Lorentz force. At Ha=100, those fine streaks are completely suppressed, and high-speed spiral streaks coming from the top and bottom walls are observed. We can understand that two types of streaks exist in the TC flow in a container at Ha=0 of Fig. 1(a). One is a fine streak generated by Görtler vortices, and the other is a high-speed spiral streak coming from the corner between inner and top (or bottom) walls (Kobayashi et al. 2025). As seen in Fig. 1(c), the triplet high-speed streak composed of two spiral streaks and the centerline streak is a good marker to understand the criterion of MHD interaction. We investigate what determines the criterion hereafter.

Figure 2 exhibits the instantaneous azimuthal and radial velocity distributions at Re=5000 and Ha=62.5, Re=8000 and Ha=100, and Re=10000 and Ha=125 near the inner wall. We can observe the triplet streaks for all the figures, although the width of the streak becomes finer for higher Reynolds numbers. The criterion where the triplet steaks are generated is defined as $Hr = Ha/Re \times 10^3 = 12.5$. Therefore, we can conclude that the criterion of MHD interaction is expressed by Hr for the MHD turbulent state near the inner wall.

We will present and discuss the effect of the radius ratio on MHD interaction and streaks at the conference. This effect is particularly interesting when considering centrifugal instability. The above criterion is modified using Taylor number Ta as follows: $Ht = Ha/Ta^{1/2} \times 10^3 = 12.5$, where $Ta = Re^2(1/\eta - 1)$.

[1] Corresponding author: hkobayas@keio.jp
[2] Keio University, Yokohama, Japan
[3] University of Tsukuba, Tsukuba, Japan
[4] Tohoku University, Sendai, Japan

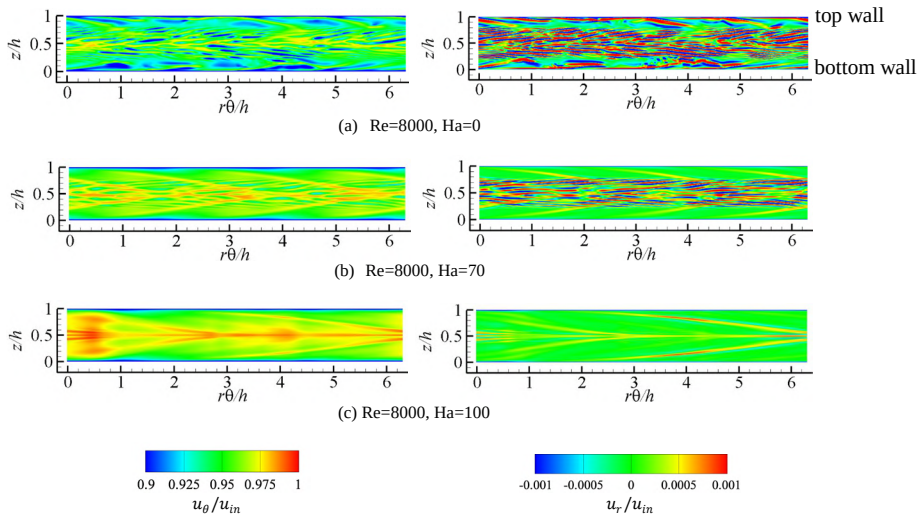

Figure 1: Instantaneous azimuthal (left) and radial velocity (right) distributions for Re=8000 at (a) Ha=0, (b) Ha=70, and (c) Ha=100 in the vicinity of the inner wall.

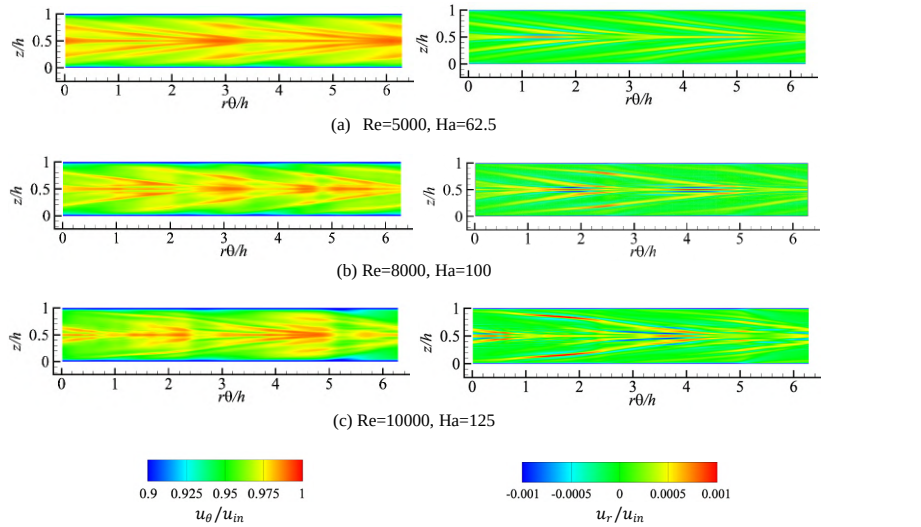

Figure 2: Instantaneous azimuthal (left) and radial velocity (right) distributions at (a) Re=5000 and Ha=62.5, (b) Re=8000 and Ha=100, and (c) Re=10000 and Ha=125 in the vicinity of the inner wall.

References

Hasebe, T., Sasaki, R., Fujino, T., Takana, H., & Kobayashi, H. (2023) "Experimental and theoretical analyses on power generation characteristics of co-axial MHD energy conversion device", *Electr. Eng. Jpn.*, **216** e23446.

Kobayashi, H. (2005) "The subgrid-scale models based on coherent structures for rotating homogeneous turbulence and turbulent channel flow", *Phys. Fluids*, **17** 045104.

Kobayashi, H., Shionoya, H., & Okuno, Y. (2012) "Turbulent duct flows in a liquid metal magnetohydrodynamic power generator", *J. Fluid Mech.*, **713** 243-270.

Kobayashi, H., Hasebe, T., Fujino, T., & Takana, H. (2025) "Turbulent Taylor–Couette flow with magnetohydrodynamic interaction in axial magnetic field", *Phys. Fluids*, **37** 027165.

Takana, H., & A. Tanida, A. (2017) "Development and fundamental characteristics of co-axial MHD energy conversion device", *Mech. Eng. J.*, **4** 16-00500.

Mean Flow Generation in Rotating Spherical Layers Under Colored Noise

O. Krivonosova[1], M. Gritsevich[2], D. Zhilenko[1]

The presence of random fluctuations over time is a fundamental characteristic of most natural processes and systems. Random variations in rotational velocity can be considered external noise that influences large-scale flows in both the atmosphere and the Earth's liquid core. In this study we numerically investigate how noise alters flow intensity, focusing on axisymmetric flows of viscous, incompressible fluid in spherical layers, where the boundaries rotate with equal angular velocities. Building on previous experiments (Zhilenko et al., 2018), random fluctuations with zero mean value are introduced into the otherwise constant rotation velocity of the inner sphere, thereby incorporating noise into the flow. Calculations were conducted for layers with relative thicknesses $\delta = 1$ and $\delta = 1.76$, and Reynolds numbers Re = 2000 and Re = 4000, based on the outer boundary parameters. Two types of noise were considered: $\alpha = 0.1$ and $\alpha = 1$, where α defines the slope of the noise spectrum $1/f^{\alpha}$. The results demonstrate that increasing the noise amplitude, N, leads to an increase in the time-averaged values of the azimuthal and meridional components of flow kinetic energy. This effect was previously observed when adding white noise (Krivonosova et al., 2023). In this study, for all noise spectra, relative thicknesses, and Reynolds numbers analyzed, we found that at equivalent noise amplitudes, the relative increase in the meridional kinetic energy component is several orders of magnitude higher than that of the azimuthal component. Conversely, the opposite trend is observed for the root mean square (RMS) deviations of kinetic energy components: the increase in RMS deviations of the azimuthal component is several orders of magnitude higher than that of the meridional component at equivalent noise amplitudes. We demonstrate that relative flow parameters—including frictional moments on the outer sphere, fluctuations, and mean values of the azimuthal and meridional kinetic energy components—follow power-law relationships with respect to the noise amplitude, N. All exponents fall within the range of 1 to 2. Moreover, this scaling appears to be independent of δ, the Reynolds number, and the noise spectrum type. A simplified analytical model qualitatively aligns with the numerical results, indicating that the slope of the noise spectrum does not affect the nature of energy component variations. We hypothesize that this power-law scaling of flow parameters with noise amplitude will extend beyond colored noise to periodic fluctuations in rotational velocity. Future research could focus on investigating this hypothesis.

We sincerely thank Peter Read for valuable discussions and insightful comments, which contributed to the development of this work.

References

Zhilenko, D., Krivonosova, O., Gritsevich, M., and Read, P. (2018). "Wave number selection in the presence of noise: Experimental results", *Chaos* 28, 053110; doi: 10.1063/1.5011349

Krivonosova, O., Gritsevich, M., Zhilenko, D., and Read, P. (2023). "Noise induced effects in the axisymmetric spherical Couette flow", *Phil. Trans. Roy. Soc. A,* 381: 20220124; doi: 10.1098/rsta.2022.0124

[1] Corresponding author at the Institute of Mechanics, Lomonosov Moscow State University: olga@imec.msu.ru
[2] University of Helsinki, Gustaf Hällströmin katu 2a, P.O. Box 64, FI-00014 Helsinki, Finland

Stability of a material interface in a two-phase system with a free surface

J. Labarbe*†

The well-known Rayleigh–Taylor instability describes the stability of an interface between two liquids of distinct densities but without surface properties (Rayleigh, 1883; Taylor, 1950; Chandrasekhar, 1961). Although the classical stability criterion for inviscid motionless layers is well-known, it still remains unknown whether the interface can be excited when coupled to an external forcing (e.g. a second moving interface). It has recently been demonstrated that the Rayleigh–Taylor phenomenon can be inhibited if the interface is allowed to slip along the side walls of the domain and if surface tension is strong enough (Wilke, 2022). On the contrary, interfacial instability has been established in the context of hydrochemical dynamics when considering surface tension gradients and viscosity (Ibanez and Velarde, 1977). More generally in most studies involving fluid interfaces, the surface rheology is often neglected on account of its small density. Nevertheless, in practice, there are several applications that necessitate the rheological behaviour of the interface in order to accurately model the dynamics of two-phase flows. To allow for such effects to be considered, a general mathematical description of the physics at the interface is required. For this reason, local formulations of jump conditions across a Newtonian interface have been derived within the most general context (Scriven, 1960; Delhaye, 1974). However, considering a two-phase system when the two layers are not semi-infinite is notoriously difficult to study (Sternling and Scriven, 1959).

This study examines the stability of a motionless two-phase fluid layer when the interface incorporates surface properties and interacts with a free surface located above. We introduce the exact jump conditions at the interface (the so-called Boussinesq–Scriven conditions, cf. Scriven (1960); Delhaye (1974)) and we solve the associated boundary eigenvalue problem by means of analytical and numerical methods. The spectral analysis demonstrates the onset of a new interfacial instability when the free surface and the material properties of the interface are present simultaneously. Remarkably, this instability takes place within the domain of stability of the Rayleigh–Taylor mechanism, i.e. when the acceleration due to gravity acts from the lighter to the heavier fluid (Rayleigh, 1883; Taylor, 1950; Chandrasekhar, 1961).

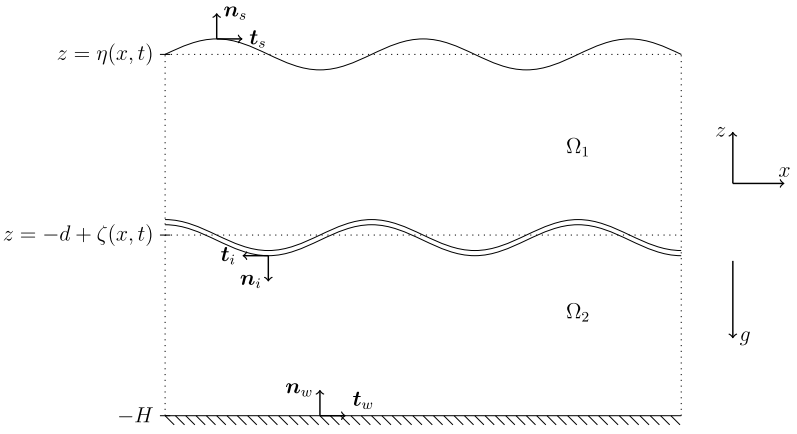

Figure 1: Sketch of a two-phase system with a material interface enclosed by two viscous fluid layers while a free surface is located above. The system is not represented at rest intentionally to highlight the presence of interfacial instability.

*Corresponding author: joris.LABARBE@univ-cotedazur.fr
†Laboratoire J. A. Dieudonné, Nice, France

References

Wilke, M. 2022 On the Rayleigh–Taylor instability for the two-phase Navier–Stokes equa- tions in cylindrical domains. Interfaces Free Bound. 24 (4), 487–531.

Taylor, G. I. 1950 The instability of liquid surfaces when accelerated in a direction perpen- dicular to their planes. I. Proc. R. Soc. Lond. A 201 (1065), 192–196.

Rayleigh, Lord 1883 Investigation of the character of the equilibrium of an incompressible heavy fluid of variable density. Proc. London Math. Soc. 14, 170–177.

Chandrasekhar, S. 1961 Hydrodynamic and Hydromagnetic Stability. Oxford: Clarendon Press.

Ibanez, J. L. & Velarde, M. G. 1977 Hydrochemical stability of an interface between two immiscible liquids: the role of Langmuir–Hinshelwood saturation law. J. Phys. 38 (12), 1479–1483.

Scriven, L. E. 1960 Dynamics of a fluid interface equation of motion for Newtonian surface fluids. Chem. Eng. Sci. 12 (2), 98–108.

Delhaye, J. M. 1974 Jump conditions and entropy sources in two-phase systems. Local instant formulation. Int. J. Multiph. Flow 1 (3), 395–409.

Sternling, C. A. & Scriven, L. E. 1959 Interfacial turbulence: hydrodynamic instability and the Marangoni effect. AICHE J. 5 (4), 514–523.

Taylor-Couette flow of complex suspensions: particle-polymer interactions, instability and mixing

T. Lacassagne*†, C. Carré †, M. Moazzen †, S.A. Bahrani †

Suspensions of solid particles in Newtonian or non-Newtonian liquids are ubiquitous in nature and industrial processes. These fluids exhibit a wide range of nonlinear dynamics, driven by inertia or the complex rheology of the suspending phase, complicating the control of their stability, mixing, and heat transfer, as well as the prediction of process performance.
In this context, recent studies have illustrated and revived the potential of the canonical Taylor-Couette flow for investigating hydrodynamic instabilities and the dynamics of complex fluids, including viscoelastic and elasto-inertial flows (Boulafentis et al., 2023; Song et al., 2023) and non-colloidal particle suspension flows (Baroudi et al., 2023). In this contribution, we use Taylor-Couette flow to combine those two complexity factors and explore the dynamics of complex suspensions composed of (mostly non-colloidal) particles in non-Newtonian viscoelastic base fluids. Direct visualization of the flow structure (figure 1, central part) is combined with torque measurements on the rotating inner cylinder (the outer one being stationary) to identify transitions to inertial or elasto-inertial regimes and to characterize the associated friction dynamics.

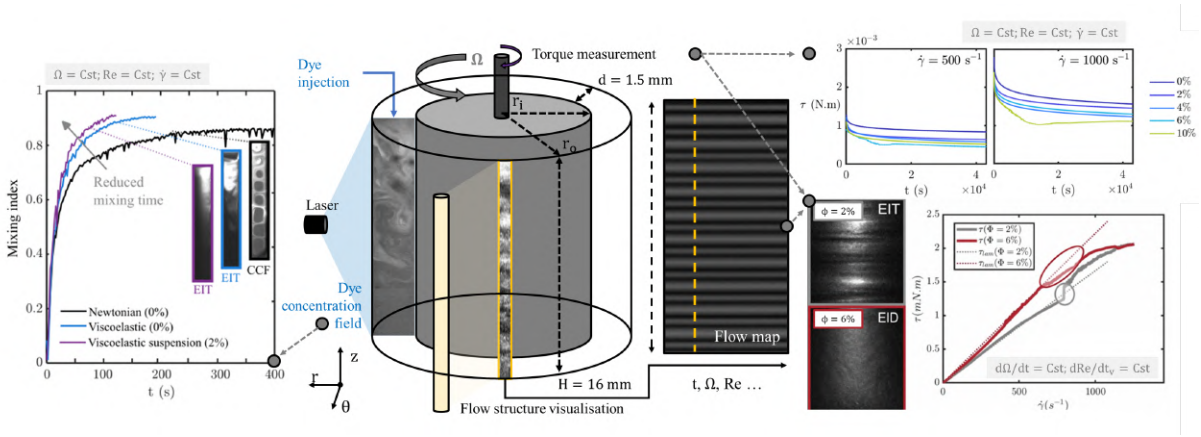

Figure 1: Taylor-Couette flow of complex suspensions: detection of elasto-inertial transitions using flow visualization and torque measurement (center and bottom right), quantification of polymer degradation (top right), and laser induced fluorescence measurement of mixing times (left).

As initially suggested in (Lacassagne et al., 2021), a notable observation is that at low particle volume fractions (dilute regime), particle addition promotes earlier onset of instabilities and transition to elasto-inertial turbulence (EIT) in terms of control parameters (Reynolds or Weissenberg numbers). However, this trend reverses in the semi-dilute regime, where particles either stabilize the flow (Lacassagne et al., 2021) or completely suppress EIT (Carré et al., 2024).
An elasto-inertial dissipation (EID - figure 1, bottom right part) mechanism is uncovered (Carré et al., 2024), and its physical origin is discussed here through the lens of local particle-polymer interactions. These interactions may be reversible or lead to irreversible polymer degradation, both strongly promoted by inter-particle contacts at sufficient particle concentrations. To probe this latter mechanism, the degradation rate of particle-laden viscoelastic fluids is systematically measured as a function of particle volume fraction and shear rate, revealing that polymer degradation is indeed enhanced in the semi-dilute regime (figure 1, top right).

*Corresponding author: tom.lacassagne@imt-nord-europe.fr
†IMT Nord Europe, Institut Mines Télécom, Univ. Lille, Center for Energy and Environment, F-59000 Lille, France

Finally, laser-induced fluorescence measurements are conducted to visualize passive scalar transport and quantify mixing times across various complex suspensions and flow regimes (figure 1, left part). This approach enables assessment of the potential of such complex suspensions for mixing and conducto-convective transfer intensification, in comparison with suspensions of colloidal or non-colloidal particles in Newtonian solvents and with particle-free viscoelastic fluids, opening prospects for the formulation of innovative heat transfer fluids.

References

Boulafentis, T., Lacassagne, T., Cagney, N. & Balabani, S. (2023) "Experimental insights into elasto-inertial transitions in Taylor–Couette flows", *Phil. Trans. Roy. Soc. A.*, **381**, 2243.

Song, J., Zhu, Y., Lin, F., Liu, N. & Khomami, B. (2023) "Turbulent Taylor–Couette flow of dilute polymeric solutions: a 10-year retrospective", *Phil. Trans. Roy. Soc. A.*, **381**, 2243.

Baroudi, L., Majji, M. V., Peluso, S. & Morris, J. F. (2023) "Taylor–Couette flow of hard-sphere suspensions: overview of current understanding", *Phil. Trans. Roy. Soc. A.*, **381**, 2243.

Lacassagne, T., Boulafentis, T., Cagney, N. & Balabani, S. (2021) "Modulation of elasto-inertial transitions in Taylor–Couette flow by small particles", *J. Fluid. Mech.*, **929** R2.

Carré, C., Moazzen, M., Lacassagne, & Bahrani, S.A. (2024) "Elasto-inertial dissipation in particle-laden viscoelastic Taylor–Couette flow", *J. Fluid. Mech.*, **997** A19.

Macroscopic pilot-wave dynamics in density-stratified fluids

P. Le Gal*†, S. Gsell†

Inspired by bouncing drop experiments that revealed how macroscopic systems can exhibit wave-particle properties previously thought to be exclusive to quantum systems (see Couder et al. (2005), Fort et al. (2006), Bush (2015)), we introduce here a new wave-particle system based on internal gravity waves propagating in density-stratified fluids. Recent experiments by Le Gal et al. (2022) on particles (called ludions) oscillating in such a fluid medium suggest that wave-particle interactions can induce symmetry breaking, leading to spontaneous self-propulsion of the particle in the horizontal plane. Here we use direct two-dimensional lattice Boltzmann / immersed-boundary simulations (see Gsell et al. (2020)) to decipher the wave-particle interactions underlying this dynamics. Figure 1 illustrates the self-propulsion of the ludion wrapped in its inernal wave field.

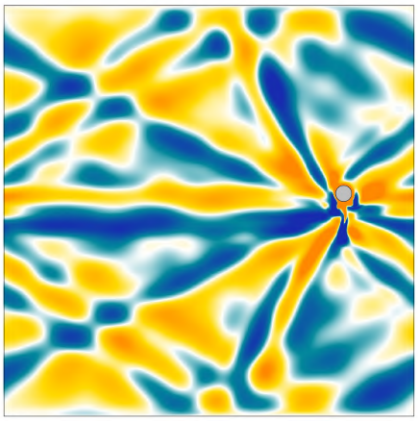

Figure 1: Snapshot from a numerical simulation using the Lattice Boltzmann Method of a self-propelled ludion (here towards the right) in a density-stratified fluid domain (here in a 2D periodic domain with a vertical oscillation frequency half the Buoyancy frequency: $\omega/N = 0.5$).

To explain this propulsion, we propose a minimal hydrodynamic theory showing that this instability can be explained by a Doppler force emerging from interactions between the ludion and its own wave field. We demonstrate that the Doppler effect breaks the forward/backward symmetry of the system by modifying the angles of the internal gravity wave vectors and thus leads to the ludion self-propulsion. We validate our theoretical predictions using direct numerical simulations and new experiments which confirm the predicted effect and show that the growth of the instability is determined by the particle oscillation amplitude.

In wall-bounded domains, the reflected internal waves react back on the ludion creating a radiative force on it. We have measured this force at different positions of the ludion along the horizontal axis and we show that a Casimir-like potential rapidly develops and constrains the particle motion as can be seen on figure 2.

Despite the presence of the Doppler force, the Casimir-like potential governs the ludion long-term dynamics, leading to capture the ludion in fixed points for the simplest cases (see Figure 3-a) or chaotic attractors (see Figure 3-b) near the potential wells (see Figure 2).

Our findings establish the ludion as a novel hydrodynamic pilot-wave system, offering a new platform for exploring macroscopic wave-particle duality, particularly in three-dimensional configurations to be explored in the future.

*Corresponding author: patrice.LE-GAL@univ-amu.fr
†Aix Marseille Univ., CNRS, Centrale Med., Marseille, France

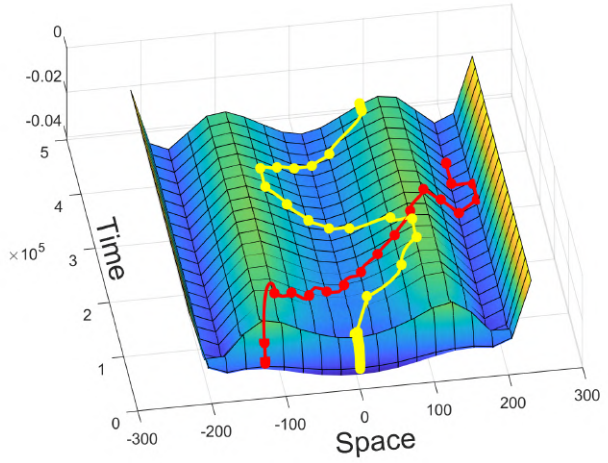

Figure 2: In a bounded domain, the waves reflect off the walls and create a Casimir-like potential (here for $\omega/N = 0.5$) capable of trapping the ludion, regardless of its original location along the horizontal direction.

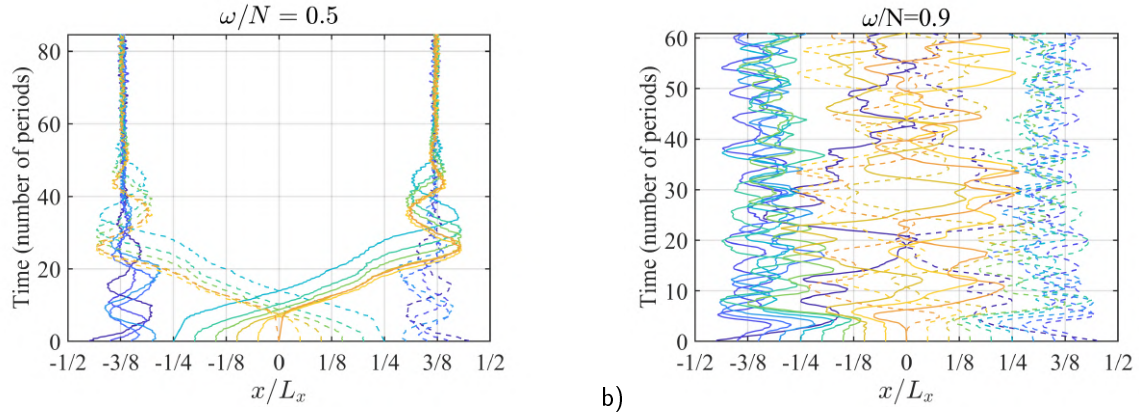

a) b)

Figure 3: Some trajectories of the ludion self-propelled by its own internal gravity waves and trapped by the Casimir-like potential generated by the wave reflections on the distant walls. The Reynolds number based on the vertical oscillations is $Re = 25$ and the ratio of the forcing frequency to the Brunt–Väisälä frequency is $\omega/N = 0.5$ in a) and $\omega/N = 0.9$ in b).

References

Y. Couder, S. Protière, E. Fort and A. Boudaoud.(2005). "Walking and orbiting droplets", *Nature*, **437**, 208.

Y. Couder and E. Fort. (2006). "Single-particle diffraction and interference at a macroscopic scale",*Phys. Rev. Lett.*, **97**,154101.

J. W. M. Bush. (2015). " Pilot-wave hydrodynamics", *Ann. Rev. Fluid Mech.*, **47**, 269.

P. Le Gal, B. Morales Castillo, S. Hernandez-Zapata and G. Ruiz Chavarria, G. (2022). "Swimming of a ludion in a stratified sea", *J. Fluid Mech.*, **931**, A14.

S. Gsell, U. D'Ortona and J. Favier. (2020). "xplicit and viscosity-independent immersed-boundary scheme for the lattice Boltzmann method", *Phys. Rev. E*, **101**, 023309.

Turbulent zonal jets interacting with local topography: an experimental study

D. Lemasquerier*†, C. David‡, R. Monville‡, J. Aurnou‡

Zonal jets are coherent east-west winds or currents observed –or expected to emerge– in many planetary fluid layers, from the Earth's oceans and atmosphere, to the atmospheres of gas giants, the subsurface oceans of icy moons and the liquid metallic cores of telluric planets. In many of these systems, zonal jets interact with a solid boundary with topography: the bathymetry in Earth's oceans is known to influence the dynamics of the Antarctic Circumpolar Current, flows in liquid cores interact with the topography at the Core-Mantle boundary, and icy moon oceans are in direct contact with a global ice crust of spatially varying thickness.

In this talk, I will present laboratory experiments to study the interaction between turbulent zonal jets and a local topography. We use the Coreaboloid device at UCLA(Lonner et al., 2022) to robustly produce turbulent zonal jets. The setup is a 75cm-diameter water tank rotating at speeds up to 72 revolutions per minute. The deflection of the free surface due to the fast rotation provides a strong topographic β-effect. The flow is forced by thermal convection, driven by starting the experiment with hot water, and cooling the inner cylinder with a block of ice. To simulate a local topography, we attach acrylic disks of different radii and heights on the bottom plate. We visualise the flow using 1) a thermal infrared camera to image the temperature field at the free surface 2) particle image velocimetry (PIV) on a horizontal laser plane and 3) ultrasonic doppler velocimetry (UDV) along three chords. Preliminary results show the formation of stationary Rossby waves downstream of the topography (Figure 1), that feed back on the amplitude, number and position of zonal jets.

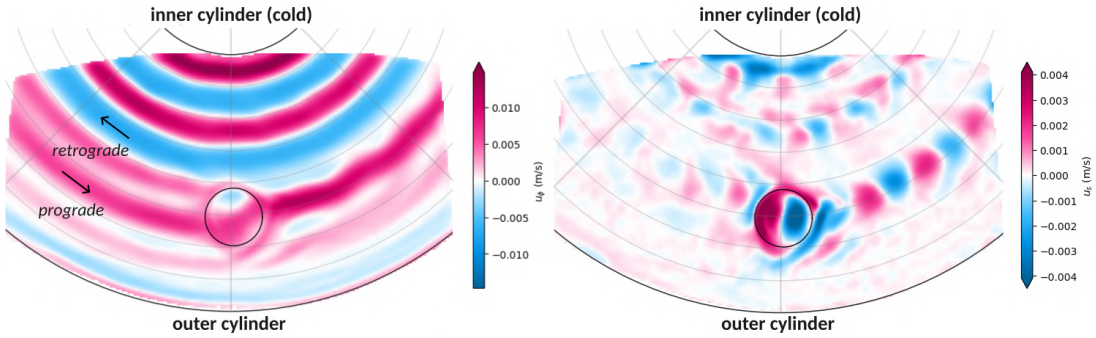

Figure 1: Time-averaged velocity fields obtained from PIV in a typical experiment at 72 rpm with a 6cm-wide, 4.5cm-high topography. The black circle is the horizontal position of the topography. Only a fraction of the total cylinder is visible. **Left**: Azimuthal component of the velocity. Red is prograde (same direction as the background rotation), blue is retrograde. **Right**: Radial component of the velocity. Red is outward, blue is inward.

References

Lonner, T. L., Aggarwal, A., & Aurnou, J. M. (2022). "Planetary core-style rotating convective flows in paraboloidal laboratory experiments", *Journal of Geophysical Research: Planets*, **127(10)** e2022JE007356.

*Corresponding author: d.lemasquerier@st-andrews.ac.uk
†University of St Andrews, UK
‡University of California, Los Angeles, USA

ICTW 2025 23rd INTERNATIONAL COUETTE-TAYLOR WORKSHOP 14th-16th JULY DURHAM, UK

Transition to ultimate Taylor-Couette turbulence

Detlef Lohse*†, Luuk Blaauw ‡, Sander G. Huisman §

We provide experimental evidence that the transition towards the ultimate turbulence regime of Taylor-Couette flow is of non-normal-nonlinear nature, showing sensitive dependences on distortions and being hysteretic and subcritical.

1 Introduction

The Rayleigh–Bénard (RB) system ([1]; [2]; [3]; [4]) – the flow in a container heated from below and cooled from above – and the Taylor–Couette (TC) system ([5]; [6]) – the flow between two coaxial co- or counterrotating cylinders – are perhaps the two most popular playgrounds to test new concepts in physics of fluids, be it instabilities, pattern formation, or turbulence. This also holds for ultimate turbulence ([7]; [8]; [9]; [10]), i.e., the state of turbulence in which also the boundary layers have become fully turbulent, displaying a logarithmic mean velocity profile and enhanced transport properties of the flow, either for the heat in RB flow or for the angular velocity in TC flow. While in RB flow it has been difficult to reach the ultimate state, due to the inefficiency of thermal driving, in TC it is much easier ([11]), due to the efficiency of mechanical driving. Therefore the TC system offers great opportunities to study the nature of the *transition* towards the ultimate regime in detail. This is what we do in this work.

For large enough driving, in any flow the boundary layers of (laminar) Prandtl–Blasius type get unstable and undergo a transition towards turbulent, so-called Prandtl–von Karman boundary layers, with a logarithmic velocity profile. This transition also occurs in RB and in TC flow ([12]; [4]). The transition is in direct analogy to the laminar-to-turbulent transitions of the boundary layer around a plate or within a pipe. It is subcritical (meaning that around the transition different states coexist) and of non-normal/nonlinear nature and can arise when (i) the shear is sufficiently strong and (ii) there are large enough disturbances (such as small wall roughnesses, inhomogeneities of the temperature boundary conditions, vibrations, etc.) to trigger the onset ("double threshold behavior") ([13]) so that the system "jumps" from one state to another. Typically, such an onset of the shear instability in a wall-parallel flow happens when the shear Reynolds number $\mathcal{R}e_s$ exceeds a value of about 420, as estimated by Walter Tollmien almost a century ago. With this, for a Prandtl number of $\mathcal{P}r \approx 0.7$ and an aspect ratio of $\Gamma \sim 1$, the critical Rayleigh number for the onset of the ultimate regime in RB convection can be estimated to occur at a Rayleigh number $\mathcal{R}a$ around 10^{14} ([14]), but given the double-threshold feature of the transition, for different small disturbances it may also be earlier or later. In TC flow, the same critical shear Reynolds number $\Re_s \approx 420$ is already achieved around a Taylor number of $\mathcal{T}a \sim 3 \times 10^8$.

2 Non-normal-nonlinear nature of the transitions towards the ultimate turbulence regime in TC flow

In this work we have analysed the detailed nature of the transition towards ultimate turbulence in TC flow. The main result is the dimensionless angular velocity transport $\mathcal{N}u_\omega$ as function of $\mathcal{T}a$. While for weak driving the local slope γ in an effective scaling law $\mathcal{N}u_\omega \sim \mathcal{T}a^\gamma$ is smaller than $1/3$ ("classical regime"), beyond the transition around $\mathcal{T}a \sim 3 \times 10^8$ we find $\gamma > 1/3$, namely $\gamma \approx 0.39$ ([11]). The important point here is to show the *nature of this transition*: When slowly increasing the driving strength $\mathcal{T}a$, the transport property $\mathcal{N}u_\omega$ suddenly *jumps* to a higher value, at a non-reproducible value of $\mathcal{T}a$, in a range of $\mathcal{T}a$ between 2.5×10^8 and $\sim 4 \times 10^8$. Moreover, when slowly reducing $\mathcal{T}a$ again, $\mathcal{N}u_\omega$ does not jump back to the values before

*Corresponding author: d.lohse@utwente.nl
†University of Twente
‡University of Twente
§University of Twente

the system underwent the transition, but stays at a higher value (green curves in the figure). Both properties support the non-normal-nonlinear nature of the transition. We doubled-checked that the hysteretic properties are not caused by the torque sensor, which is used to deduce $\mathcal{N}u_\omega$, but that they are really a property of the flow, as the same features of the transition are also seen in measurements of the Reynolds number, using Laser Doppler velocimetry. We note that in addition to the question on whether the flow has turbulent type BLs above the transition or laminar type BLs below the transition, also the number of vertically stacked Taylor rolls can change (16), which presumably is the reason why $\mathcal{N}u_\omega$ does not recover at the value it had prior to the transitions into and out of the ultimate regime.

In conclusion, our experimental results give strong evidence that the transition towards ultimate TC turbulence is of non-normal-nonlinear nature. Further studies are necessary to further explore the transition and in particular to check how it can best be triggered by controlled distortions and how these distortions then decay, depending on the value of the control parameter $\mathcal{T}a$. Exciting and versatile times to better understand the details of the non-normal-nonlinear transition to ultimate turbulence in TC and RB flow are ahead of us.

References

[1] L. P. Kadanoff, Phys. Today **54**, 34 (2001).

[2] G. Ahlers, S. Grossmann, and D. Lohse, Rev. Mod. Phys. **81**, 503 (2009).

[3] F. Chillà and J. Schumacher, Eur. Phys. J. E **35**, 58 (2012); K.-Q. Xia, Theor. Appl. Mech. Lett. **3**, 052001 (2013).

[4] D. Lohse and O. Shishkina, Phys. Today **76**, 26 (2023); Rev. Mod. Phys. bf 96, 035001 (2024).

[5] S. Grossmann, D. Lohse, and C. Sun, Annu. Rev. Fluid Mech. **48**, 53 (2016).

[6] M. A. Fardin, C. Perge, and N. Taberlet, Soft Matter **10**, 3523 (2014).

[7] R. Kraichnan, Phys. Fluids **5**, 1374 (1962).

[8] X. Chavanne *et al.*, Phys. Rev. Lett. **79**, 3648 (1997).

[9] S. Grossmann and D. Lohse, Phys. Fluids **23**, 045108 (2011).

[10] X. He *et al.*, Phys. Rev. Lett. **108**, 024502 (2012).

[11] S. G. Huisman *et al.*, Phys. Rev. Lett. **108**, 024501 (2012).

[12] P.-E. Roche, New J. Phys. **22**, 073056 (2020).

[13] P. Manneville, Mech. Eng. Reviews **3**, 15 (2016); M. Avila, D. Barkley, and B. Hof, Annu. Rev. Fluid Mech. **55**, 575 (2023).

[14] S. Grossmann and D. Lohse, Phys. Rev. Lett. **86**, 3316 (2001).

[15] S. G. Huisman *et al.*, Phys. Rev. Lett. **110**, 264501 (2013).

[16] S. G. Huisman, R. C. A. van der Veen, C. Sun, and D. Lohse, Nat. Commun. **5**, 3820 (2014); J. Wen *et al.*, J. Fluid Mech. **901**, A30 (2020).

Rayleigh-Taylor Instability Drives Axial Band Formation in Granular Flow

U. D'Ortona*, R. M. Lueptow†‡, N. Thomas*

Rayleigh-Taylor (RT) instabilities arise when a denser fluid is placed atop a lighter one in a gravitational field. The horizontal interface between the layers becomes wavy, eventually resulting in downward high density plumes and upward low density plumes. Rayleigh-Taylor instabilities can also occur in granular flows. Unlike the fluid instability, which occurs under quiescent conditions, the granular material must be flowing for the instability to occur (static granular layers would remain unchanged without the input of energy via the flow). For example, as a layer of large dense particles above a layer of small light particles flows down an inclined plane, the interface between the layers destabilizes to form ascending plumes of the small light particles and descending plumes of the large dense particles in the flow (D'Ortona *et al.*, 2020).

We show here that this granular Rayleigh-Taylor instability is the answer to the long-standing question about the mechanism for the formation of large and small particle axial bands in rotating tumblers. This axial segregation of different sizes of particles into bands occurs in long horizontal cylindrical rotating tumblers that are partially filled with a mixture of small and large particles that have the same density. Upon rotation, particles tumble down the inclined surface in a thin flowing layer, while particles below this flowing layer are in a static zone that is in solid body rotation with the tumbler. It is well-known that size segregation occurs as particles flow down the sloped surface in which small particles percolate to the bottom of the surface flowing layer forcing large particles to rise to the top of the flowing layer. Within a few tumbler rotations, this results in a segregation pattern in the static zone consisting of a core of small particles with large particles at the periphery of the tumbler. After hundreds more tumbler rotations following radial segregation, axially spaced bands rich in small and large particles appear, as shown in Figure 1. Although this phenomenon was first reported in 1940 (Oyama, 1940), the mechanism for axial segregation was unresolved prior to this work.

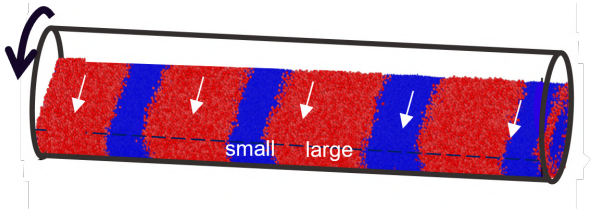

Figure 1: DEM simulation showing segregated axial bands after 350 rotations, when the bands are stationary, in a 100 cm long, 18 cm diameter tumbler rotating at 15 rpm that is half filled with equal volume fractions of 2 mm (blue) and 5 mm (red) spherical particles with periodic boundary conditions.

Using Discrete Element Method (DEM) simulations, we show that this axial segregation is due to the Rayleigh-Taylor instability. For initially mixed particles having two sizes but the same density, segregation and collisional diffusion in the flowing layer lead to a three-layer system for the flowing particles at the surface of the granular bed as the tumbler rotates. To explain, as a mixture of large and small particles flow down the sloped free surface, the small particles fall through the interstices between the large particles, resulting in a layer of large particles over a layer of small particles. Due to diffusion at the interface between the two layers, a layer of mixed particles is interposed between the upper large particle layer and the lower small particle layer. However, mixed particles pack more densely than particles of the same size, so the middle layer of mixed particles is more dense than the layer of nearly pure small particles below it, thereby inducing the Rayleigh-Taylor instability, evident as waviness in the interface between the layers. The waviness destabilizes

*Aix-Marseille University, CNRS, Centrale Marseille, Marseille, FRANCE
†Corresponding author: r-lueptow@northwestern.edu
‡Northwestern University, Evanston, IL, USA

into ascending plumes of small particles and descending plumes of mixed particles with large particles enriched near the surface of the flow. After many tumbler rotations, this become evident as axially-spaced small and large particle bands visible at the free surface. Rolls driven by segregation at the tilted interface between plumes sustain the pattern of upward and downward plumes to reinforce and maintain the bands of small and large particles.

References

D'Ortona, U. & Thomas, N. "Self-induced Rayleigh-Taylor instability in segregating dry granular flows", *Phys. Rev. Lett.*, **124** 178001 (2020).

Oyama, Y. "Studies on mixing of solids. Mixing of binary system of two sizes by ball mill motion", *Sci. Pap. Phys. Chem. Res.*, **37** 17 (1940).

D'Ortona, U., Lueptow, R. M., & Thomas, N. "Origin of granular axial segregation bands in a rotating tumbler: An interface-mixing driven Rayleigh-Taylor instability", *Phys. Rev. Res.*, **6** L032038 (2024).

Particle tracking and tracer evolution using Lagrangian means

C. Maitland-Davies*†, H. Kafiabad†

Lagrangian time averaging, where averages are taken along particle trajectories rather than at fixed spatial locations (Eulerian averaging), has long been recognised as a useful tool for understanding fluid behaviour with multiple timescales, especially in oceanic and atmospheric flows. Despite the theory's advantages, calculating these Lagrangian means has generally been unattractive due to difficulties associated with tracking particle trajectories, until recently when an alternative approach was proposed that circumvented this (Kafiabad & Vanneste, 2023; Baker et al., 2025). Using this approach, one can calculate Lagrangian means online (i.e. simultaneously with solving the governing equations) and save mean fields of interest with a slow save interval, lightening the memory footprint that comes with storing model output at high temporal resolution. This memory-light output can be used to investigate the mean transport of tracers as well as mean particle paths, which may be useful in analysing the ocean's large scale circulation, for example. Preliminary results in this regard are very encouraging, and support the wider use of Lagrangian means in the field. Figure 1 shows an example using a rotating shallow water system, consisting of a fast wave and a slow balanced flow. Particle advection is used to reconstruct a tracer field that is materially conserved. The result of advecting particles with a large timestep using the Lagrangian mean velocity bears much greater resemblance to the 'truth' than advection with the same large timestep but using the instantaneous velocity.

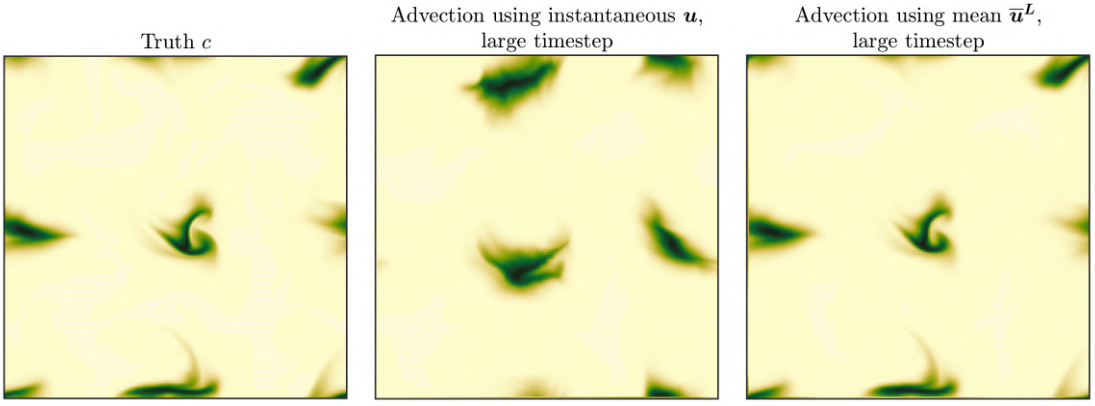

Figure 1: Snapshots of tracer fields that have been advected by a doubly-periodic rotating shallow water flow with a small timestep (left), and reconstructed from tracked particle trajectories with a large timestep, using the instantaneous velocity field (centre) and the Lagrangian mean velocity field (right).

References

Kafiabad, H.A. & Vanneste, J. "Computing Lagrangian means", *J. Fluid Mech.*, **960** A36.

Baker, L.E., Kafiabad, H.A., Maitland-Davies, C. & Vanneste, J. "Lagrangian filtering for wave–mean flow decomposition", *J. Fluid Mech.*, **1009** A40.

*Corresponding author: gqft45@durham.ac.uk
†Department of Mathematical Sciences, Durham University, Durham, UK

Blind identification of subcritical dynamo equilibria

F. Marcotte*†, P.Mannix†, Y.Ponty‡, C. Skene§, S.Tobias¶

In some astrophysical flows known to be linearly stable, finite-amplitude perturbations with a favourable spatial structure can nonlinearly trigger a transition from a non-magnetic, non-turbulent state to self-sustained dynamo action and turbulence. However, observations of magnetic fields in astrophysical objects are scarce and therefore poorly constrain the resulting dynamo field and driving mechanisms. I will show how optimal control of a finite-amplitude disturbance over a freely evolving flow can successfully identify subcritical dynamo branches without requiring prior knowledge of the magnetic field amplification process. Following an approach developed in the context of subcritical transition to turbulence in shear flows, the method also identifies both the structure and amplitude of critical perturbations. I will discuss some applications to the modeling of astrophysical dynamos, such as Keplerian discs dynamos and the Geodynamo.

*florence.marcotte@inria.fr
†Centre Inria d'Université Côte d'Azur, Laboratoire J.A. Dieudonné, Nice, France.
‡Observatoire de la Côte d'Azur, Laboratoire Lagrange, Nice, France.
§University of Leeds, Department of Applied Mathematics, Leeds, United Kingdom.
¶University of Edinburgh, School of Physics and Astronomy, Edinburgh, United Kingdom.

Optimal body force for heat transfer in turbulent vertical heated pipe flow

S. Chu*, E. Marensi†‡, A.P. Willis*

As buoyancy can help drive a flow, the vertical heated-pipe arrangement is widely used in thermal engineering applications. However, buoyancy suppresses and can even laminarise turbulence in the flow, thereby seriously damaging the heat transfer, measured by the Nusselt number *Nu*. As buoyancy, measured by the parameter C, is increased, three typical flow regimes are possible: shear-driven turbulence, laminarised flow, and convective turbulence (Parlatan, 1996; Yoo, 2013; Marensi, 2021; Chu, 2024). Here, we develop an optimisation method, based on a variational technique, to maximise heat transfer in each of these three flow regimes by optimising a time-independent body force. Optimisations are performed at $Re = 3000$.

Beginning with the laminarised state, at $C = 3$, optimisation improves heat transfer substantially, and when turbulence is triggered by the force, *Nu* experiences a strong increase, see figure 1. The optimal force presents roll structures of different azimuthal wavenumber m (figure 1(a-d)), consistent with previous computations for steady flow, e.g. Jia (2014); Meng (2005), which are similar to the linear optimal for growth of velocity perturbations. Computing optimal forces with different rotational symmetries, we found that *Nu* is maximized

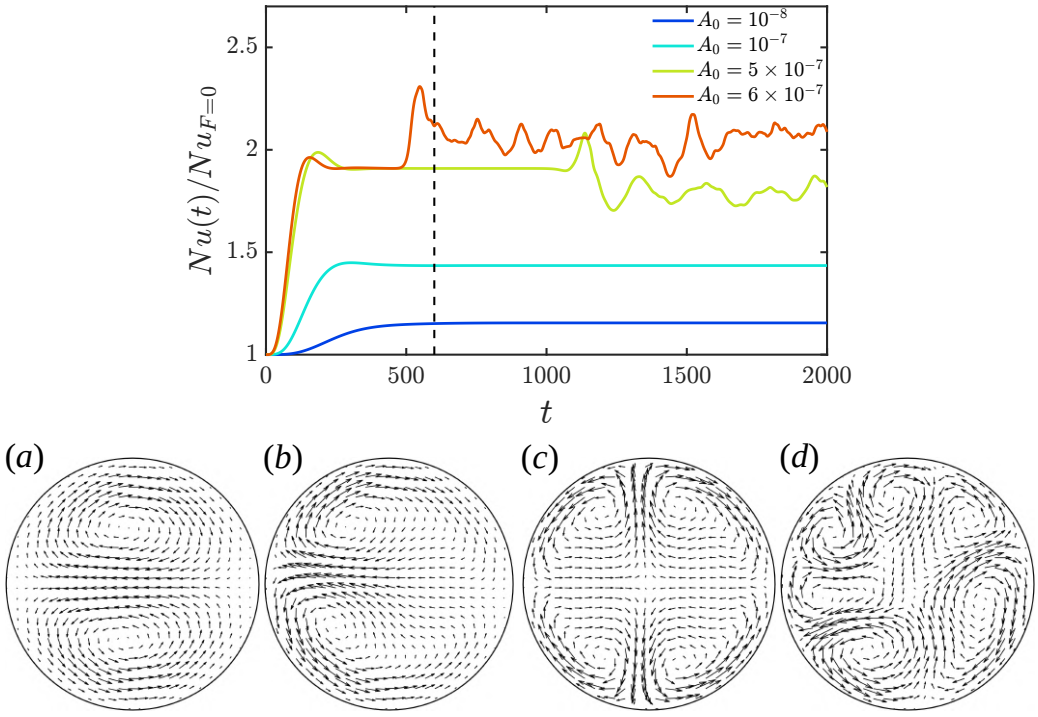

Figure 1: Top: Time evolution of instantaneous Nusselt number, normalised by the mean for the unforced flow, for increasing force amplitudes, starting from a laminar initial condition at $C = 3, Re = 3000$. The vertical dashed line indicates the optimisation target time $\mathcal{T} = 600$. Bottom: Contours of optimal body force for corresponding force amplitudes A_0: (*a*) $A_0 = 10^{-8}$, (*b*) $A_0 = 10^{-7}$, (*c*) $A_0 = 5\times10^{-7}$, (*c*) $A_0 = 6\times10^{-7}$. The arrows represent the cross-stream components of body force and their magnitude increases with A_0. As the axial component of the body force is at least an order of magnitude smaller, it is not shown.

*Applied Mathematics, School of Mathematical and Physical Sciences, University of Sheffield, Sheffield S3 7RH, UK
†Corresponding author: e.marensi@sheffield.ac.uk
‡School of Mechanical, Aerospace and Civil Engineering, University of Sheffield, Sheffield S1 3JD, UK

for azimuthal wavenumber $m = 1$ for very small amplitudes of the force A_0, and the optimal m increases as A_0 increases. At intermediate A_0, a stable nonlinear travelling wave solution is observed. At larger A_0, turbulence is triggered by strong rolls, but whether laminar or turbulent, *Nu* is found to depend only weakly on m. Interestingly, at larger A_0 turbulence does not necessarily lead to an increase in *Nu*. Visualisation of heat flux reveals that the streamwise vortices in forced turbulent states are not as efficient for heat transfer as those in forced laminar states. At larger force amplitude, unsteadiness of the rolls inhibits heat transfer.

Optimisation in the shear-turbulence regime, at $C = 1$, is most challenging, as it is highly chaotic, preventing long target times. However, the method is found to still be effective for much shorter target times, with $\mathcal{T} = 50$. In this case, despite turbulence being already effective for heat transfer, substantial further enhancement was still possible. Optimisations with a short target time $\mathcal{T}$ but turbulent flow are compared with optimisations that assume a steady state. Roll structures for the short-$\mathcal{T}$ optimisation are found to be located closer to the wall than those with the steady flow assumption, and the enhancement of *Nu* is greater. Like for the laminar state, the enhancement of *Nu* is found to be robust to the choice of forcing wavenumber m. In the convective turbulence regime, for $C \approx 4-6$, the force is found to laminarise convective turbulence, and for $C \approx 7-8$, the flow is only weakly chaotic, so that the results for steady flow are effectively extended over a larger range. For strong chaotic convective turbulence $(C = 16, 32)$, like for shear turbulence, the short-$\mathcal{T}$ optimisation with large enough A_0 leads to greater heat transfer than optimisations with the steady state assumption and also in this case the roll structures of the force optimised with the short $\mathcal{T}$ at all amplitudes are found to be located closer to the wall than for the corresponding steady calculation, see figure 2.

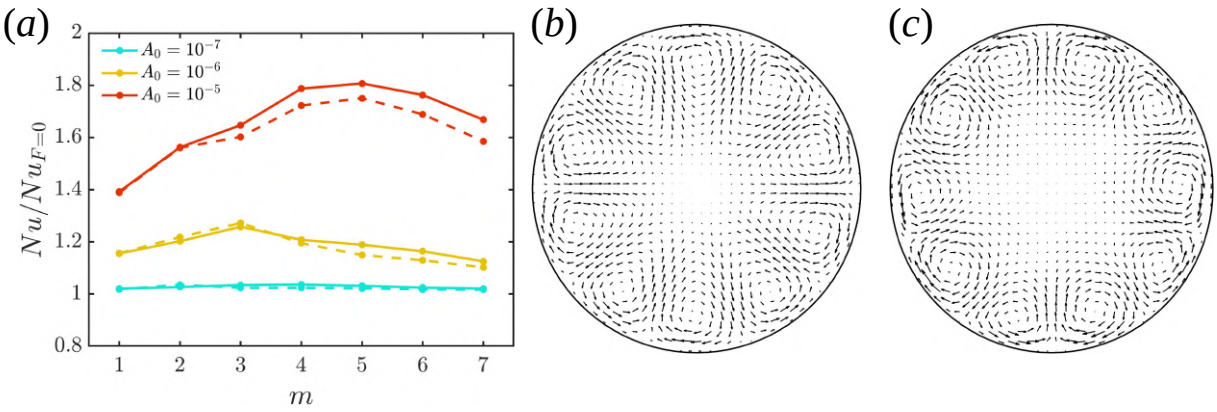

Figure 2: (*a*) Comparison between optimal body forces with different rotational symmetry m optimised in unsteady convective turbulence (solid line) and a steady two-dimensional laminar state (dashed line) at $A_0 = 10^{-5}$, $C = 16$, $Re = 3000$ and target time $\mathcal{T} = 100$. The cross-sections show an example of optimal force (with $m = 5$) optimised from: (*b*) a steady laminar state, and (*c*) the convective turbulence state. The largest arrow has magnitude 1.4×10^{-3} in (*b*) and 1.9×10^{-3} in (*c*).

References

Parlatan Y., Todreas N.E. & Driscoll M.J. (1996) Buoyancy and property variation effects in turbulent mixed convection of water in vertical tubes. *Journal of heat transfer* **118** (2), 381–387.674

Yoo, Jung Yul (2013) The turbulent flows of supercritical fluids with heat transfer. *Annual Review of Fluid Mechanics* **45**, 495–525.

Marensi E., He S. & Willis A. P. (2021) Suppression of turbulence and travelling waves in a vertical heated pipe. *Journal of Fluid Mechanics* **919**, A17

Chu S., Willis A. P. & Marensi E. (2024) The minimal seed for transition to convective turbulence in heated pipe flow. *Journal of Fluid Mechanics* **997**, A46.

Jia, H., Liu, Z.C., Liu, W. & Nakayama, A. (2014) Convective heat transfer optimization based on minimum entransy dissipation in the circular tube. *International Journal of Heat and Mass Transfer*, **73**, 124-–129.

Meng, Ji-An, Chen, Ze-Jing, Li, Zhi-Xin & Guo, Zeng-Yuan (2005) Field-coordination analysis and numerical study on turbulent convective heat transfer enhancement. *Journal of Enhanced Heat Transfer* **12** (1)

Flow regimes in turbulent co- and counter-rotating Taylor–Couette flows of very wide gaps.

S. Merbold*†, M.H. Hamede ‡C. Egbers ‡

In this study, flow regimes in co- and counter-rotating Taylor-Couette flow (Taylor (1923)) of very wide radius ratios for various Reynolds numbers up to 1.5×10^4 are discussed. The study aims to understand the effect of curvature on the Taylor-Couette flow, particularly in cases where the circumferential length of the inner cylinder is smaller than the gap width, which occurs for $\eta < 0.14$. In the investigation centrifugally stable as well as centrifugally unstable flow regimes are realized. The flow is investigated using a visualization method as well as Particle Image Velocimetry. Here, flow states in the centrifugally-unstable regime are investigated in the case of counter-rotating cylinders and pure inner cylinder rotation. Beside classical known flow states as Taylor-Vortex flow and Wavy Vortex flow, a variety of new flow patterns in the cylindrical annulus is observed, especially for the transition to turbulence (see Merbold et al. (2023)). For strong counter rotation coexisting turbulent and laminar regions inside the system are observed and investigated in detail. Small turbulent Spots and bursts of turbulent motion detatching the wall are observed, as well as an irregular Taylor-Vortex flow and non-stationary turbulent Vortices. Especially, a single Axially-aligned Columnar Vortex between the inner and outer cylinder is found. The principle regimes observed in flow between independently rotating cylinders are summarized in a flow-regime diagram. For a more detailed quantitative study, a time-resolved velocity field measurement has been conducted using a High-speed Particle Image Velocimetry technique through the TC system end plate, taking into account the curvature of the cylinder wall /Hamede et al. (2023)). These measurements record the radial and azimuthal velocity components in the 2D horizontal plane, which is traversed at different axial positions to include known axial wavelengths. The recorded flow field is used to compute the angular momentum transport in terms of the quasi-Nusselt number. The results show a maximum in angular momentum transport for low counter-rotating rates of $0.011 < \mu_{max} < 0.0077$, which is associated with large-scale structures that span the entire gap. Moreover, the angular momentum transport decreases for counter-rotation rates higher than μ_{max} until it reaches a minimum value and then tends to increase again for higher counter-rotation cases,where second maximum of angular momentum transport is expected for higher speeds. The occurrence of such behaviour was attributed to the presence of novel structures observed during the investigation of flow configurations. It was determined that these flow structures emerge from the outer cylinder boundary layer and travel inward, thereby enhancing the momentum transport at such flow configurations (Hamede et al. (2023)).

References

Taylor, G.I. "Stability of a Viscous Liquid contained between Two Rotating Cylinders", *Phil. Trans. Roy. Soc. A*, **223** 289–343.

Merbold, S., Hamede, M.H., Froitzheim, A. & Egbers C. (2023). "Flow regimes in a very wide-gap Taylor–Couette flow with counter-rotating cylinders" *Phil. Trans. Roy. Soc. A*, **381** 2246..

Hamede, M.H., Merbold, S., Egbers, C. (2023) "Experimental investigation of turbulent counter-rotating Taylor–Couette flows for radius ratio $\eta = 0,1$." *Journal of Fluid Mechanics* **964**:A36. doi:10.1017/jfm.2023.392

*Corresponding author: sebastian.merbold@dlr.de
†German Aeropspace Center, Institute of electrified Aero Engines, Cottbus, Germany
‡Brandenburg University of Technology Cottbus-Senftenberg

Sensitivity of Bifurcation Scenarios of Time-Periodic Flows in a cavity

A. Meseguer*†, A. Alonso†, O. Batiste†, F. Mellibovsky†

Abstract:

Time-periodic lid-driven flows arising in a four-sided $\mathbb{D}_2$-symmetric square cavity are identified. The reported oscillatory flows result from a rich variety of local and global bifurcations. Local Hopf bifurcations of steady flows arising in this setting were originally found in Meseguer (2024) using a spectral Chebychev discretization of the Navier-Stokes equations. Starting near these Hopf bifurcations, stable and unstable orbits are accurately found and tracked as a function of the Reynolds number using Poincaré-Newton-Krylov methods. Overall, three families of periodic orbits have been identified. Two of these families are unstable and are destroyed at global heteroclinic or homoclinic collisions with other steady flows. The only stable orbit found has a long period and is also born at a global bifurcation.

Preliminary numerical explorations, carried out using a Lattice Boltzmann (LB) method with non-regularized boundary conditions, identify two of the families of periodic orbits found by the spectral DNS method, albeit at different Reynolds numbers. However, the LB computations reveal a different bifurcation scenario and stability nature for one particular family of periodic orbits. More specifically, whereas one of the periodic orbits detected by DNS is unstable, being born at a subcritical Hopf bifurcation, the LB method identifies it as stable, in a supercritical fashion.

We conclude that, overall, regularization of the boundary conditions may affect the structural stability of the bifurcation diagrams, sometimes leading to higher-codimension (Bautin) scenarios for time-periodic flows. The discrepancies between the regularized-DNS and non-regularized-LB results will be shown, time permitting.

Acknowledgements:

This research is supported by the Ministerio de Ciencia, Innovación y Universidades (Agencia Estatal de Investi- gación, project nos. PID2020-114043GB-I00 (MCIN/AEI/10.13039/501100011033) and PID2023-150029NB-I00 (MCIN/AEI/10.13039/501100011033/feder, ue).

References

Meseguer, A., Alonso, A., Batiste, O., An, B. and Mellibovsky, F. (2024). "Bifurcation analysis in the regularized four-sided cavity flow: Equilibrium states in a $\mathbb{D}_2$-symmetric fluid system.", *Phys. Fluids*, **36** 064104(1-11).

*Corresponding author: alvaro.meseguer@upc.edu
†Universitat Politècnica de Catalunya BarcelonaTech, Barcelona, Spain

Experimental investigation of the thermoconvective instability in a cylindrical annulus for a high Prandtl number fluid.

A. Meyer[1 2], A. Hiremath[2], A. Prigent[2], I. Mutabazi[2]

We consider a Newtonian fluid of density ρ, kinematic viscosity ν, and thermal diffusivity κ confined in a vertical cylindrical annulus of height H with a radial temperature gradient. The inner cylinder of radius R_1 is maintained at the temperature T_1 and the outer cylinder of radius $R_2 = R_1 + d$ is maintained at the temperature $T_2 = T_1 - \Delta T$, where d is the gap size and ΔT is the temperature difference between the two cylinders (Figure 1-a). Under the condition of an infinite aspect ratio $\Gamma = H/d$, the base flow consists of a vertical flow ascending near the hot cylindrical wall and descending near the cold one. The temperature of the base flow has a logarithmic decreasing profile and the velocity has a cubic profile with an inflexion point. The control parameters of the flow are the radius ratio η, the Prandtl number $Pr = \nu/\kappa$ and the Grashof number $Gr = \alpha \Delta T g d^3/\nu^2$.

For a finite length cylindrical annulus, Lopez *et al.* (2015) have shown that the base flow may be either in a conduction regime when the boundary layers at the endplates do not significantly affect the temperature profile base flow or in a convective regime in the opposite case. These authors have provided an analytic expression $Ra_*(\eta, \Gamma) = a(\eta)\Gamma$ which allows to determine the separation between the conduction and convective regimes. For a cylindrical annulus with $\eta = 0.8$ and $\Gamma = 114$, Kang *et al*. (2023) have shown that $Ra_* \cong 46\,446$. This suggests that for the experiments to be conducted from the base flow with a temperature conduction state, the working fluids (i.e. the values of Pr) and the values of Gr should be chosen such that $Gr\ Pr < Ra_*$.

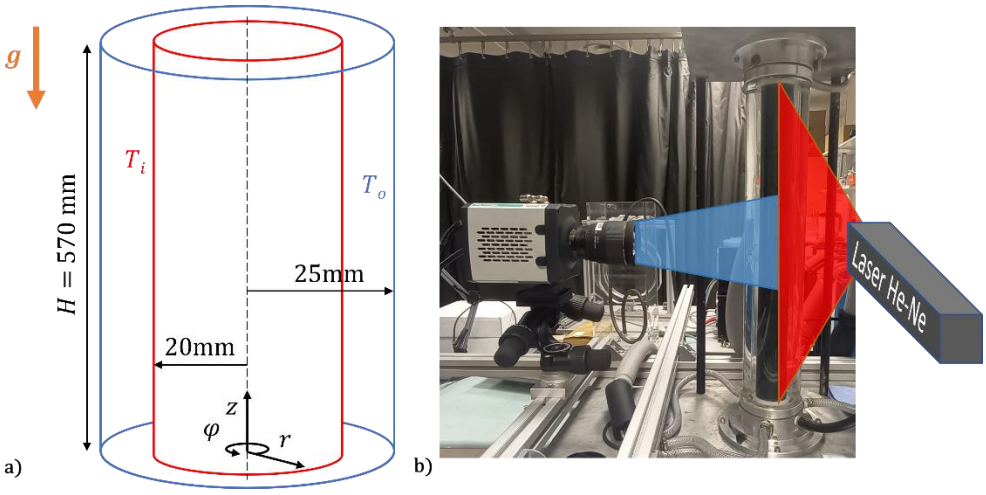

Figure 1: Geometry of the studied cylindrical annulus (a), and photography of the experimental apparatus (b).

[1] Corresponding author: antoine.meyer@univ-lehavre.fr
[2] University of Le Havre Normandie, LOMC UMR 6294, Le Havre, France

For the base flow with a temperature conduction regime, above a critical value Gr_c of the Grashof number, the flow becomes unstable and the nature of instability depends on Pr and of the radius ratio η (Bahloul *et al*., 2000). For low values of Pr, the instability is induced according to the Rayleigh-Fjörtfört criterion [Drazin, 2002] by the presence of the inflexion point in the velocity profile and leads to hydrodynamic modes. Because of curvature, these modes are oscillatory. The threshold Gr_c of these modes is independent of Pr. For large values of Pr, the instability is due to the development of temperature perturbations leading to thermal modes which are oscillatory and the threshold depends on Pr. For a radius ratio $\eta = 0.8$, hydrodynamic modes occur for $Pr < 12.5$ and thermal modes appear for $Pr > 12.5$.

We have performed an experiment with a silicone oil with $Pr = 30$ in a cylindrical annulus of gap size $d = 5$mm, radius ratio $\eta = 0.8$ and aspect ratio $\Gamma = 114$. With this configuration, it is possible to observe instability in a regime close to the conduction one. To observe the instability, Polyamide particles are dispersed in the fluid and we measure the velocity using the PIV technique (Figure 1-b). The thermoconvective instability is observed at a critical value very close to the predictions of linear stability analysis. The secondary flow consists in the superposition of two modes with similar wave numbers, but traveling in opposite directions (Figure 2). We have performed spectral analysis and the demodulation of the spacetime diagrams; the results are compared with the results from the linear stability analysis. In particular, the Ginzburg-Landau equation is used to characterize the interaction between the two instability modes.

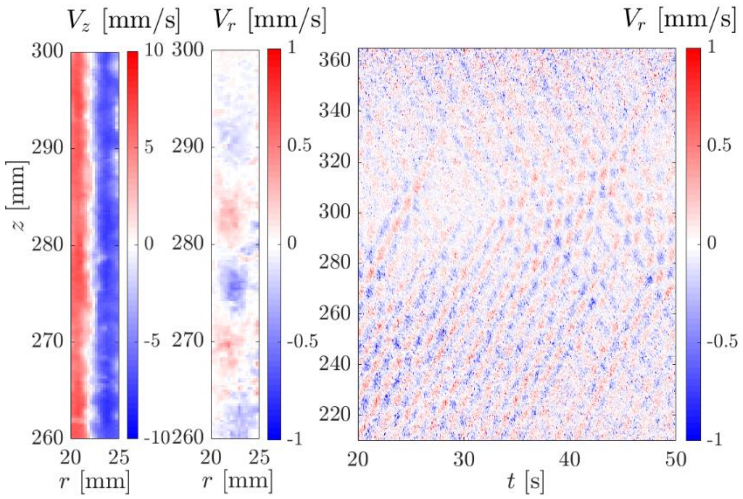

Figure 2: Thermal mode observed with $Gr = 2127$. Axial velocity component (left), radial velocity component (middle), and spacetime diagram of the radial component of the velocity measured at the mid-gap.

References

Lopez, J.M., Marques, F. & Avila, M. (2015). "Conductive and convective heat transfer in fluid flows between differentially heated and rotating cylinders", *International journal of Heat and Mass Transfer* **90**, 959-967.

Kang C., Yoshikawa H.N., Ntarmouchant Z, Prigent A. & Mutabazi I. (2023). "Solitary-like and modulated wavepackets in the Couette-Taylor flow with a radial temperature gradient", *Phil. Trans. R. Soc*. A **381**, 20220117.

Bahloul, A., Mutabazi, I. & Ambari, A. (2000). "Codimension 2 points in the flow inside a cylindrical annulus with a radial temperature gradient", *The European Physical Journal-Applied Physics* **9**(3), 253-264.

Drazin P.G., *Introduction to Hydrodynamic Stability*, Cambridge University Press, 2002.

On-the-fly Lagrangian averaging

Abhijeet Minz*†, H. Amini-Kafiabad†, Lois E. Baker‡, Jacques Vanneste‡§

Abstract

Many fluid dynamical phenomena involve temporal and spatial scales that cannot be fully resolved by measuring instruments or numerical simulations. Their modelling requires coarse graining, typically in the form of temporal or spatial averaging of the equations of motion, and the parameterisation of the impact of the unresolved scales. Eulerian averaging, in which flow variables are averaged at fixed spatial locations, is widely used. The alternative of Lagrangian averaging, which involves averaging flow variables along the particle trajectories, has benefits because it respects the advective structure of the equations modelling fluid motion.

The numerical computation of Lagrangian (time) averages from simulation data is challenging, however. It can be carried out by tracking a large number of particles or, following a recent approach, by solving a dedicated set of partial differential equations (PDEs). Both approaches are computationally demanding because they require an entirely new computation for each time at which the Lagrangian mean fields are desired.

We overcome this drawback by developing a PDE-based method that delivers Lagrangian mean fields for all times through the single solution of evolutionary PDEs. This allows for an on-the-fly implementation, in which Lagrangian averages are computed along with the dynamical variables. This is made possible by the use of a special class of temporal filters whose kernels are sums of exponential functions in Minz (2024). We implement these in the rotating shallow-water model and demonstrate their effectiveness at filtering out large-amplitude Poincaré waves.

References

Minz, A., Baker, L. E., Kafiabad, H. A., and Vanneste, J., "The exponential Lagrangian mean", *arXiv preprint arXiv:2406.18243*.

*Presenting author:abhijeet.minz@Ed.ac.uk
†Durham University, Durham, UK
‡School of Mathematics and Maxwell Institute for Mathematical Sciences, University of Edinburgh, Edinburgh EH9 3FD, UK
§School of Mathematics and Maxwell Institute for Mathematical Sciences, University of Edinburgh, Edinburgh EH9 3FD, UK

Stratified turbulence forced by large scale waves

N. Mordant[1] [2], M. Magnier[2], T. Valran[2], S. Viboud[2], P. Augier[2], J. Sommeria[2]

Ocean is stratified in density due to vertical variations of temperature or salt density. This makes its dynamics sensitive to gravity. One consequence is the ability of the fluid to sustain internal gravity waves that propagate in its bulk. Another consequence is that the motion is anisotropic due to the symmetry breaking by gravity. We investigate experimentally turbulence in such a stratified fluid when the horizontal Froude number Fr_h is low (~ 0.01 in our case), the Reynolds number Re is large ($\sim 10^4$ in our case) and the buoyancy Reynolds number $Re_b = Fr_h^2 Re$ is much larger than 1 (~ 50 in our case). This range is expected for the submesoscale motions in the bulk of the ocean (although with more extreme values of the Reynolds numbers). In these regimes, field data from mid-latitude northern Atlantic show the Garrett & Munk spectrum in which the energy spectrum follows power laws as function of frequency or vertical wave numbers with exponents -2 (with some observation scatter between -2.5 and -1.5 roughly) that is associated with wave turbulence (Polzin & Lvov, 2011, Pollman, 2020). In this range of parameters, scaling analysis predicts the LAST (Layered Anisotropic Stratified Turbulence) in which the vertical and horizontal spectrum of horizontal velocity are different due to anisotropy. The horizontal spectrum is predicted to scale as $k_h^{-5/3}$ for all scales while the vertical spectrum should have a first range with a scaling k_v^{-3} followed, at smaller scales, by a scaling $k_v^{-5/3}$ with a return to isotropy (Brethouwer *et al.* , 2007).

To investigate experimentally these flow regimes, we use the Coriolis facility in our laboratory that is a large-scale turntable, 13m in diameter and 1m deep. We set a linear stratification in water by varying the vertical concentration of salt or of a mixture of salt and alcohol (for optical index matching). Rotation can be added as well. We force the motion by generating large scale waves using 4 large oscillating panels (6m long) so that to generate large amplitude, large scale internal waves (Savaro *et al.*, 2020, Rodda *et al.* 2022, 2023). Measurements are:
- time-resolved Particle Image Velocimetry either in horizontal or vertical cuts of the flow
- Particle Tracking Velocimetry in a volume near the center of the tank to investigate particle dispersion
- Density measurements with conductivity probes either at fixed locations or through vertical profiling.

We use all these measurements to provide a detailed characterization of the statistical properties of turbulence in our flow.

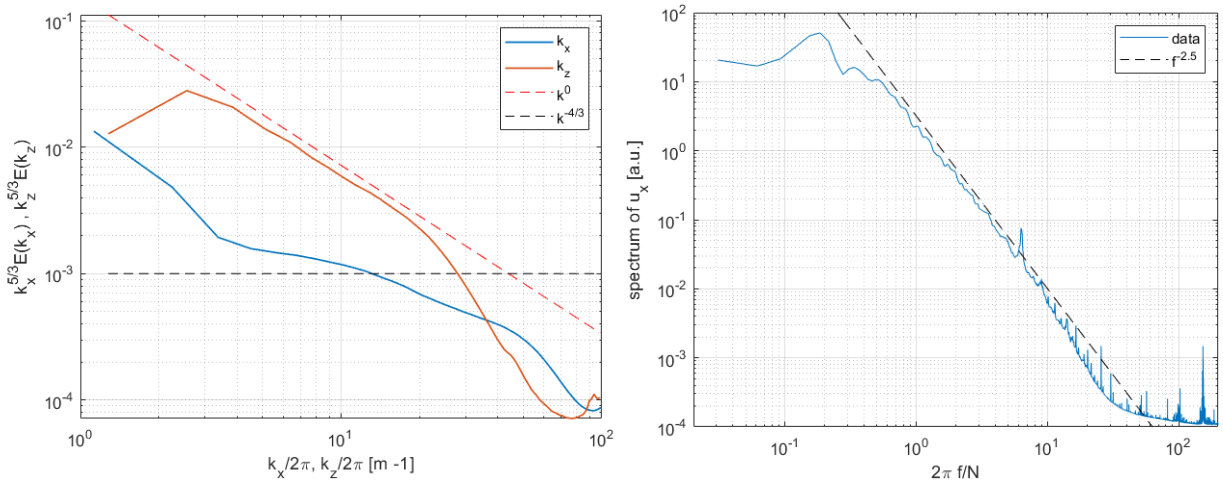

Figure 1: (left) Vertical and horizontal Fourier spectra of the horizontal velocity for an experiment at strong forcing. (right) Frequency spectrum. Dashed lines are power law decays with exponents given in the legend

[1] Corresponding author: nicolas.mordant@univ-grenoble-alpes.fr
[2] Université Grenoble Alpes, Grenoble, France

At the highest forcing intensity, we can achieve, the velocity spectrum of the horizontal velocity is shown in figure 1. One can see that the vertical spectrum decays following a k_z^{-3} and the horizontal spectrum shows a small range of decay close to $k_x^{-5/3}$. This strongly suggest that our flow is in the LAST regime. The frequency spectrum displays a power law decay with exponent -2.5 compatible with the Garrett & Munk spectrum. Previous investigation showed that the large-scale flow is made of internal wave turbulence.

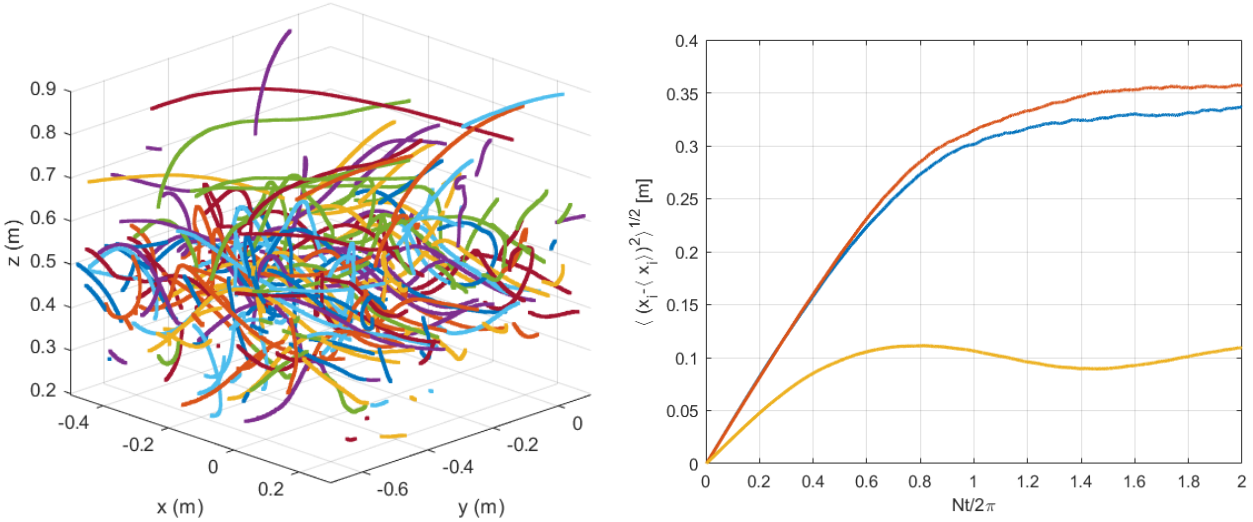

Figure 2: Left: example of Lagrangian trajectories measured at the strongest forcing. Right: statistics of single particle dispersion for the same experiment as a function of time.

Figure 2 shows some Lagrangian data obtained from the PTV system for a similar experiment as in figure 1. We show the dispersion of a single particle from its initial position as a function of time. It can be seen that the vertical dispersion saturates much faster than the horizontal one. While the saturation of the horizontal dispersion is a bias of the finite size of the measurement, the saturation of the horizontal dispersion is due to the stratification and highlights the impact of gravity on the flow and its strong anisotropy.

We will present further characterization of this flow during the presentation.

References

Polzin, K.L. & Lvov Y.V., (2011) "Toward regional characterizations of the oceanic internal wavefield", Rev. Geophys. 49 RG4003

Pollmann F. (2020), Global Characterization of the Ocean's internal wave spectrum, *J. Phys. Oceanogr*. **50**, 1871

Brethouwer, G., Billant, P., Lindborg, E., & Chomaz, J.-M. (2007), "Scaling analysis and simulation of strongly stratified turbulent flows", *J. Fluid Mech.* **585**, 343

Savaro, C., Campagne, A., Calpe Linares, M., G., Augier, P., Sommeria, J., Valran, T., Viboud, S., Mordant, N. (2020) "Generation of weakly nonlinear turbulence of internal gravity waves in the Coriolis facility", Phys. Rev. Fluids, **5**, 073801

Rodda, C., Savaro, C., Davis, G., Augier, P., Sommeria, J., Valran, T., Viboud, S., Mordant, N. (2022) "Experimental observations of internal wave turbulence transition in a stratified fluid", *Phys. Rev. Fluids,* **7**, 094802

Rodda, C., Savaro, C., Bouillaut, V., Augier, P., Sommeria, J., Valran, T., Viboud, S., Mordant, N. (2023), "From Internal Waves to Turbulence in a Stably Stratified Fluid", *Phys. Rev. Lett.* **131,** 264101

Instability modes in viscoelastic Taylor-Couette flow with Boger fluids : linear stability theory and experiments

I. Mutabazi[1 2], Y. Bai[2], F. Kelai[2], O. Crumeyrolle[2] and N. Latrache[3]

We investigate the instabilities modes in viscoelastic Taylor-Couette flow of a Boger fluid using linear stability analysis, space-time diagrams of cross-section visualization and particle image velocimetry (PIV). The working solution is an aqueous mixture of the polymer solution of Polyethylene oxide (PEO) and Polyethylene glycol (PEG). The concentrations of the PEG and the POE are chosen in such a way to obtain solutions with constant shear viscosity η i.e. solutions without shear-thinning because of the presence of PEG. Viscoelastic solutions are characterized by the viscosity ratio $S = \eta_p/\eta$ with η_p the polymer contribution to the viscosity and the elasticity number $E = \lambda/\tau_v$ where λ is the polymer relaxation time and $\tau_v = \rho d^2/\eta$ is viscous diffusion time in the gap annulus [1]. The shear of the viscoelastic fluid is characterized by the Weissenberg $W_i = \lambda\dot{\gamma}$ which is the analog of the Reynolds $Re = \tau_v\dot{\gamma}$ where $\dot{\gamma}$ is the shear rate. The ratio $E = \frac{Wi}{Re} = \frac{\lambda}{\tau_v}$ defines the elasticity of the polymer solution and it is an intrinsic property of the polymer solution in a given flow configuration. The cylinders are rotated independently with angular velocities Ω_i and $\Omega_o = \mu\,\Omega_I$ so that we define associated Reynolds numbers as follows: $Re_i = \Omega_i ad/\nu$ and $Re_o = \Omega_o bd/\nu$ where $d = b - a$ with a and b being the radii of the inner and outer cylinder respectively. Another set of control parameters consists of the rotation ratio $\mu = \Omega_o/\Omega_i$ and the Taylor number $Ta = Re_i\left(\frac{d}{a}\right)^{1/2}$. So a viscoelastic flow in the Taylor-Couette with given radius a/b ratio is determined by 4 control parameters: (S, E, Re_i, Re_o) or (S, E, μ, Ta).

We will present results from viscoelastic flow instabilities in three different cases: rotating inner cylinder with fixed outer cylinder, rotating outer cylinder and fixed inner one, and both rotating cylinders in quasi-Keplerian regimes. The flow patterns have been investigated using flow visualization by seeded anisotropic particles and by particle image velocimetry (PIV). Linear stability analysis has been performed to determine the critical parameters for different solutions. In the viscoelastic Taylor-Couette flow, there are two destabilizing mechanisms : the centrifugal force (the inertia force) and the elasticity [2]. The interplay between the elasticity of the polymer solution

[1] Corresponding author: innocent.mutabazi@univ-lehavre.fr
[2] Université Le Havre Normandie, LOMC, UMR 6294 CNRS/ULHN, Le Havre, France
[3] Université de Bretagne Occidentale, IRDL, UMR 6027 CNRS/UBO, Brest, France.

and the inertia forces leads to different critical modes : stationary Taylor vortices for very small values of the elasticity, ribbons i.e. superposition of spirals of opposite helicity for intermediate values of the elasticity and disordered elastic vortices for large values of the elasticity and weak inertia forces. The effect of the inertia force can be suppressed by choosing the Rayleigh-stable flows in which the centrifugal force does not destabilize the flow (Keplerian regime or fixed inner cylinder and rotating outer cylinder). A generalized Rayleigh criterion for viscoelastic curved flows shows that the elasticity is always destabilizing. We will present the critical states from both experiments and linear stability theory for different flow situations. The centrifugal force induces Taylor vortices while the elasticity induces oscillating vortices which superimpose to generate ribbons for intermediate values of elasticity and disordered elastic vortices for large values of elasticity.

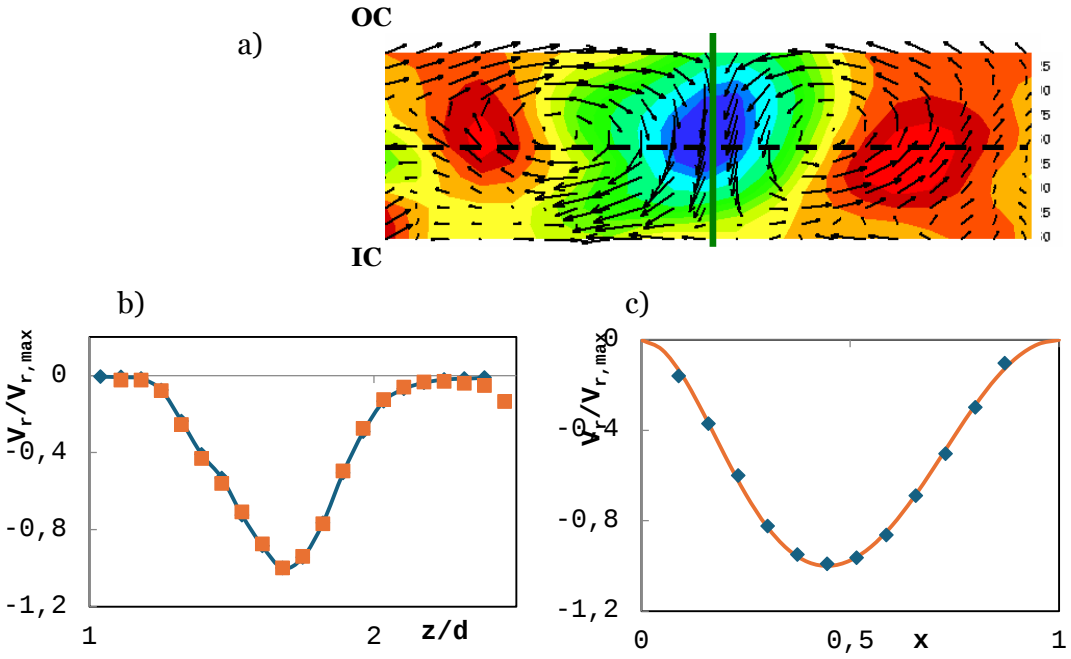

Figure 1: Instantaneous radial velocity $(V_r/V_{r,max})$ in the (r, z) plane (IC : inner cylinder, OC : outer cylinder); b) Axial profile of the radial velocity in the middle of the gap ; c) Radial profile of the radial velocity profile in the inflow position of the elastic vortices.

References

1. R.G. Larson, S. J. Muller and E. S. G. Shaqfeh, A purely elastic instability in Taylor-Couette flow, *J. Fluid Mech.* 218, 573- 600(1990).

2. Y. Bai, N. Latrache, F. Kelai, O. Crumeyrolle and I. Mutabazi, Viscoelastic instabilities of Taylor-Couette flows with different rotation regimes, *Phil. Trans. R. Soc. A* **301**, 20220133 (2023).

The present work was funded by the French National Research Agency (ANR) through the programme d'Investissements d'Avenir (grant n°.ANR-LABX-09-01) LABEX EMC³ TUVECO and HILIMBA.

ICTW 2025 23rd INTERNATIONAL COUETTE-TAYLOR WORKSHOP 14th-16th JULY DURHAM, UK

Spiral vortex flows of the Taylor-Couette system in the narrow-gap limit

M. Nagata*†

Taylor-Couette flow describes the closed fluid motion between two concentric cylinders rotating about their common axis. Considering a vast number of experiments that have been explored, one interesting question arises regarding how the experimental observations change when the gap is reduced to zero, that is, when the radius ratio, $\eta \equiv r_i/r_o$, approaches 1, where r_i and r_o are the radii of the inner and the outer cylinders, respectively. In this so-called narrow-gap limit, the circular geometry of the cylinder walls approaches a plane geometry. In the present work, we extend the recent linear and nonlinear analyses for axisymmetric cases in the narrow-gap limit by (Nagata, 2023 and 2024), to non-axisymmetric cases, and obtain finite-amplitude solutions in the form of spiral vortex flows numerically.

Formulation:

We consider incompressible motion of a fluid with density ρ and kinematic viscosity ν, which is confined between two coaxial cylinders of infinite extent in the axial direction, where the inner and outer cylinders at radii r_i and r_o, rotate with angular velocities, ω_i and ω_o, respectively. We assume that $\omega_i \neq 0$.

After appropriately scaled by $\sqrt{1-\eta}$ or $1/\sqrt{1-\eta}$, depending on the variables and the coordinates, the disturbance velocity and pressure $[\hat{\boldsymbol{u}}^*; \hat{p}^*]$ which are superimposed on the basic state, $i.e.$ on circular Couette flow (CCF), $[U_B^*; P_B^*]$, are governed by

$$\nabla^* \cdot \hat{\boldsymbol{u}}^* = 0, \tag{1}$$

$$(\partial_t - \nabla^{*2})\hat{\boldsymbol{u}}^* = -\nabla^*\hat{p}^* - U_B^*\partial_{x^*}\hat{\boldsymbol{u}}^* + Re^*\,\hat{u}_{z^*}^*\hat{\boldsymbol{i}} - \frac{1}{2}Q^*z^*\hat{u}_{x^*}^*\hat{\boldsymbol{k}} - \frac{1}{2}(\hat{u}_{x^*}^*)^2\boldsymbol{k} - \Omega^*\hat{\boldsymbol{j}}\times\hat{\boldsymbol{u}}^* - (\hat{\boldsymbol{u}}^*\cdot\nabla^*)\hat{\boldsymbol{u}}^*, \tag{2}$$

where $\hat{\boldsymbol{i}}$, $\hat{\boldsymbol{j}}$ and $\hat{\boldsymbol{k}}$ are the unit vectors in the azimuthal (x^*), axial (y^*) and wall-normal (z^*) directions, and Re^* is the Reynolds number, Ω^* is the rotation number and Q^* represents the effect of inertia with the following constraints: $\Omega^* = \frac{1+\mu}{1-\mu}Re^*$ and $Q^* = 2Re^*$. In the present analysis, we choose $\tau = Q^*Re^* = 2(Re^*)^2$ and the angular velocity ratio, $\mu \equiv \omega_o/\omega_i$, as the two controlling parameters. We call τ the modified Taylor number. See (Nagata, 2023 and 2024) for the derivation of (1) and (2).

Results and Discussion:

We anticipate that nonlinear flows possess a spiral vortex flow (SVF) structure, $\propto \exp[im\{\alpha(x^*-ct)+\beta y^*\}]$ with $m \in \mathbb{Z}$, travelling in the x^*-direction with the phase speed c, where α and β are the wavenumbers in the x^*- and the y^*-directions. It is found that, consistent with the results of linear stability analysis by (Krueger et al., 1966), SVFs bifurcate directly from CCF before axisymmetric Taylor vortex flows (TVF) set in, as shown in Figure 1(a) for $\mu = -1$. The figure shows the bifurcation branches of SVFs with various values of α for $\beta = 2.0$ and α =0.44721 for β=1.821. It is seen that the bifurcation of TVF ($\alpha = 0$) is subcritical. As α is increased from zero, the bifurcation remains subcritical with the bifurcation point below the critical τ_c for TVF. As α is further increased, the bifurcation nature changes gradually from subcritical to supercritical.

At the point of bifurcation from CCF, the phase speed, c, of SVF satisfies

$$c = -\sigma^I/\alpha, \tag{3}$$

where σ^I is the imaginary part of the eigenvalue σ of the perturbation at the criticality $\tau = \tau_c$, which is determined by the linear stability analysis. (The real part of σ corresponds to the growth rate of the perturbation.) This is checked in Figure 1(b), where c of SVF and $-\sigma^I/\alpha$ of infinitesimal perturbations near the critical point are plotted. It is seen that c is less than $-\sigma^I/\alpha$ for all α.

*Corresponding author: nagata.masato.45x@st.kyoto-u.ac.jp
†Kyoto University, Kyoto, JAPAN

To see the flow pattern, we plot the stream function Ψ on the (z^*, y^*) cross-section along one wavelength in the x^*-direction in Figure 2. It is seen that the vortex centre moves along a direction inclined from the x^*-axis. The spiral flow pattern propagates in the azimuthal (x^*) direction with the phase velocity c like the barber's pole.

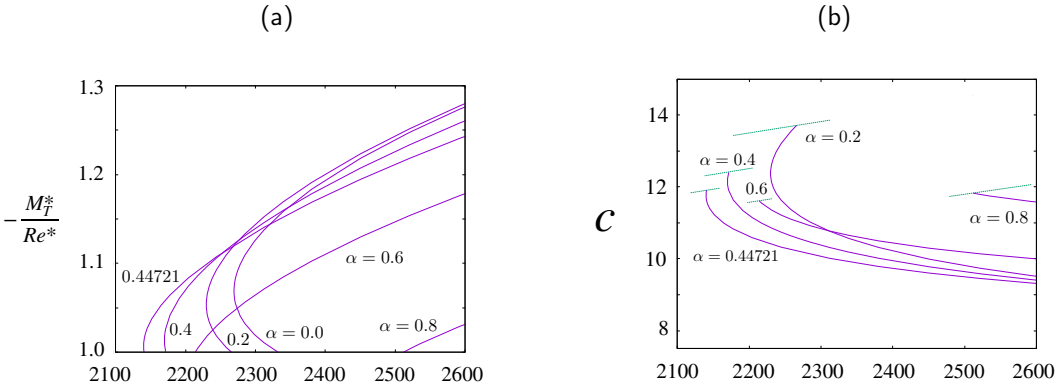

Fig
τ f
for
co
(b
lin
an

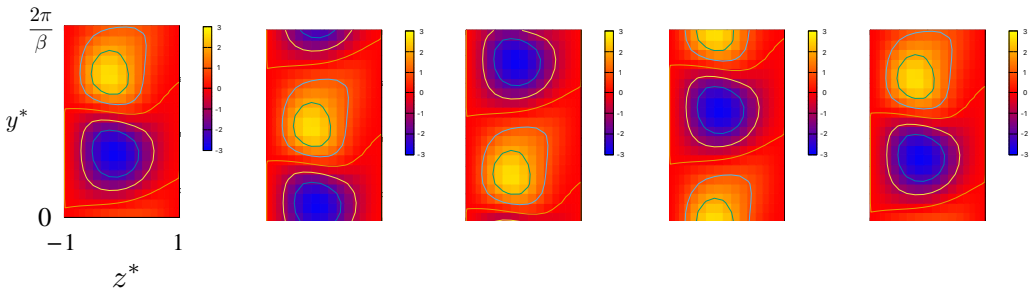

Figure 2: The stream function, Ψ, on the (z^*, y^*)-plane at $x^* = 0$, $0.5\pi/\alpha$, π/α, $1.5\pi/\alpha$ and $2\pi/\alpha$ from left to right, at $\tau = 3000$ for $\mu = -1$. $\alpha = 0.44721$ and $\beta = 1.821$.

We shall discuss other nonlinear characteristics of SVF, such as the mean flow in the azimuthal direction as well as in the axial direction. Also, comparisons with available experimental observations shall be attempted.

References

Krueger E.R., Gross A. & Di Prima R.C. (1966). "On the relative importance of Taylor-vortex and non-axisymmetric modes in flow between rotating cylinders". *J. Fluid Mech.* **24**, 521-538.

Nagata M. (2023). "Taylor-Couette flow in the narrow-gap limit". *Phil, Trans. Roy. Soc. A,* **381**, 20220134.

Nagata M. (2024). "Taylor-Couette system in the narrow-gap limit, revisited, with a corrigendum to the paper by Nagata (2023, Philosophical Transaction A.)". *Proc. Roy. Soc. A,* **480**, 20230890.

Rapidly Rotating Wall-Mode Convection

J. S. Oishi*[†], G. M. Vasil[‡], K. J. Burns[§], D. Leconaet[¶], B. P. Brown[‖]
K. Julien[**]

In the rapidly rotating limit, we derive a balanced set of reduced equations governing the strongly nonlinear development of the convective wall-mode instability in the interior of a general container. The model illustrates that wall-mode convection is a multiscale phenomenon where the dynamics of the bulk interior diagnostically determine the small-scale dynamics within Stewartson boundary layers at the sidewalls. The sidewall boundary layers feedback on the interior via a nonlinear lateral heat-flux boundary condition, providing a closed system. Outside the asymptotically thin boundary layer, the convective modes connect to a dynamical interior that maintains scales set by the domain geometry. The final system of equations resembles boundary-forced planetary geostrophic baroclinic dynamics coupled with barotropic quasi-geostrophic vorticity. The reduced system provides a new avenue for investigating wall-mode convection in the strongly nonlinear regime. We also derive the dominant Ekman-flux correction to the onset Rayleigh number for large Taylor number, $Ra \approx 31.8\, Ta^{1/2} - 4.43\, Ta^{5/12} + O(Ta^{2/3})$ for no-slip boundaries. However, we find that the linear onset in a finite cylinder differs noticeably compared to a Cartesian channel. We demonstrate some of the reduced model's nonlinear dynamics with numerical simulations in a cylindrical container.

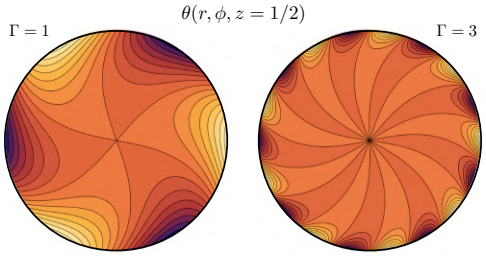

Figure 1: Midplane linear temperature perturbations at aspect ratio $\Gamma = 1$ (left) and $\Gamma = 5$ (right).

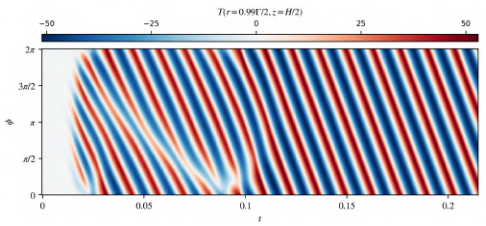

Figure 2: Temperature space-time propagation diagram at $R/R_c = 2$ with no-slip boundaries.

References

Vasil G.M., Burns, K. J., Lecoanet, D., Oishi, J. S., Brown, B. P., & Julien, K. "Rapidly Rotating Wall-Mode Convection", *J. Fluid Mech, in review*. arxiv:2409.20541

*Corresponding author: jeff.oishi@unh.edu
[†]University of New Hampshire, Durham, NH USA
[‡]University of Edinburgh, Edinburgh, UK
[§]Massachusetts Institute of Technology, Cambridge, MA USA
[¶]Northwestern University, Evanston, IL USA
[‖]Universty of Colorado, Boulder, CO USA
**Deceased

Non-linear instabilities in stratified Taylor-Couette flow

Junho Park*†, Abhishek Kumar†, Jacopo Gianfrani†

It is not uncommon for various naturally-occurring and engineering flow systems to have stratification of density or temperature along the vertical direction of gravity. Taylor-Couette flow with stable stratification along the vertical/axial direction has served as a laboratory model for complex flow systems as the flow allows us to investigate effectively how a complex interplay between stratification and rotation in shear flow leads to instability and turbulence. The stratification plays a dual role in Taylor-Couette flow. On the one hand, it delays the onset of centrifugal instability (CI) and its transition to turbulence by suppressing the vertical motion of fluid (see e.g. Withjack and Chen , 1974; Boubnov *et al.*, 1995; Caton *et al.*, 2000). On the other hand, stratification can promote another type of instability called strato-rotational instability (SRI) as its restoring force can generate an inertia-gravity wave and the SRI can be triggered by a resonant interaction between the waves trapped near the two cylinders (see e.g. Yavneh *et al.*, 2001; Shalybkov and Rüdiger , 2005). It is noteworthy that while the CI is characterised by a profile of rotation (i.e. a necessary condition for centrifugal instability is $\mu < \eta^2$ where $\mu = \Omega_o/\Omega_i$ and $\eta = R_i/R_o$ are the angular velocity and radius ratios, respectively) as it originates from the centrifugal imbalance, the SRI depends not on a rotation profile but on stratification as it originates from the resonance of inertia-gravity waves, which can be triggered when the stratification is sufficiently strong. This leads to our finding of SRI in centrifugally-stable regimes such as the Keplerian regime ($\mu \sim \eta^{3/2}$) or super-rotation regime ($\Omega_o > \Omega_i$) (Le Bars and Le Gal , 2007; Park and Billant , 2013; Ibanez *et al.*, 2016). There have been recent advances on further understanding on the dynamics of SRI such as a variant SRI due to a coupling with critical layers (Wang and Balmforth , 2018) or the SRI driven by centrifugal buoyancy (Lopez and Marques , 2020, 2022).

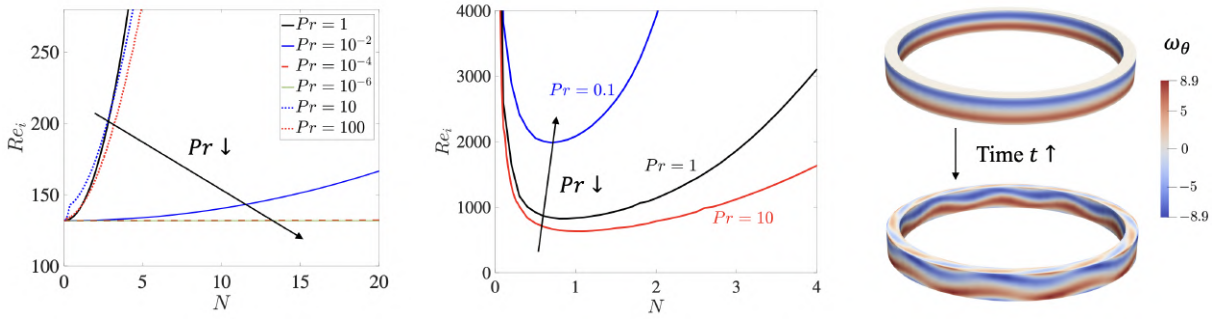

Figure 1: (Left) Neutral stability curves for centrifugal instability at $\eta = 0.9$ and $\mu = 0$. (Middle) Neutral stability curves for strato-rotational instability at $\eta = 0.9$ and $\mu = \eta^2$. (Right) Transition from axisymmtric Taylor vortices to wavy vortices via secondary instability at $N = 1$, $Re_i = 200$, $Pr = 0.01$.

Our work aims to address how the centrifugal and strato-rotational instabilities develop nonlinearly in Taylor-Couette flow when a fluid is stratified and thermally diffusive. We focus on the regime where the Prandtl number $Pr = \nu/\kappa$, which denotes a ratio between kinematic viscosity ν and thermal diffusivity κ, is low as $Pr < 1$. The low-Pr regime is of particular interest to astrophysicists due to its relevance to various astrophysical flows (see e.g. Garaud , 2021) From linear stability analysis, it is found that strong thermal diffusion with low Pr promotes centrifugal instability (Figure 1 left) while it delays strato-rotational instability (Figure 1 middle). Such a contrary role of thermal diffusion on these two instabilities is based on the dynamics in which stratification is favoured and disfavoured by SRI and CI, respectively, while the effect of stratification is suppressed by strong thermal diffusion.

*Corresponding author: junho.park@coventry.ac.uk
†Centre for Fluid and Complex Systems, Coventry University, Coventry, UK

At the 23rd ICTW in 2025, we will present details of how these instabilities change with thermal diffusion in both linear and non-linear regimes. Our recent work (Park , 2024) revealed how CI develops nonlinearly and leads to different stages: saturation, secondary instability or chaotic states, depending on the Prandtl number Pr, non-dimensional Brunt-Väisälä frequency N and Reynolds number Re_i. At a relatively low Pr in the range $10^{-3} < Pr < 1$ at $N = 1$, it is found that thermal diffusion delays the onset of secondary instability, which appears as non-axisymmetric wavy vortices (Figure 1 right). For lower $Pr < 10^{-3}$, the flow behaves as an unstratified Taylor-Couette flow due to the suppression of stratification effect by strong thermal diffusion. Chaotic flow states, a precursor to turblence, have also been examined in this work to unveil the non-linear dynamics of stratified Taylor-Couette flow. In the presentation, we will also present how SRI develops nonlinearly to secondary states (see also, Leclercq *et al.*, 2016; Lopez and Marques , 2022) and transitions to turbulent states when the Prandtl number Pr is low. Results from parametric investigations on SRI and subsequent flow patterns with varying Pr, N and Re and other parameters will also be presented. Furthermore, the Nusselt number Nu as a measure of the torque at the inner cylinder will be explored in wide parameter space for both CI and SRI to address how the angular momentum transport varies with instabilities and parameters.

References

Withjack, E. M. & Chen, C. F., "An experimental study of Couette instability of stratified fluids", *J. Fluid Mech.*, **66** 725–737 (1974).

Boubnov, B. M. & Gledzer, E. B. & Hopfinger, E. J., "Stratified circular Couette flow: instability and flow regimes", *J. Fluid Mech.*, **292** 333–358 (1995).

Caton, F. & Janiaud, B. & Hopfinger, E. J., "Stability and bifurcation in stratified Taylor-Couette flow", *J. Fluid Mech.*, **419** 93–124 (2000).

Yavneh, I. & McWilliams, J. C. & Molemaker, M. J., "Non-axisymmetric instability of centrifugally stable staratified Taylor–Couette flow", *J. Fluid Mech.*, **448** 1-–21 (2001).

Shalybkov, D. & Rüdiger, G., "Stability of density-stratified viscous Taylor–Couette flows", *A&A*, **438** 411-–417 (2005).

Le Bars, M. & Le Gal, P., "Experimental Analysis of the Stratorotational Instability in a Cylindrical Couette Flow", *PRL*, **99** 064502 (2007).

Park, J. & Billant, P., "The stably stratified Taylor-Couette flow is always unstable except for solid-body rotation", *J. Fluid Mech.*, **725** 262-–280 (2013).

Ibanez, R. & Swinney, H. L. & Rodenborn, B., "Observations of the stratorotational instability in rotating concentric cylindres", *Phys. Rev. Fluids*, **1** 053601 (2016).

Wang, C. & Balmforth, N. J., "Strato-rotational instability without resonance", *J. Fluid Mech.*, **846** 815–833 (2018).

Lopez, J. M. & Marques, F., "Impact of centrifugal buoyancy on strato-rotational instability", *J. Fluid Mech.*, **890** A9 (2020).

Lopez, J. M. & Marques, F., "Stratified Taylor-Couette flow: nonlinear dynamics", *J. Fluid Mech.*, **930** A2 (2022).

Garaud, P., "Journey to the center of stars: The realm of low Prandtl number fluid dynamics", *Phys. Rev. Fluids*, **6** 030501 (2021).

Park, J., "Centrifugal instability of Taylor-Couette flow in stratified and diffusive fluids", submitted to *J. Fluid Mech.*, (2024).

Leclercq, C. & Partridge, J. L. & Augier, P. & Caulfield, C. P. & Dalziel, S. B. & Linden., P. F., "Nonlinear waves in stratified Taylor–Couette flow. Part 1. Layer formation", arXiv:1609.02885, (2016)

Experimental and numerical investigation of multi-humped mode-2 internal solitary waves

Niraj Kr Prasad*[†], Alex Doak[‡], Ricardo Barros[§], Paul A Milewski[¶], Magda Carr[‖]

Internal solitary waves (ISWs) are solitary waves that occur within stably stratified water columns where density changes are due to changes in temperature or salinity or both. The pycnocline, where density changes relatively quickly with depth, acts as a wave guide for such internal wave motion. ISWs are characterized by different modes. Mode-1 ISWs are the most frequently observed mode, and they displace isopycnals in one direction only (depression or elevation). Mode-2 ISWs displace isopycnals in two directions and are characterized by concurrent elevation and depression of isopycnals into the upper and bottom layers respectively. Mode-2 ISWs are commonly observed as convex bulges propagating along the pycnocline, but recent studies have suggested the presence of other types of profiles.

Strongly nonlinear theory of large amplitude ISWs has reported a unique class of mode-2 ISWs characterized by multi-humped profiles (Doak,2022). So far, limited investigations have been made of these unique mode-2 waves. Thus, experimental and numerical studies were performed to investigate the physical generation of such waves. Simulations were performed on an open-source solver, Spectral Parallel Incompressible Navier-Stokes solver (SPINS) (Subich,2013) to observe the formation of mode-2 waves with double, triple, and quadruple humped profiles. A numerical domain mimicking the laboratory wave flume was used. The computational domain represents a rectangular flume filled with fluids of three different densities (ρ_1, ρ_2, ρ^*). The domain was divided into two parts of length l_g (Domain 1) and l_m (Domain 2) by a partition (gate). The two portions of the computational domain were filled with different thicknesses of the fluid layer of density of ρ^*. The difference in the thickness of the said layer generates the mode-2 waves. Free-slip boundary conditions were applied at the top and bottom boundary. The thickness of each fluid layer for the present numerical investigation is shown in Fig. 1. The domain was discretized into 1024 $\times$ 256 grid elements. The values of the parameters taken for the study are ρ_1 = =1025 kg/m^3, $\nabla\rho$ = 0.024, l_g = 30 cm and h = 40 cm.

.

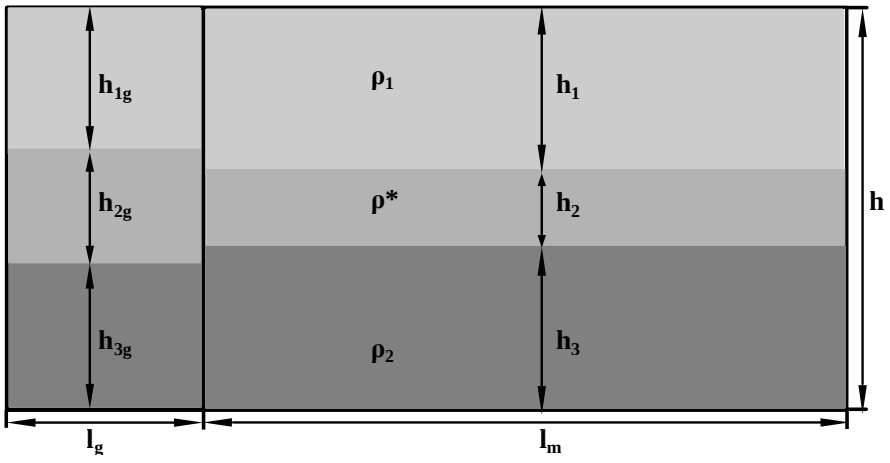

Figure 1: Computational domain mimicking the laboratory wave flume

*Corresponding author: niraj.prasad@newcastle.ac.uk
[†]Newcastle University, UK
[‡]Univesity of Bath, UK
[§]Loughborough University, UK
[¶]Penn State University, USA
[‖]Newcastle University, UK

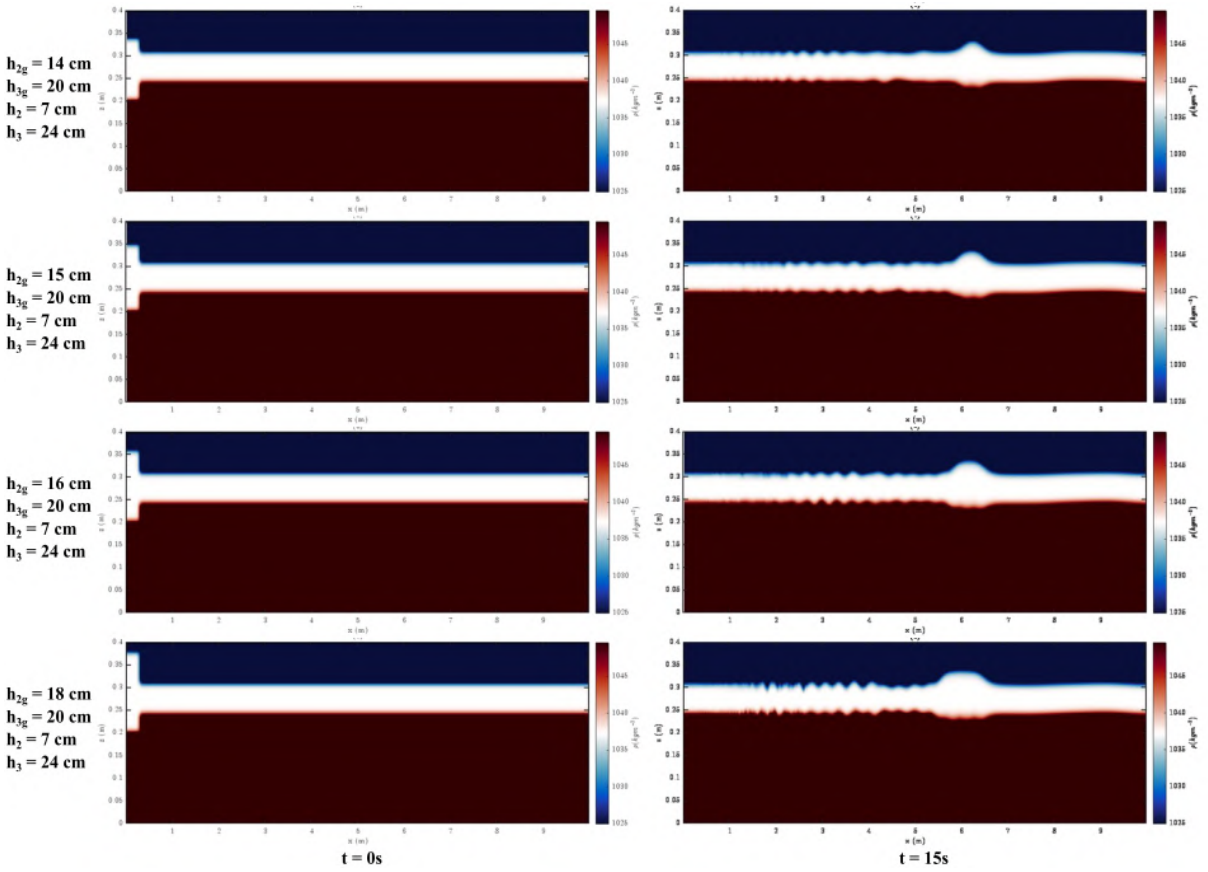

Figure 2: Map showing the effect of generating volume thickness (h_{2g}) on morphology of mode-2 waves

The water column was stably stratified, and a lock release method used to generate the ISWs due to buoyancy adjustment. Simulation results revealed that the mode-2 wave profile changes from double to triple hump when the wave generating volume behind the lock increases (Fig. 2). Furthermore, the waves generated were more stable when the pycnocline in the main part of the domain was at a higher distance from the bottom of the domain. The effect of offsetting the generating volume from alignment with the pycnocline in the main section of the flume was investigated and shown to be crucial in generating multi-humped waves. Preliminary experimental investigation in a 7m long wave flume has taken place and results will be presented to illustrate the physical flow.

References

[Doak,2022] Doak, Alex, Ricardo Barros, and Paul A. Milewski. "Large mode-2 internal solitary waves in three-layer flows." Journal of Fluid Mechanics 953 (2022): A42.

[Subich,2013] Subich, Christopher J., Kevin G. Lamb, and Marek Stastna. "Simulation of the Navier–Stokes equations in three dimensions with a spectral collocation method." International Journal for Numerical Methods in Fluids 73.2 (2013): 103-129.

From internal waves to turbulence in a stably stratified fluid

C. Rodda*†, C. Savaro‡, V. Bouillaut†, P. Augier†, J. Sommeria†, T. Valran†, S. Viboud†, N. Mordant†

We report on the statistical analysis of stratified turbulence forced by large-scale waves. The setup mimics some features of the tidal forcing of turbulence in the ocean interior at submesoscales. Our experiments are performed in the large-scale Coriolis facility in Grenoble, which is 13 m in diameter and 1 m deep. Four wave makers excite large-scale waves of moderate amplitude. In addition to weak internal wave turbulence at large scales, we observe strongly nonlinear waves, the breaking of which triggers intermittently strong turbulence at small scales. A transition to strongly nonlinear turbulence is observed at smaller scales. Our measurements are reminiscent of oceanic observations. Despite similarities with the empirical Garrett and Munk spectrum that assumes weak wave turbulence, our observed energy spectra are rather to be attributed to strongly nonlinear internal waves.

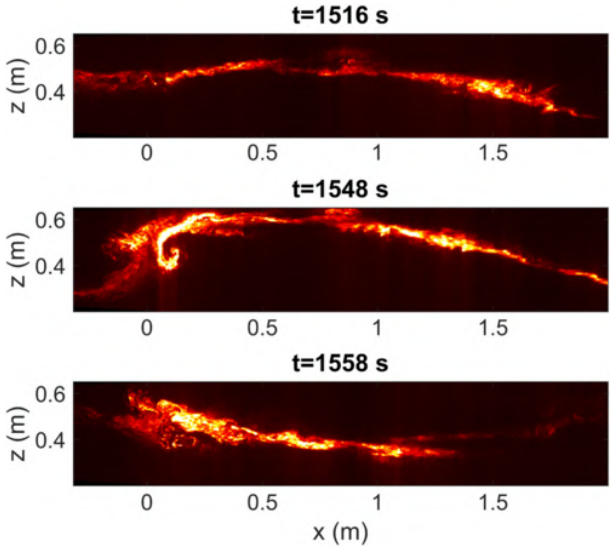

Figure 1: Snapshots in a vertical plane of a volumetric laser scan of a fluorescent dye layer showing a overturning internal wave.

References

Costanza Rodda, Clément Savaro, Vincent Bouillaut, Pierre Augier, Joël Sommeria, Thomas Valran, Samuel Viboud, Nicolas Mordant. "From Internal Waves to Turbulence in a Stably Stratified Fluid", *Phys. Rev. Lett.*, **131(26)**.

Costanza Rodda, Clément Savaro, Géraldine Davis, Jason Reneuve, Pierre Augier, Joël Sommeria, Thomas Valran, Samuel Viboud, Nicolas Mordants. "Experimental observations of internal wave turbulence transition in a stratified fluid." *Phys. Rev. Fluids*, **7(9)**.

*Corresponding author: c.rodda@imperial.ac.uk
†Imperial College London, London, UK
‡University of Grenoble Alpes, France

Data-Driven Numerical Investigation of Dielectrophoretic Force-Enhanced Annular Flows

J. Roller*†, M.H. Hamede‡, A. Meyer§, Ch. Egbers‡, V. Heuveline†

The enhancement of heat transfer in dielectric fluids by electric fields has raised the interest of researchers in both fundamental and applied fields over the past decades. In this study, we investigate the comparison between experimental and numerical dynamics of a fluid between two concentric, differentially heated cylinders where a high-frequency electric voltage is applied to the inner cylinder, while the outer cylinder is grounded. This setup induces the dielectrophoretic (DEP) force, creating an additional source of buoyancy along with Earth's gravity. We refer to the corresponding partial differential equation (PDE) model as the thermal electrohydrodynamical (TEHD) Boussinesq equations. The complex PDE model – usually three-dimensional and instationary – leads to challenging and CPU-intensive computations, which we address with tailored finite element method (FEM) discretizations and solvers.

Our contribution is focused on two particular sets of experiments. In the first set, the horizontally aligned cylinders remain at rest. We could demonstrate numerically that the heat transfer is enhanced by the DEP force. Upon a sufficient voltage increase, the two-dimensional base flow destabilizes and becomes fully three-dimensional. The destabilization of the base flow is beneficial as it is closely related to a further jump in the heat transfer. As seen in figure 1, we could verify a close match between numerical and experimental data (Hamede et al., 2024). We achieved this level of agreement in part by calibration of the computational model using experimental results. The experimental-numerical match gives credence to our above statements about the heat transfer, as it is a quantity that could only be evaluated numerically. The second set of experiments concerns vertically aligned cylinders. Here, the unicellular base flow can also be destabilized by a sufficient voltage, producing columnar vortices with a corresponding increase in heat transfer (Seelig et al., 2019). When the inner cylinder is set to rotate, the voltage threshold required for destabilization changes. We intend to compute such threshold numerically and compare with the values obtained from the associated physical experiment. Based on an adequate calibration, we aim to provide reliable numerical methods in the context of the highly challenging problems in TEHD flows.

References

Hamede, M. H., & Roller, J., & Meyer, A., & Heuveline, V., & Egbers, Ch. (2024). "Dielectrophoretic force-enhanced thermal convection within a horizontal cylindrical annulus", *Phys. of Fluids*, **36** 124106.

Seelig, T. & Meyer, A. & Gerstner, P. & Meier, M. & Jongmanns, M. & Baumann, M. & Heuveline, V., & Egbers, Ch. (2019). "Dielectrophoretic force-driven convection in annular geometry under Earth's gravity", Int. J. Heat Mass Transf., **139**, 386–398. https://doi.org/https://doi.org/10.1016/j.ijheatmasstransfer.2019.04.068

*Corresponding author: jonas.roller@uni-heidelberg.de
†Engineering Mathematics and Computing Lab, Heidelberg University, Heidelberg, Germany
‡Department of Aerodynamics and Fluid Mechanics, BTU Cottbus-Senftenberg, Cottbus, Germany
§LOMC, UMR6294, CNRS-Universite´ Le Havre Normandie, Le Havre

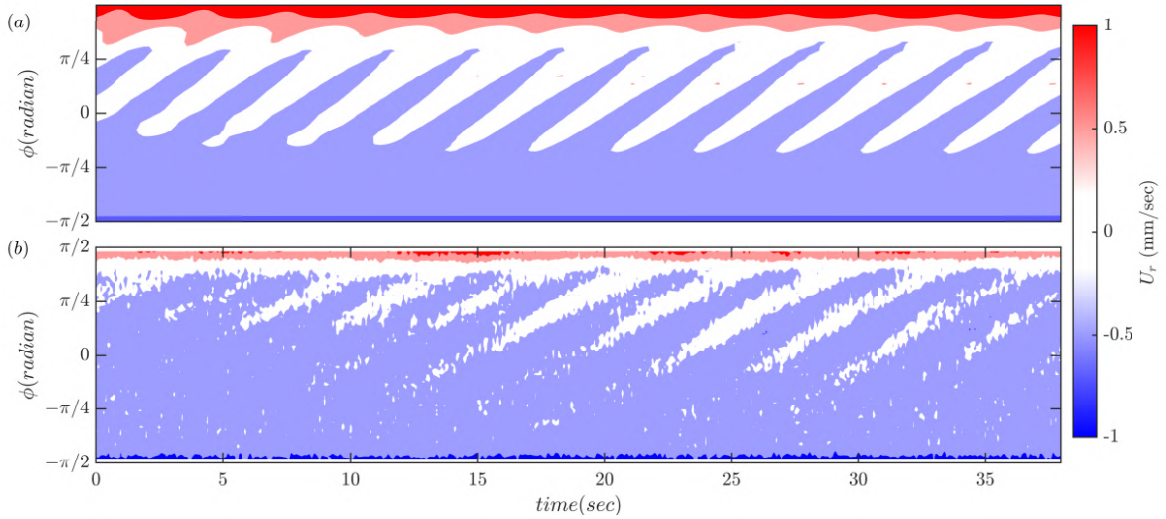

Figure 1: Space-time plots (*Hovmøller diagrams*) of the radial fluid velocity U_r at the mid-gap position between horizontally aligned cylinders. The velocities have been axially averaged and are presented here for different azimuthal positions. The lowest positional value $-\pi/2$ denotes the bottom of the annulus, while $\pi/2$ represents the top. Both plots correspond to a flow with temperature differential $\Delta T = 9K$ between the inner and outer cylinders and imposed peak voltage $V_p = 17\ kV$. The respective Rayleigh number is $Ra = \frac{\alpha g \Delta T d^3}{\nu \kappa} = 2.78 \times 10^4$, where d denotes the gap size. In plot (a) the velocities are calculated from numerical simulations, for (b) the velocities are obtained from experiments. A substantial qualitative and quantitative fit can be observed. This figure was originally published in (Hamede et al., 2024).

ICTW 2025 23rd INTERNATIONAL COUETTE-TAYLOR WORKSHOP 14th-16th JULY DURHAM, UK

Simultaneous Generation and Scattering of Internal Waves by Bottom Topography

Sai Saandeep Sampatirao*, Michael Allshouse†, Hanut Vemulapalli‡, Manikandan Mathur*§

The dissipation mechanisms of low-mode internal tides, which propagate far from their topographic generation sites, are crucial for understanding large-scale circulation and the energy budget in the ocean. Scattering by bottom topography is one of the identified pathways to dissipation [Johnston and Merrifield, 2003]. Modelling studies so far, have treated internal wave generation and scattering as independent problems, but in reality, they occur together. In this study, we model the combined effects of internal wave generation by a barotropic forcing and scattering of an incident mode-1 internal wave, at an isolated bottom topography in uniform stratification using a semi-analytical Green function approach. This approach was previously used to model topographic generation [Pétrélis et al., 2006] and scattering [Mathur et al., 2014] of internal waves. Four different parameters govern the problem - the non-dimensional topographic height (height ratio h^*) and slope (criticality ϵ), and the amplitude ratio of barotropic forging-to-incident mode-1 internal wave (U_0) and phase (Θ) of the barotropic forcing with respect to the incident mode-1 internal wave.

Figure 1 shows a schematic of the problem studied. A bottom topography of maximum height h_0 and criticality ϵ is present in an inviscid ocean of depth $H = h_0/h^*$. The topography experiences forcings from two sources: (i) a barotropic forcing modelled as a uniform oscillatory flow throughout the depth, and (ii) a baroclinic left-to-right mode-1 internal wave which is generated far away from the topography under consideration. The simultaneous presence of barotropic and baroclinic forcings results in a combined occurrence of internal wave generation and scattering. The boundary conditions are no normal flow on the rigid lid and no normal flow on the bottom topography and ocean floor.

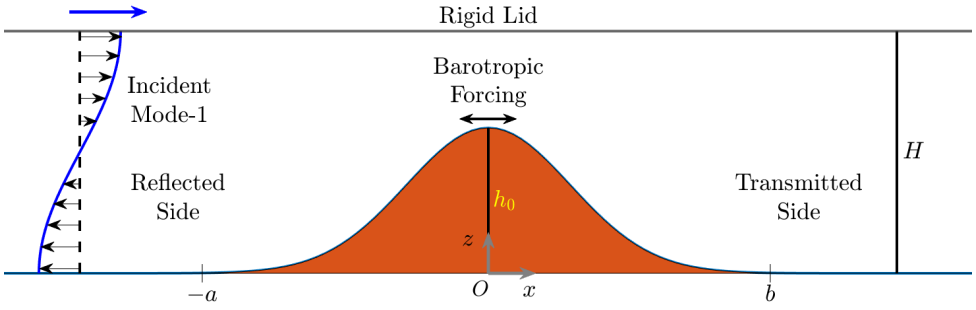

Figure 1: A schematic showing a bottom topography of height h_0 in an ocean of depth H, with a rigid lid representing the ocean surface. The forcing includes a barotropic oscillation and an incident baroclinic mode-1 internal wave, with a phase difference between the two.

The theory is first validated using numerical simulations. Figure 2 shows a snapshot of the horizontal velocity field (excluding the barotropic component) for topographic parameter values of $(h^*, \epsilon) = (0.3, 0.3)$. Figures 2(a) and (b) correspond to the individual generation only and scattering only problems. Figures 2(c) and (d) correspond to the combined forcing problems with phase differences $\Theta = 0, \pi$ respectively. The flow field in combined forcing problems has significant differences from the individual problems. We can also observe a noticiable difference in wavefields between $\Theta = 0$ and π. The snapshots from simulations (figures 2e

*Geophysical Flows Lab and Department of Aerospace Engineering, Indian Institute of Technology Madras, India
†Department of Mechanical and Industrial Engineering, Northeastern University, Boston, MA 02115, USA
‡Institute for Power Systems and High Voltage Technology, ETH Zürich, Switzerland
§Corresponding author: manims@smail.iitm.ac.in

and f) agree qualitatively and quantitaively with theory. We then proceed to do a detailed parameter sweep after validation with simulations.

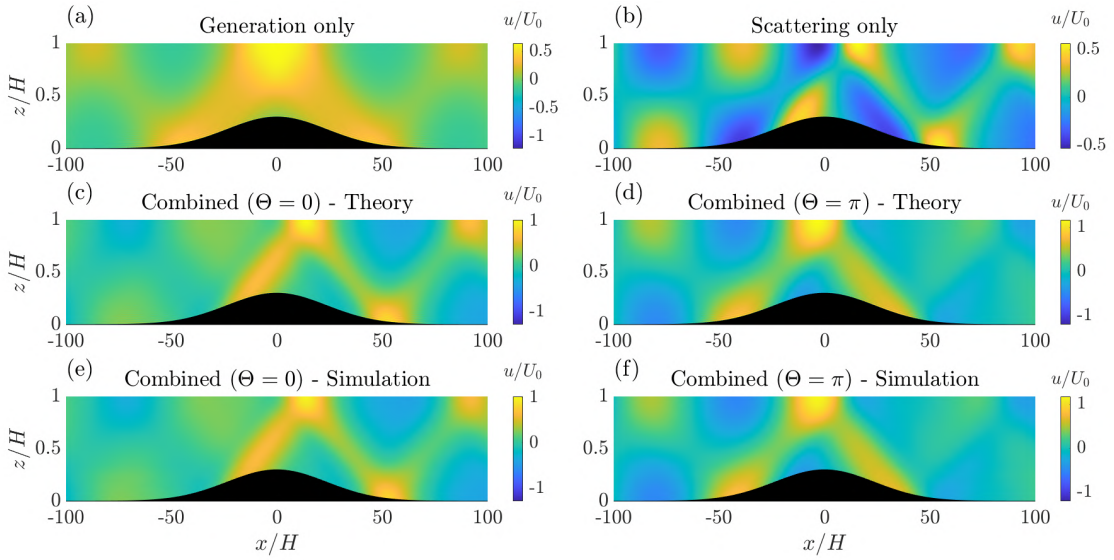

Figure 2: Snapshots of horizontal velocity (without the barotropic component) for (a) scattering only, (b) generation only, and combined scattering and generation with $U_0 = 2.79$ and (c) $\Theta = 0$, (d) $\Theta = \pi$. Figures (a) - (d) are based on Green function theory. (e)-(f) are same as (c)-(d), but based on numerical simulations. All the figures correspond to $(h^*, \epsilon) = (0.3, 0.3)$.

For a given topography and U_0, as Θ is varied, the energy flux of the combined forcing deviates significantly from mean value, which is the sum of the energy fluxes associated with generation in the presence of the barotropic forcing alone and the incident mode-1. This occurs for a wide range of topographies and forcing amplitudes. These deviations, which occur due to construction/destruction of individual modes, can lead to two scenarios: (i) additional or lower or no new internal wave generation, which can be interpreted as the influence of the incident internal wave on the internal wave generation, (ii) "loss" of incident internal wave energy to other forms, which can be interpreted as the influence of barotropic tide on the scattering. These energy flux gain or loss effects are typically predominant for short subcritical ($h^* \lesssim 0.4$, $\epsilon < 1$) and sufficiently steep, tall ($h^* \gtrsim 0.4$) topographies.

References

TM Shaun Johnston and Mark A Merrifield. Internal tide scattering at seamounts, ridges, and islands. *Journal of Geophysical Research: Oceans*, 108(C6), 2003.

Manikandan Mathur, Glenn S Carter, and Thomas Peacock. Topographic scattering of the low-mode internal tide in the deep ocean. *Journal of Geophysical Research: Oceans*, 119 (4):2165–2182, 2014.

François Pétrélis, Stefan Llewellyn Smith, and WR Young. Tidal conversion at a submarine ridge. *Journal of Physical Oceanography*, 36(6):1053–1071, 2006.

Transition to Turbulence in the Stokes Boundary Layer: Edge States and the Periodic Self-Sustaining Process

Jorge Sandoval*†, Tom Eaves†

The Stokes boundary layer is an oscillatory flow above an infinite plate, with oscillations driven either by (1) a transverse sinusoidal motion of the plate or (2) a sinusoidal applied pressure gradient. Beyond a critical Reynolds number of 2511, the laminar solution of the Stokes boundary layer is susceptible to linear instability. However, this instability is subcritical given that turbulence is observed for Reynolds numbers above approximately 700, despite the flow being linearly stable in this range.

The state space of a subcritical flow consists of two basins of attraction: that of the laminar flow and that of turbulence. A saddle point separates these basins, termed the 'edge state', and its codimension-one stable manifold termed the 'edge manifold', or simply 'edge'. The edge states may be found by 'edge tracking', an iterative procedure in which the trajectories of initial conditions on either side of the edge are computed and bisected.

Edge states in the Stokes boundary layer are composed of vortical structures of the same nature as canonical shear flows, namely streaks, rolls and waves (see Figure 1). For non-oscillating shear flows, these structures are known to coexist and mutually balance through a mechanism known as the Self-Sustained Process. However, in the Stokes boundary layer, these structures are inherently periodic and utilise the oscillating base flow in a novel way. Structures migrate upwards to align with the location of the maximum shear of the laminar velocity profile, and large-scale rolls form to periodically create new streaks near the wall. This talk will present these edge states in the Stokes boundary layer, compare them to their known non-oscillatory counterparts, and provide insights about their effects on momentum and energy transport among structures near the wall.

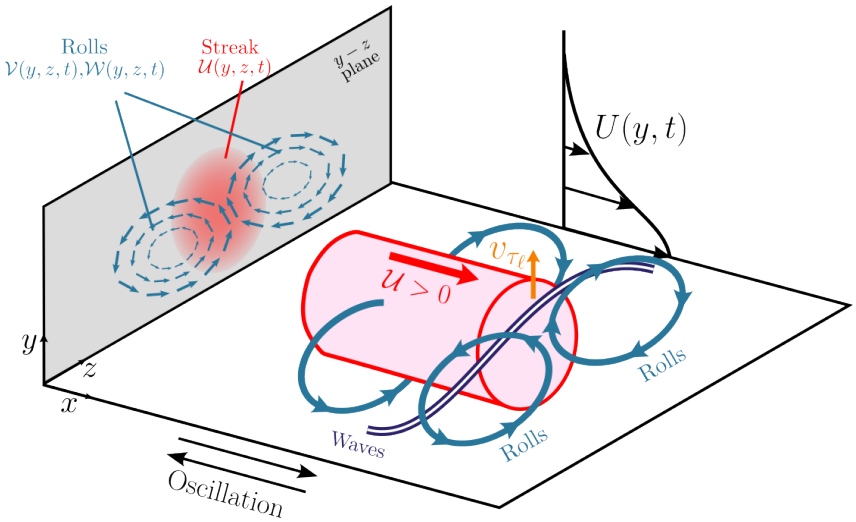

Figure 1: Schematic representation of the structures involved in the PSSP.

*Corresponding author: jsandoval@dundee.ac.uk
†University of Dundee, Dundee, UK

Role of interfacial surfactant and wall deformability on linear stability of film flows

G. Sharma[1 2], N. Jain[2]*, M. Baingne[3], D. S. Tomar[4]

Abstract

Liquid film flows find widespread applications in numerous technologies as well as in physiological flows such as in lung airways. A planar Newtonian liquid film falling down a rigid inclined plane becomes unstable above a critical Reynolds number (Re) for long-wave disturbances, and this long-wave instability is referred as gas-liquid (GL) free-surface mode (Yih, 1963). In contrast to the planar liquid films, a cylindrical Newtonian liquid film lining inside of a tube exhibits Rayleigh-Plateau (RP) capillary instability in creeping flow limit for long-wave disturbances. The effect of presence of interfacial surfactant is known to be stabilizing for both planar and cylindrical films on GL mode and RP mode, respectively (Craster & Matar, 2009). Further, an additional mode, known as surfactant mode, appears in presence of interfacial surfactant. This surfactant mode is known to remain stable for both planar and cylindrical films. For planar film, the stability of surfactant mode is established in presence/absence of basic flow. However, for cylindrical film, the surfactant mode stability is explored only for the case of a stationary film (i.e. zero basic flow). Here, we report the results for the linear stability of surfactant-laden Newtonian cylindrical film lining inside of a tube in presence of the basic flow (Figure-1). We demonstrate the differences that arise in the stability behavior of RP mode due to surfactant for a flowing film in comparison to a stationary film. More importantly, we show that the surfactant mode becomes unstable in presence of basic flow and can be the most unstable mode depending on process parameters. For surfactant-laden planar film falling down an inclined plane (Figure-1), we show that the stability behavior is dramatically affected when the inclined plane is coated with a soft solid layer.

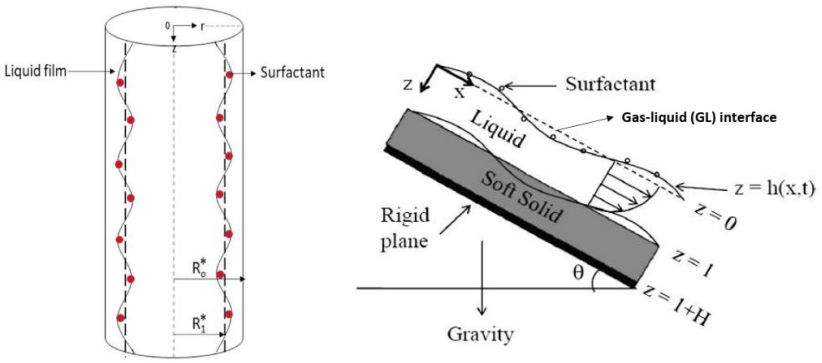

Figure-1: Schematic of cylindrical and planar film flow configurations.

We first present the results of surfactant-laden liquid film flowing inside of a tube. We have considered creeping flow limit and the relevant non-dimensional parameters are: (i) the mean gas-liquid interface location (R_1), (ii) Bond number ($Bo = \rho g h_0^2/\gamma_0^2$, where ρ is the density, h_0 is the film thickness, and γ_0 is the surface tension with constant mean surfactant concentration Γ_0) characterizing the strength of flow ($Bo = 0$ implies absence of basic flow), and (iii) Marangoni number ($Ma = E\Gamma_0/\gamma_0$) denoting the presence ($Ma \neq 0$) or absence of surfactant ($Ma = 0$). The early work on stationary film have shown that the surfactant reduces the growth rate of RP instability but is unable to completely eliminate it, and the surfactant mode always remain stable. In contrast, the present work demonstrated that the RP instability is completely suppressed and the surfactant mode becomes unstable when basic flow is incorporated in stability analysis (Jain, Sharma & Das, 2022). Figure-2 shows the growth rate vs.

[1] Corresponding author: gaurav.sharma@ch.iitr.ac.in
[2] Indian Institute of Technology Roorkee, Roorkee, Uttarakhand, India. * Currently at Anton Paar, India.
[3] Babasaheb Ambedkar University, Raigad, Maharashtra, India
[4] Lovely Professional University, Jalandhar, Punjab, India

wavenumber data for both RP and surfactant modes. This clearly demonstrates that the RP instability is completely suppressed when Ma increases above a threshold value for non-zero Bond number. In contrast, the surfactant mode exhibits significant positive growth rates (i.e. unstable) for any non-zero Ma. Further, this surfactant-mode instability starts from low-wavenumber and extends to sufficiently high wavenumbers. In fact, the highest growth rates are observed for wavenumbers greater than unity, and thus, there is a shift in nature of instability from long-wave to finite-wave dominated instability in presence of flow (due to excitation of surfactant mode instability). We have also carried out a long-wave asymptotic analysis which helps us to elucidate the mechanism behind the surfactant mode instability in presence of basic flow.

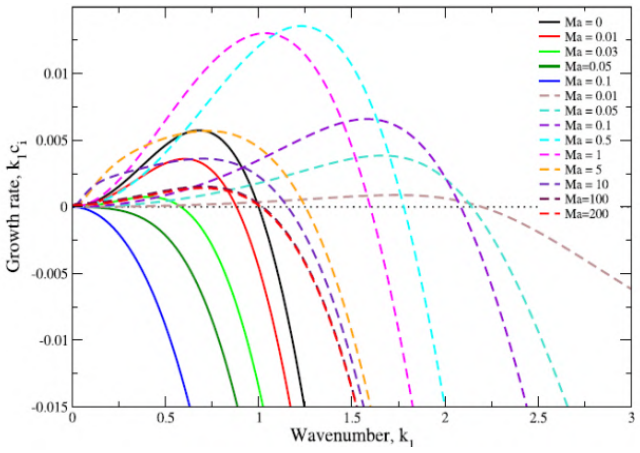

Figure-2: Growth rate vs. wavenumber data for RP (continuous line) and surfactant mode (dashed line) for $R_1 = 0.7,\ Bo = 1$ at different values of Ma.

We now discuss the effect of presence of soft solid coating on the stability of surfactant-laden planar film flowing down an inclined plane (Tomar, Baingne & Sharma, 2017). In absence of soft solid coating, the GL interface remains stable for $Re = 0$, and the surfactant mode has been shown to remain stable for zero/non-zero Reynolds number. We have shown that the presence of soft solid layer triggers the surfactant mode instability even for $Re = 0$ when the wall deformability parameter ($G = \mu V/ER$) increases above a critical value (refer Figure-3). It is important to note that the GL interface allows two modes: GL mode and surfactant mode, and one additional mode called as liquid-solid (LS) mode also appears because of the presence of a deformable LS interface. Figure-3 shows that the LS mode becomes unstable at higher values of G than required for triggering surfactant mode instability. Thus, in creeping flow limit, the wall-deformability induced surfactant mode remains the most dominant mode for the system. For $Re \neq 0$, the GL mode instability becomes operational, and it has been shown that the presence of soft solid coating can suppress this GL mode instability without exciting surfactant or LS modes. For example, Figure-4 shows that the region between upper and lower neutral curves, the GL interface is stabilized by soft solid coating while all other modes remaining stable. Thus, this work shows the dual role of soft solid coating for surfactant-laden planar films.

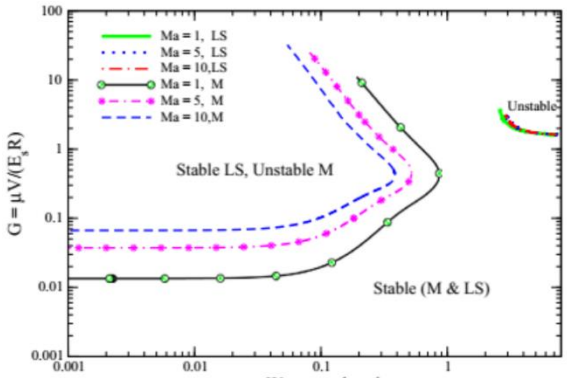

Figure-3: Neutral curves showing destabilization of surfactant mode for $H = 5, Re = 0, \theta = 45^o$

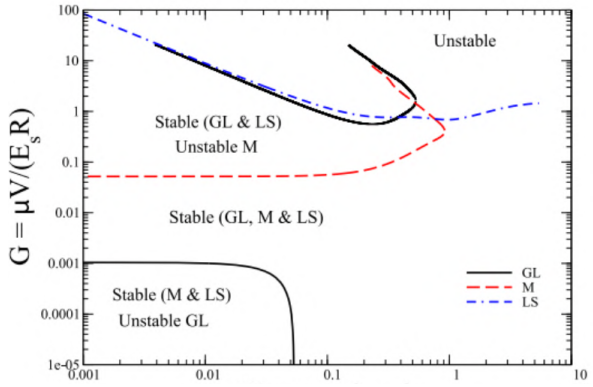

Figure-4: Neutral curves showing stabilization of film flow for $H = 2, Re = 1.5, Ma = 025, \theta = 45^o$

References

Craster, R.V., and Matar, O.K. "Dynamics and stability of thin liquid films", Rev. Mod. Phys. 81, 1131-1198, 2009.

Jain, N., Sharma, G. & Das, S. "Instability of liquid film flow inside of a vertical tube in presence of an interfacial surfactant", Phys. Rev. E, 106, 055101, 2022.

Tomar, D.S., Baingne, M. & Sharma, G. "Stability of gravity-driven free surface flow of surfactant-laden liquid film flowing down a flexible inclined plane", Chem. Engg. Sc., 165, 216-228, 2017.

Yih, C.S. "Stability of liquid flow down an inclined plane", Phys. Fluids, 6, 321-334, 1963.

Hagen-Poiseuille Flow in the pipe layered by porous medium is linearly unstable

Ajay Sharma *, P. Bera*† and Gaurav Sharma*

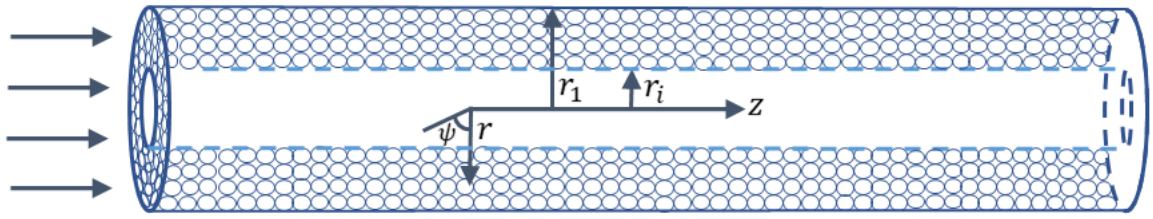

Figure 1: Physical sketch of the dimensional flow domain

The long-standing linearly stable Hagen-Poiseuille flow is shown to become unstable when a low-permeable porous medium layers the inner surface of the pipe (Reynolds, 1883). The configurational layout for the current problem as shown in Figure 1, comprises of a long pipe of radius r_1 with the inner surface layered by the fluid-saturated porous medium. The interface is located at $r = r_i$. The flow is driven by an external pressure gradient in the axial direction. An unsteady Darcy's law is used to model the Newtonian fluid flow inside the porous domain (Nield & Bejan, 2017). The instability of the system is governed by five key dimensionless parameters: the thickness ratio ($\hat{t}$), Darcy number (Da), Reynolds number (Re), porosity (ϵ), and the Beaver-Joseph interfacial slip-constant (α_{BJ}). The D^2-Chebyshev-spectral-collocation method is utilized to determine the instability boundary numerically, in terms of Re_c as a function of Da, $\hat{t}$ and α_{BJ}, while fixing the porosity at 0.3 (Chen & Chen, 1989).

The analysis indicates that depending upon the media permeability, a threshold value of the fluid layer thickness exists below which the onset of instability occurs under axisymmetric disturbances, whereas above the threshold value, the same occurs under non-axisymmetric disturbance. In the former case, the instability is induced due to the interaction of the dynamics of base flow with the porous layer and leads to the porous mode of instability. The latter case is due to the combined effect of Reynolds stress in the fluid regime and slip porous boundary at the interface, and gives rise to the fluid mode of instability. For instance, when the Darcy number and Beavers-Joseph slip coefficient are fixed at $Da = 10^{-6}$ and $\alpha_{BJ} = 0.1$, respectively, the threshold value of $\hat{t}$, at which the instability mode changes is around 0.0336. Our results show that the threshold value of $\hat{t}$ increases monotonically with an increase in Da. In the fluid mode, energy production due to Reynolds stress is balanced by energy loss via viscous dissipation, whereas in the porous mode, the same is balanced mainly by combined energy loss via surface drag and work done at the interface (Boomkamp & Miesen, 1996). In addition, keeping the thickness of porous region fixed, the fluid layer thickness for which almost similar instability characteristics are found varies directly as the square root of media permeability. Our rigorous analysis also shows that α_{BJ} destabilizes the flow, and the onset of instability takes place at a Reynolds number as small as 695, when $Da = 10^{-6}, \alpha_{BJ} = 0.3$ and $\hat{t} = 0.016$. Furthermore, an increase in α_{BJ} invites the fluid mode of instability for a relatively low values of fluid layer thickness. The present study is the first to demonstrate that the fluid-porous interface can render the system linearly unstable when the flow in porous layer is modelled using unsteady Darcy's law, which is otherwise stable under rigid and impermeable conditions.

*Indian Institute of Technology, Roorkee, Roorkee, India
†Corresponding author: p.bera@ma.iitr.ac.in

References

Reynolds, O. 1883. "Stability of a Viscous Liquid contained between Two Rotating Cylinders", *Proc. R. Soc. London A*, **223** 84–99.

Chen, F. & Chen, C. F. 1989. "Experimental investigation of convective stability in a superposed fluid and porous layer when heated from below", *J. Fluid Mech.*, **207** 311–321.

Nield, D. A. & Bejan A. 2017. "Convection in porous media", *Springer*.

Boomkamp, P. & Miesen, R. 1996. "Classification of instabilities in parallel two-phase flow", *Int. J. Multi. Flow*, **22** 67–88.

Centrifugal Convection

Zhongzhi Yao, Mohammad S. Emran, Andrei Teimurazov, & Olga Shishkina*†

We study Centrifugal Convection (CC) in an annular container, heated at the outer sidewall and cooled at the inner wall, under constant vertical-axis rotation. For a container of a fixed size and a given fluid, the strengths of centrifugal and thermal driving in such a system are characterized, respectively, by the dimensionless Froude number Fr and Rayleigh number Ra.

The setup considered in our Direct Numerical Simulations (DNS) (Yao et al., 2025) mimics the Annular Centrifugal Rayleigh–Bénard Convection (ACRBC) experiments conducted in C. Sun's lab at Tsinghua University (Jiang et al., 2020, 2022), and the studied parameter range spans from 0 to 100 for Froude number and from about 10^5 to 10^9 for Rayleigh number. As Fr increases from 0 (no rotation) to 100 (strong centrifugal buoyancy) at a fixed value of Ra, the global flow structure and heat transport scaling transition from those typical in vertical convection, where the temperature gradient is orthogonal to the gravitational buoyancy force, to those typical in Rayleigh–Bénard convection, where the gradient aligns with centrifugal buoyancy. With increasing centrifugal buoyancy, the flow first transitions from a quasi-two-dimensional $(r-z)$ through fully three-dimensional to another quasi-two-dimensional $(r-\phi)$ global flow structure, which is characterized by reduced vertical mixing in accordance with the Taylor-Proudman theorem. To trigger the latter transition, for higher Ra values, larger Fr values are generally required.

Although the CC system gets closer to the Rayleigh–Bénard (RB) system for large Fr and Ra, there are still several principal differences between them. These differences are reflected in a generally higher mean temperature in CC compared to RB (even in the fully Oberbeck–Boussinesq case), which is caused by the CC container geometry, and by generally earlier transition to the ultimate regime (Lohse and Shishkina, 2024) in CC, caused by the additional shear in CC due to the gravitational buoyancy. The similarities and differences between the RB and CC systems are discussed in the talk.

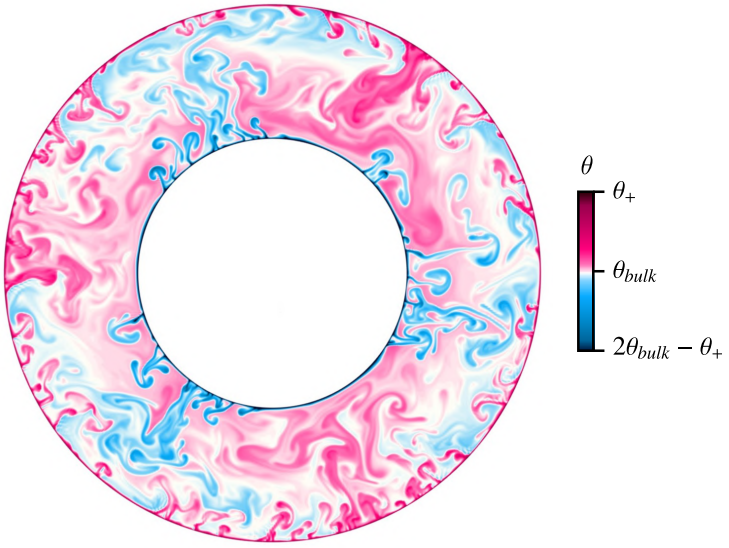

Figure 1: Instantaneous flow structure obtained in the DNS for $Ra = 8.88 \times 10^8$, $Fr = 6.53$, visualised with horizontal cross-section of the temperature field at the mid plane.

*Corresponding author: Olga.Shishkina@ds.mpg.de
†Max Planck Institute for Dynamics and Self-Organization, Göttingen, 37077 Germany

The authors acknowledge the financial support from the Deutsche Forschungsgemeinschaft under the grants Sh405/20, Sh405/22 and the China Scholarship Council (CSC) under grant No. 202208460009.

References

Yao, Z., Emran, M.S., Teimurazov, A., & Shishkina, O. "Direct numerical simulations of centrifugal convection: From gravitational to centrifugal buoyancy dominance", *Int. J. Heat Mass Transfer*, **236** 126314 (2025).

Jiang, H., Zhu, X., Wang, D., Huisman, S. G., & Sun, C. "Supergravitational turbulent thermal convection", *Sci. Adv.*, **6** (40) eabb8676 (2020).

Jiang, H., Wang, D., Liu, S., & Sun, C. "Experimental evidence for the existence of the ultimate regime in rapidly rotating turbulent thermal convection", *Phys. Rev. Lett.*, **129** (20), 204502 (2022).

Lohse, D., & Shishkina, O. "Ultimate Rayleigh–Bénard turbulence", *Rev. Modern Physics*, **96** (3), 035001 (2024).

Enhancement of heat transfer due to the thermoelectrohydrodynamic (TEHD) force in a cylindrical annulus under μg conditions.

Y. Sliavin*†, M. H. Hamede†, V. Motuz†, A. Meyer‡, Ch. Egbers†

The effect of the dielectrophoretic force on a dielectric fluid's flow under microgravity conditions was experimentally examined during parabolic flight campaigns. The fluid is confined in a vertically aligned, differentially heated cylindrical annulus and is subjected to an alternating electric field (200 Hz) during repeated 22-second microgravity intervals. The combined effect of permittivity stratification due to the radial temperature gradient and of the electric field inhomogeneity due to curvature induces an artificial radial buoyancy that is able to trigger the so-called thermoelectric instability (1). The flow field is quantitatively analyzed using two-plane Particle Image Velocimetry (PIV), with one axial plane and two radial planes located at the top and bottom of the cell. This multiplane arrangement offers valuable spatial information on the evolution of flow structures during the microgravity intervals, providing a more comprehensive view compared to single-plane measurements. In addition, a heat flux measurement system was used for the first time.

The experiments focused on the onset and saturation of the instability, examining the effects of varying aspect ratios ($\Gamma = 10, 15, 20$) and initial flow conditions upon entering the microgravity phase (2). The results demonstrated that breaking the initial convective cells via controlled mixing during the hypergravity phases leads to homogenization of the fluid and accelerates the transition to instability (Figure 1). In addition, it was shown that the effect of the top and bottom boundaries of the cell stabilizes the flow. Indeed, for the same forcing parameters, the instability arises and saturates faster for cells with higher aspect ratios. Complementary, heat flux measurements provided new insights into the interplay between thermal and electrical driving forces, allowing for a comprehensive characterization of the instability and served as clear evidence of heat flux modification.

These findings advance the understanding of thermoelectrohydrodynamic instabilities in microgravity, offering valuable benchmarks for comparison with theoretical predictions and future experimental designs.

References

[1] Harunori N. Yoshikawa, Olivier Crumeyrolle, Innocent Mutabazi, Dielectrophoretic force-driven thermal convection in annular geometry. *Physics of Fluids*, 25, 2, (2013), 10.1063/1.4792833.

[2] Antoine Meyer, Olivier Crumeyrolle, Innocent Mutabazi, Martin Meier, Marcel Jongmanns, Marie-Charlotte Renoult, Torsten Seelig, Christoph Egbers, Flow Patterns and Heat Transfer in a Cylindrical Annulus under 1g and low-g Conditions: Theory and Simulation. *Microgravity Science and Technology*, 30 (2018), 10.1007/s12217-018-9636-3.

*Corresponding author: Yaraslau.Sliavin@b-tu.de
†Department of Aerodynamics and Fluid Mechanics, BTU Cottbus-Senftenberg, Cottbus, Germany
‡LOMC, UMR6294, CNRS-Université Le Havre Normandie, Le Havre, France

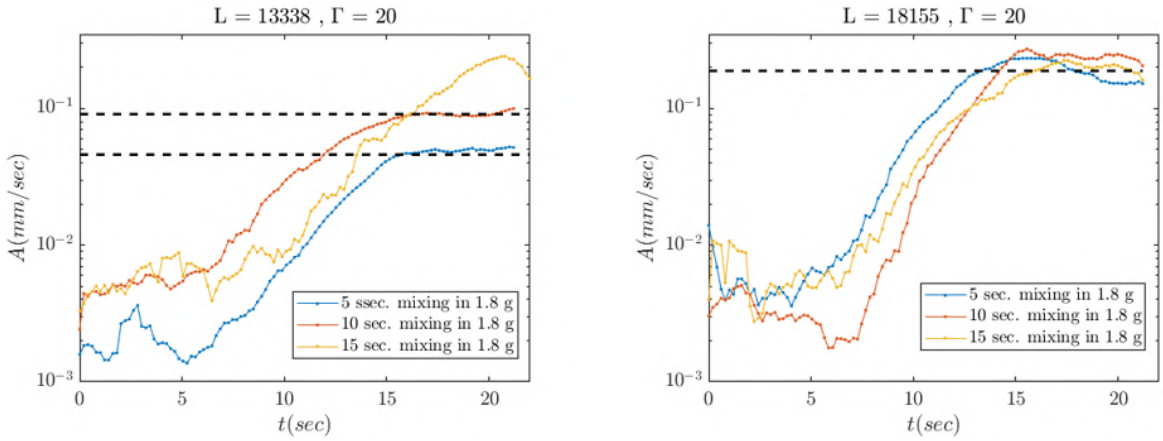

(a) (b)

Figure 1: Perturbation amplitude for aspect ratio $\Gamma = 20$ and (a) $L = 13338$ and (b) $L = 18155$, where $L = \frac{\alpha \Delta T \, g_e(\overline{R}) \, d^3}{\nu \kappa}$. For mixing times in hypergravity of 5s and 10s, instability reaches its saturation under the lower electric Rayleigh number, while for 15s, saturation is delayed. For the higher electric Rayleigh number (b), the instability reaches its saturation regardless of the mixing time length.

Dielectrophoretic-driven convection in the spherical shell

Y. Gaillard [*], P.S.B. Szabo[*†], C. Egbers

Laboratory investigations of large-scale flows in planetary atmospheres and interiors are often performed using cylindrical or spherical shell test beds that preserve the fundamental physical dynamics. AtmoFlow is one such experiment, designed with concentric spherical shells to simulate a planetary atmosphere, where thermal forcing is achieved through equatorial heating and polar cooling. Planetary rotation is given via shell rotation, while an artificial gravity-like force is generated by a central electric field. To eliminate buoyancy-driven natural convection, the experiment is scheduled to operate aboard the International Space Station (ISS) in 2026. The artificial central force, as described by Futterer et al. (Futterer , 2008), arises from a dielectrophoretic effect, which decreases with distance following a $1/r^5$ dependence. The resulting thermo-electrohydrodynamic (TEHD) convection has been previously explored in the Geophysical Flow Simulator (GeoFlow), an ISS-based experiment conducted from 2008 to 2017 to model geophysical flow phenomena. Building on the findings of Futterer et al. (Futterer , 2008), the present study focuses on the AtmoFlow experiment, which incorporates a spherical shell aspect ratio of $\eta = 0.7$ to investigate fundamental flow dynamics.

The principle of dielectrophoretic thermo-electrohydrodynamic (TEHD) convection can be described in a non-isothermal fluid that is subjected to an electric tension, which induces an intrinsic or externally generated inhomogeneous electric field, such as that arising from geometric curvature. The central force field driving this phenomenon is governed by Gauss's law and gives rise to convective flow analogous to Rayleigh-Bénard convection. By employing the continuity, momentum, and energy equations, a forcing parameter analogous to the Rayleigh number can be derived by

$$Ra_{\mathsf{E}} = \frac{\epsilon_0 \epsilon_{\mathsf{r}} \gamma_{\mathsf{e}} V_0^2}{2\rho_0 \nu \kappa}, \qquad \text{with} \quad \gamma_{\mathsf{e}} = e\Delta T \tag{1}$$

where ϵ_0 is the vacuum electric permittivity, ϵ_{r} the relative electric permittivity, γ_{e} the thermoelectric parameter, V_0 the applied electric tension, ρ_0 the reference density, ν the kinematic viscosity and κ the thermal diffusivity.

In this study, we expand the parameter space explored by Futterer et al. (Futterer , 2008) to investigate the flow fields within the parameter range of the AtmoFlow experiment, covering Ra_{E} values from 1×10^5 to 2×10^7. Three distinct flow regimes are identified: (1) a steady-state regime characterized by plume structures forming quadratic-shaped mode-6 patterns, (2) a transient periodic regime marked by the emergence of sheet-like structures and mode reduction, and (3) an irregular regime distinguished by structural variations and fluctuations in mode amplitude, which form clusters that diminish as Ra_{E} increases.

Quantitative analysis based on integral values indicates that the Nusselt number (Nu) increases with both Ra_{E} and γ_{e}. However, the kinetic energy (E_{kin}) does not scale linearly with the forcing, highlighting the presence of non-linear energy dissipation. Comparisons with the findings of Moore and Weiss (Moore , 1973) reveal similar, though not identical, trends in Nu. Steady-state simulations demonstrate good agreement with GeoFlow results when normalized by the critical Rayleigh number. Additionally, regime transition thresholds are broadly consistent with those reported by Futterer et al. (Futterer , 2008), with slight discrepancies attributed to differences in the definitions of transient and irregular regimes, as well as the incorporation of a temperature-sensitive Gauss equation in this study to account for thermal feedback effects.

The relationship between Nu and E_{kin} demonstrates independence from both the Prandtl number and the aspect ratio, in line with previous observations by Futterer et al. (Futterer , 2013). This investigation provides novel insights into the dynamics of thermoelectrohydrodynamic (TEHD) convection in spherical shells, its heat transport mechanisms and offering valuable implications for the experimental study of geophysical flow phenomena in small-scale laboratory experiments.

*Department of Aerodynamics and Fluid Mechanics, Brandenburg University of Technology Cottbus-Senftenberg, Siemens-Halske-Ring 15a, 03046 Cottbus, Germany

†Corresponding author: peter.szabo@b-tu.de

Acknowledgement

The AtmoFlow project is supported by the BMWi via the German Space Administration (Deutsches Zentrum für Luft- und Raumfahrt) under Grant No. 50WP1709, 50WM1841, 50WM2141 and 50WM2441 and via the National High Performance Computing centre NHR with Grant No. bbi00021.

References

Futterer, B., Hollerbach, R., & Egbers, C. (2008, November). "GeoFlow: 3D numerical simulation of supercritical thermal convective states", *In Journal of Physics: Conference Series*, **137**, No. 1, p. 012026. IOP Publishing.

Moore, D. R., & Weiss, N. O. (1973). "Two-dimensional Rayleigh-Bénard convection", *Journal of Fluid Mechanics*, **58**(2), 289-312.

Futterer, B., Krebs, A., Plesa, A. C., Zaussinger, F., Hollerbach, R., Breuer, D., & Egbers, C. (2013). "TSheet-like and plume-like thermal flow in a spherical convection experiment performed under microgravity", *Journal of Fluid Mechanics*, **735**, 647-683.

Effective eddy viscosity profiles in viscoelastic Taylor-Couette flow

A. Takano[1 2], Y. Tasaka[2], Y. Murai[2]

We developed a method termed *"eddy viscosity profiler"* to quantify momentum transportation in turbulent flows for drag reduction studies. In such flows, additives such as polymers and bubbles modulate flows by altering the large-scale structures, which significantly affects friction characteristics. This method aims at evaluating the inter-scale dissipation from large-scales to smaller scales. Mean velocity profile is measured by the ultrasonic velocity profiler in Taylor Couette flow and substituted to the Reynolds-averaged Navier-Stokes (RANS) equation. The Reynolds shear stress is modeled by the eddy viscosity concept. In the derived equation, kinematic viscosity, mean velocity and eddy viscosity remain as unknowns. By analyzing this equation with experimentally obtained velocity profiles, we derive the spatial distribution of effective eddy viscosity. To validate the present method, we first applied it to a Newtonian fluid across three classical regimes of Taylor-Couette flow. We successfully obtained radial profiles of eddy viscosity which increases from the inner cylinder wall toward the bulk. Theoretical analysis shows that the local mean shear rate, also quantified in this method, links the local eddy viscosity to angular momentum Nusselt number Nu^{ω}, and our results show a good agreement with the previous reports. Notably, we also observed a non-monotonic dependency of the bulk-mean eddy viscosity on Reynolds number, in contrast to the monotonic trend of wall-shear stress or Nu^{ω}.

As an application to non-Newtonian fluids, we demonstrated the method using a viscoelastic surfactant solution known for the drug reducing effects. In the experiment. Wall shear stress was measured via torque, and the friction coefficient was evaluated as a function of Reynolds number $Re_i(=r_i\omega_i d/\nu)$ where r_i, ω_i, d and ν are the inner cylinder radius, inner cylinder angular velocity, gap width, and kinematic viscosity of the base fluid, respectively (Fig. 1). The local slope of the friction coefficient curve (inset of Fig. 1) indicates the flow transitions between three flow regimes at $Re_i \approx 3000$, 6000 (red lines). Eddy viscosity was evaluated at Re_i indicated with red circle in Figure 1. The bulk-mean eddy viscosity $\nu_{t,mean}$, plotted as a function of Re_i (Fig. 2) shows a stepwise decrease, which is the consistent trend with the torque measurement. In the presentation, we will introduce the theoretical basis of the method and discuss the observed decrease of eddy viscosity from the experimental data including visualization and rheological measurements, and theoretical insights.

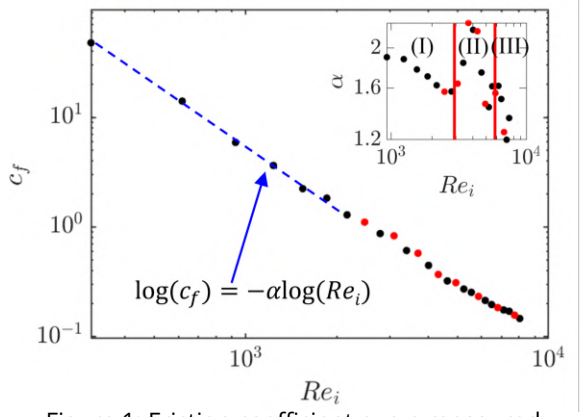

Figure 1: Friction coefficient curve measured from torque and its local slope (inset).

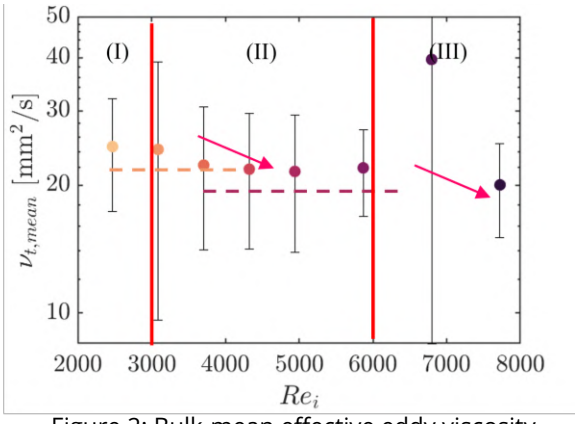

Figure 2: Bulk-mean effective eddy viscosity evaluated by the present method.

[1] Corresponding author: takano.a@eis.hokudai.ac.jp
[2] Hokkaido University, Sapporo Hokkaido, Japan

A novel instability of gravity-driven compressible plane-Poiseuille flow field

N. Taniguchi[1] [2], Y. Fukumoto[3,4]

Kagei & Nishida (2014, 2018) (KN14 in below) conducted a perturbation analysis to compressible plane Poiseuille flow driven by the gravity force in isentropic equation, and they found that the linear instability occurs in a condition of $M > 2.5, R < 10$. This instability regime is unusual considering that the critical Reynolds number of incompressible plane-Poiseuille flow is 5772.22 (Orszag, 1971), and the critical Reynolds number increases with an increase of Mach number (Malik et al., 2008). KN14 assumed the adiabatic process by ignoring the thermal conductivity, and KN14's instability has yet been detected in a more realistic setting, even in a detailed study of linear stability analysis of compressible plane-Poiseuille flow by Deka et al. (2023). For this reason, it can be pointed out that the parameter ranges intensively examined in previous studies are significantly different from the range of instability in KN14. Indeed, as shown in below, the instability of KN14 occurs in a narrow parameter setting at low Reynolds number ($R < 10^4$) and small wavenumber. Thus, it is required to clarify the instability regime of KN14 using the linear stability analysis.

The purpose of this study is to identify the instability of the compressible plane-Poiseuille flow field predicted by KN14 using linear stability analysis for the full Navier–Stokes equation and to present the physical mechanism of the instability.

In this analysis, the basic equation is compressible N–S equation. Following KN14, the equation is non-dimensionalized as

$$\partial_t \rho = -u_j \partial_j \rho - \rho \partial_j u_j,$$
$$\rho \partial_t u_i = -\rho u_j \partial_j u_i - \partial_i p + \nu \partial_j \tau_{ij} + 2\nu\rho,$$
$$\rho \partial_t T = -\rho u_j \partial_j T - (\gamma - 1)\rho T \partial_j u_j + \frac{\gamma}{P_r R} \partial_j \left(\kappa \partial_j T\right) + \gamma(\gamma - 1) M^2 \nu \tau_{ij} \partial_j u_i,$$

where ρ, u_i, p, T, τ are density, velocity in i-th direction, pressure, temperature, and viscous stress tensor. Here, flow parameters are Reynolds number $R(= 1/\nu)$, Mach number M, Prandtl number Pr, and specific heat ratio γ. For eigenvalue problem, we used the approach of Orszag (1971) with Chebyshev-Galerkin method, where we applied adiabatic boundary condition on the upper and lower boundary walls. The numerical scheme was validated by the reproducibility of inviscid modes, reported by Deka et al. (2023).

Figure 1 shows the three-dimensional visualization of linearly unstable regime, and we present the cross-sectional contour plot of growth rate in Fig. 2. In these figures, we observe the unstable regime (B) in addition to

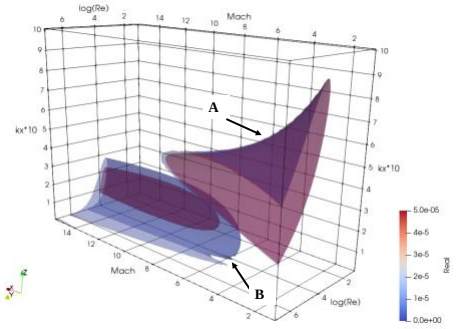

Figure 1. visualization of unstable regime at $\gamma = 1.4, Pr = 0.7$.

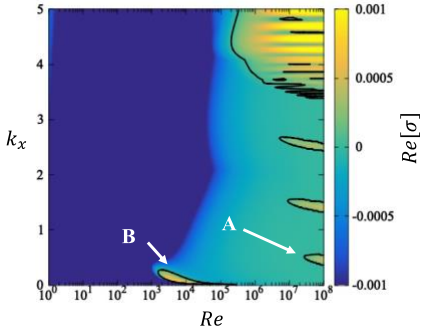

Figure 2. Marginally stable curve at $M = 10$.

[1] Corresponding author: nobutaka.taniguchi.c1@tohoku.ac.jp
[2] Tohoku University, Japan
[3] Kyusyu University, Japan
[4] Osaka Metropolitan University, Japan

conventional unstable regime (A) of Tollmien–Schlichting waves. The parameter regime is slightly different from KN14: $M > 6.0$ and $2500 < R < 10^6$. Based on the parametric study, the instability of KN14 is clearly observed for flows composed of polyatomic molecules with Pr<1.5.

Regarding the source for instability of KN14, we consider that the inviscid instability driven by the gravity term in the linearized N–S equation cause the instability. Figure 3 shows the comparison of eigenvalue of the most unstable eigenmode for isentropic compressible N–S equation. In this figure, we eliminate terms of linearized equation and compared the growth rate of eigenvalue: dissipation and gravity terms. From this figure, we confirm that the application of gravity term induces the instability in both viscous and inviscid condition. Thus, the main structure of KN14 instability is considered to be governed by the following second-order ordinary differential equation as

$$\hat{\rho}'' = \frac{2U'}{U-\sigma}\hat{\rho}' + (\alpha^2(1-(U-\sigma)^2M^2) + 2i\alpha g)\hat{\rho}.$$

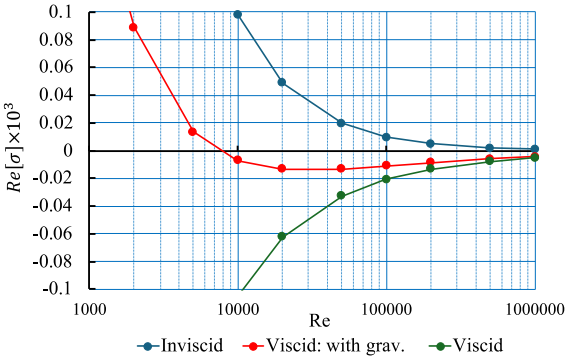

Figure 3. Changes of growth rate with R at $M = 2.5, k_x = 0.2$.

In the presentation, we will discuss the range of KN14 instability of gravity-driven compressible Navier–Stokes equation and the physical mechanism of instability based on the Euler equation.

References

Deka, M., Tomar, G., Kumaran, V., "Linear stability of a compressible flow in a channel", *Q. JI Mech. Appl.* Math, Vol. 76. No. 4, 2023.

Kagei, N., Nishida, T., "Instability of plane Poiseuille flow in viscous compressible gas", *J. Math. Fluid Mech*., 2014.

Kagei, N., Nishida, T., "Traveling waves bifurcating from plane Poiseuille flow of the compressible Navier–Stokes equation", *Arch., Rational Mech. Anal*., 2018.

Malik, M., Dey, J., Alam, M., "Linear stability, transient energy growth, and the role of viscosity stratification in compressible plane Couette flow", *Physical review E* 77, 036322, 2008.

Orszag, S. A., "Accurate solution of the Orr–Sommerfeld stability equation", J. Fluid Mech., vol. 50, part 4, pp. 689-703, 1971.

Influence of the centrifugal force on convective flow in a central force field

V.Travnikov*†, C.Egbers†

The study of large-scale convective flows within a spherical gap has been the focus of numerous theoretical and numerical investigations due to its relevance in geophysical applications, particularly in scenarios where the inner surface is warmer than the outer surface and the fluid is subject to a radial force field. The flow patterns that emerge in such a simplified model have been extensively analyzed by various researchers in both non-rotating and rotating cases.

In the non-rotating case, the behavior of supercritical states can be characterized using the critical degree of the Legendre polynomial, denoted as ℓ_c, as predicted by linear theory. In contrast, in the rotating case, the flow structure is primarily determined by the Coriolis force, which introduces the corresponding critical azimuthal wave numbers, denoted $\mathrm{m_c}$.

A further motivation for conducting numerical analyses of convective flow within a spherical gap arises from the GEOFLOW experiment (Futterer (2013)), which was performed on the International Space Station (ISS) to eliminate the influence of terrestrial gravity. In cases where the rotation rate becomes sufficiently high, the centrifugal force significantly impacts the experiment due to temperature-dependent density variations. In the context of this study, particular attention is paid to a detailed examination of the influence of centrifugal force.

We present the results of numerical investigations of thermal convection within a rotating spherical gap filled with silicon oil M5, characterized by a Prandtl number of $\mathrm{Pr} = 64.64$. The radii ratio is defined as $\eta = \frac{\mathrm{R_{in}}}{\mathrm{R_{out}}} = 0.5$, where $\mathrm{R_{in}}$ and $\mathrm{R_{out}}$ denote the inner and outer radii, respectively. The inner surface maintains a higher temperature than the outer surface, i.e., $\mathrm{T_{in}} > \mathrm{T_{out}}$. A radial force field is induced by the dielectrophoretic effect Mutabazi (2016). The buoyancy force in the Navier-Stokes equation depends on the imposed oscillating electric field and the temperature gradient according to $\mathrm{V_{rms}^2 \Delta T / r^5}$, where $\Delta \mathrm{T} = \mathrm{T_{in}} - \mathrm{T_{out}}$, $\mathrm{V_{rms}}$ is the mean square voltage between surfaces. Hence, the convective flow can be controlled by two parameters: $\Delta \mathrm{T}$ and $\mathrm{V_{rms}}$. This represents a fundamental distinction from Rayleigh-Bénard convection, in which only $\Delta \mathrm{T}$ is variable under terrestrial laboratory conditions. Under microgravity conditions, however, convection can be manipulated through both $\Delta \mathrm{T}$ and $\mathrm{V_{rms}}$, or alternatively, through artificial gravity. In the non-rotating case, the Rayleigh number defined as $\mathrm{Ra} = \frac{2\epsilon_0 \epsilon_r \gamma \Delta \mathrm{T}}{\rho \nu \kappa} \mathrm{V_{rms}^2}$, where ϵ_0 is the vacuum constant, ϵ_r is the permittivity, γ is the thermal permittivity coefficient, ρ is the density, ν is the kinematic viscosity, and κ is the thermal diffusivity serves as the sole control parameter.

The situation becomes much more complex if the system rotates. Due to the equation of state $\rho(\mathrm{T}) = \rho_{\mathrm{out}}(1 - \alpha(\mathrm{T} - \mathrm{T_{out}}))$, where α is the volume expansion coefficient, the temperature-dependent part of the centrifugal force can be expressed in the form of the additional buoyancy term. The key question in this study concerns whether $\Delta \mathrm{T}$ is constant and $\mathrm{V_{rms}}$ varies, or vice versa. In the first case, the centrifugal force can be expressed as follows: $\mathrm{F_c} \sim \mathrm{Ta}$, where $\mathrm{Ta} = (\frac{2\Omega \mathrm{d}^2}{\nu})^2$ is the Taylor number, $\mathrm{d} = \mathrm{R_{out}} - \mathrm{R_{in}}$ is the width of gap and Ω is the rotation rate. In the second case, the centrifugal force follows the relationship $\mathrm{F_c} \sim \mathrm{RaTa}$. A numerical investigation is conducted to analyze both cases systematically.

Initially, we examine the behavior of the steady two-dimensional basic flow. After that, a linear instability analysis is performed to determine the critical Rayleigh number and critical frequencies of the most unstable perturbations as functions of the Taylor number, denoted as $\mathrm{Ra_c(Ta)}$, $\omega_\mathrm{c}(\mathrm{Ta})$, respectively. The analysis reveals that the critical Rayleigh number increases with the Taylor number. We found that the basic flow becomes unstable with respect to the nonaxisymmetric perturbations. In all the cases considered, the instability sets in as a Hopf bifurcation. Furthermore, according to the numerical analysis of the three-dimensional flow, this bifurcation is supercritical. Heat transfer is performed in terms of the Nusselt number, which increases

*Corresponding author: Vadim.Travnikov@b-tu.de
†Department of Aerodynamics and Fluid Mechanics, Brandenburg University of Technology Cottbus-Senftenberg, Siemens-Halske-Ring 15a, 03046 Cottbus, Germany

drastically when the Rayleigh number exceeds the critical value. The amplitude of the supercritical flow follows the relationship $a \sim \sqrt{Ra - Ra_c}$.

Numerical research is performed using the pseudospectral method developed by R. Hollerbach Hollerbach (2000). Three-dimensional calculations have been verified using the MagIC code.

Acknowledgmend

This research is supported by Deutsche Forschungsgemeinschaft (V.T. DFG, Grant No. TR 986/6-3) and through the National High Performance Computing Center NHR with Grant No. bbi00021.

References

Futterer, B., Krebs, A., Plesa, A.-C., Zaussinger, F., Hollerbach, R., Breuer, D., & Egbers, C. "Sheet-like and plume-like thermal flow in a spherical convection experiment performed under microgravity ", *J. Fluid Mech.,* **745** 647–683.

Mutabazi, I., Yoshikawa, H., Fogaing, M., Travnikov, V., Crumeyrolle, O., Futterer, B., & Egbers, C. "Thermo-electro-hydrodynamic convection under microgravity: a review", *Fluid Dyn. Res.,* **48** 061413.

Hollerbach, R., "A spectral solution of the magneto-convection equations in spherical geometry", *Int. J. Numer. Meth. Fluids,* **32** 773–797.

ICTW 2025 23rd INTERNATIONAL COUETTE-TAYLOR WORKSHOP 14th-16th JULY DURHAM, UK

AMOC in a box: Heat and salinity transport in horizontal double-diffusive convection

G. Vacca*†, R. Yang ‡, C. Howland §, R. Verzicco †¶‖, D. Lohse †**

The Atlantic Meridional Overturning Circulation (AMOC) plays a key role in regulating global climate. Indeed, it governs the transfer of heat, salinity, and nutrients between the equator and polar regions(Buckley and Marshall , 2016). Recently a weakening of the AMOC has been observed, which has major impact of the climate in Europe; so a fundamental understanding of the AMOC dynamics is crucial.
The present study investigates the effect of the density ratio on the double-diffusive convection (DDC) flow in the presence of horizontal temperature and salinity gradients, extending the results of Li and Yang (Li and Yang , 2021). To this aim a series of 2D and 3D direct numerical simulations has been performed. The considered configuration (Figure 1 top) has been inspired by several studies of horizontal convection (Shishkina , 2017). By varying the temperature Rayleigh number Ra_T and the density ratio Λ, which represents the ratio of the buoyancy forces generated by the two active scalars on the flow field, four distinct regimes are found. These regimes are distinguished by the global response parameters of the system, namely the temperature Nusselt number Nu_T, the salinity Nusselt number Nu_S (Figure 2) and the friction Reynolds number Re_τ, as well as by the flow field structures. The two limiting regimes of horizontal convection (HC), at high and low Λ values, follow the scaling of the extended Grossmann-Lohse theory for horizontal convention(Shishkina et al. , 2016). In the other regimes, in which the competition between the buoyancy forces occurs, a clear thermohaline layering (Figure 1 bottom) and the presence of oscillating convected salt fingers are found.
Our numerical investigation sheds light on the dynamics that emerge in horizontal double-diffusive convection phenomena as the density ratio varies. Although the considered system is very simplified, it may contribute to understand the dynamics of large-scale problems such as oceanic currents and the possible effects of the climate change on these systems.

*Corresponding author: g.vacca@utwente.nl
†Physics of Fluids Group and Max Planck Center for Complex Fluid Dynamics, University of Twente, Enschede, The Netherlands
‡Department of Mechanical and Aerospace Engineering, Princeton University, Princeton, New Jersey, USA
§School of Mathematics and Statistics, University College Dublin, Belfield, Ireland
¶Dipartimento di Ingegneria Industriale, University of Rome 'Tor Vergata', Roma, Italy
‖Gran Sasso Science Institute, Viale F. Crispi, 7, 67100 L'Aquila, Italy
**Max Planck Institute for Dynamics and Self-Organization, Göttingen, Germany

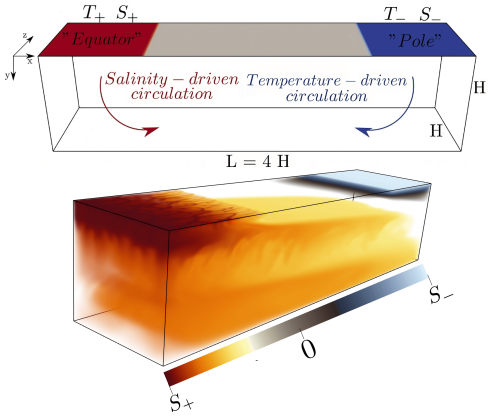

Figure 1: Sketch of the set up with boundary conditions on the upper plate. In red the hot and salty (T_+, S_+) plate and in blue the cool and fresh (T_-, S_-) plate (top). Instantaneous salinity field for the layering regime (bottom).

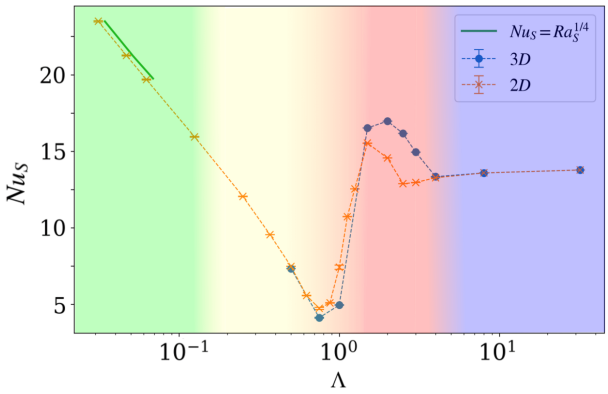

Figure 2: Density ratio dependence of the salinity Nusselt number. The colours highlight different regimes: blue represents temperature-driven HC, red oscillating regime, yellow layering regime, and green salinity-driven HC.

References

Buckley, M. W., & Marshall, J. (2016). Observations, inferences, and mechanisms of the Atlantic Meridional Overturning Circulation: A review. Reviews of Geophysics, 54(1), 5-63.

Li, J., & Yang, Y. (2021). Thermohaline interleaving induced by horizontal temperature and salinity gradients from above. Journal of Fluid Mechanics, 927, A12.

Shishkina, O. (2017). Mean flow structure in horizontal convection. Journal of Fluid Mechanics, 812, 525-540.

Shishkina, O., Grossmann, S., & Lohse, D. (2016). Heat and momentum transport scalings in horizontal convection. Geophysical research letters, 43(3), 1219-1225.

Scattering of internal waves by turbulence

J. Vanneste*†, H. A. Kafiabad‡, M. R. Cox†,‡

Atmospheric and oceanic internal waves propagate in a turbulent flow with which they interact strongly. The advection and refraction of the waves by the flow leads to a scattering process that redistributes wave energy in both physical and spectral space. This scattering can be described by an asymptotic theory which models the turbulent flow as a homogeneous random process and assumes that the typical group speed of the waves is much larger than the typical flow speed. With these assumptions, we obtain a kinetic equation governing the evolution of the wave action $a(\mathbf{x}, \mathbf{k}, t)$ in position–wavevector $(\mathbf{x}, \mathbf{k})$-space (Savva et al., 2021). The scattering is captured by an integral (collision) term which reduces to a simple wavenumber diffusion under the additional (WKB) assumption of wavelengths much shorter than the flow scale (Kafiabad et al., 2019). We analyse the kinetic model and its WKB limit and tests its predictions against numerical simulations of the rotating Boussinesq equations. We consider two aspects in details: (i) the impact of the time dependence of the flow on the frequency distribution of the waves (Cox et al., 2023), and (ii) the role played by flow-induced density fluctuations in the scattering (Cox et al., 2025).

References

Savva, M. A. C., Kafiabad, H. A. & Vanneste, J. (2021). " Inertia-gravity-wave scattering by geostrophic turbulence", *J. Fluid Mech.*, **916**, A6.

Kafiabad, H. A., Savva, M. A. C. & Vanneste J. (2019). "Diffusion of inertia-gravity waves by geostrophic turbulence", *J. Fluid Mech.*, **869**, R7.

Cox, M. R., Kafiabad, H. A. & Vanneste, J. (2023). "Inertia-gravity-wave diffusion by geostrophic turbulence: the impact of flow time dependence", *J. Fluid Mech.*, **958**, A21.

Cox, M. R., Kafiabad, H. A. & Vanneste, J. (2025). "Inhomogeneity-induced wavenumber diffusion", *J. Fluid Mech.*, **1007**, A15.

*Corresponding author: j.vanneste@ed.ac.uk
†University of Edinburgh, Edinburgh, UK
‡Durham University, Durham, UK

ICTW 2025 23rd INTERNATIONAL COUETTE-TAYLOR WORKSHOP 14th-16th JULY DURHAM, UK

Experimental study of the linear instability of the featureless turbulent flow

Arthur Viallefont[1] , Grégoire Lemoult[1], Arnaud Prigent[1]

In Taylor-Couette flow (TCF), the transition to turbulence can take different forms. When the cylinders rotate in opposite directions, the transition is characterized by the emergence of the intermittency (INT) and the spiral turbulence (SPT) regimes, two laminar-turbulent coexistence regimes, in which regions of laminar and fully turbulent flow coexist. Spiral turbulence, a turbulent helix within laminar flow produces a periodic pattern in space and time whereas the INT regime, turbulent spots surrounded by laminar flow, is spatio-temporally intermittent. These regimes have been studied since the 1960s [1-3] and have been reproduced numerically using direct numerical simulations (DNS) since 2009 [4-5]. They are not unique to TCF but are a characteristic feature of the transition to turbulence in wall-bounded shear flows. For example, in plane Couette flow (PCF), inclined stripes form at an angle of about 30°, and their number increases with the Reynolds number (Re) until the flow becomes fully turbulent [5-6]. In Poiseuille flow, the laminar-turbulent coexistence takes the form of turbulent puffs within a laminar flow. These puffs drift along the pipe and exhibit dynamic behaviors such as splitting and merging, which depend on the Reynolds number. It has been shown that these dynamics can be fully reproduced using a one-dimensional discrete model, where the turbulence is understood as a chaotic repeller [8].

Recently, it has been shown that the transition from laminar to the INT regime is well described within the domain of out-of-equilibrium critical phenomena. It is now considered as a continuous transition belonging to the directed percolation class [9]. The transition from the SPT regime to the homogeneous turbulence has traditionally been studied starting from the fully turbulent state. It has been shown that this regime can be understood as a long-wavelength instability of the turbulent flow [10]. More recently, Kashyap et al [11-12] have investigated the linear stability of turbulent plane channel flow. Their numerical studies provide evidence that the coexistence of laminar and turbulent regions indeed results from a linear instability of the fully turbulent regime. However, this result has not yet been confirmed by theoretical studies. Moreover, experimental studies are still lacking to conclusively characterize the nature of this transition. The primary objective of our work is to verify whether these coexistence regimes arise from a linear instability of the turbulent flow. We conducted our study using a double-axis rheometer with a Couette geometry characterized by a radius ratio of $\eta=0.977$ and an aspect ratio of $\Gamma=132$. Taking advantage of this configuration, we explored the state diagram (based on Andereck's diagram) while simultaneously measuring the torque. This allowed us to introduce a new order parameter based on torque measurements and to study its variation as a function of the system control parameters. We found that its variation behaves as a supercritical transition. Additionally, we present the results of the linear stability analysis of the flow by performing quenches from the turbulent state. We measured the growth rates of the modes associated with the observed patterns by visualizing the flow over a 360° view.

[1] LOMC, Université Le Havre Normandie-CNRS

References

[1] Coles, D. (1965). Transition in circular Couette flow. *Journal of Fluid Mechanics*, *21*(3), 385-425.

[2] Van Atta, C. (1966). Exploratory measurements in spiral turbulence. *Journal of Fluid Mechanics*, *25*(3), 495-512.

[3] Andereck, C. D., Liu, S. S., & Swinney, H. L. (1986). Flow regimes in a circular Couette system with independently rotating cylinders. *Journal of fluid mechanics*, *164*, 155-183.

[4] Meseguer, A., Mellibovsky, F., Avila, M., & Marques, F. (2009). Instability mechanisms and transition scenarios of spiral turbulence in Taylor-Couette flow. *Physical Review E—Statistical, Nonlinear, and Soft Matter Physics*, *80*(4), 046315.

[5] Dong, S. (2007). Direct numerical simulation of turbulent Taylor–Couette flow. *Journal of Fluid Mechanics*, *587*, 373-393.

[6] Chantry, M., Tuckerman, L. S., & Barkley, D. (2016). Turbulent–laminar patterns in shear flows without walls. *Journal of Fluid Mechanics*, *791*, R8.

[7] Avila, M., & Hof, B. (2013). Nature of laminar-turbulence intermittency in shear flows. *Physical Review E—Statistical, Nonlinear, and Soft Matter Physics*, *87*(6), 063012.

[8] Barkley, D. (2011). Simplifying the complexity of pipe flow. *Physical Review E—Statistical, Nonlinear, and Soft Matter Physics*, *84*(1), 016309.

[9] Lemoult, G., Shi, L., Avila, K., Jalikop, S. V., Avila, M., & Hof, B. (2016). Directed percolation phase transition to sustained turbulence in Couette flow. *Nature Physics*, *12*(3), 254-258.

[10] Prigent, A., Grégoire, G., Chaté, H., Dauchot, O., & van Saarloos, W. (2002). Large-scale finite-wavelength modulation within turbulent shear flows. *Physical review letters*, *89*(1), 014501.

[11] Kashyap, P. V., Duguet, Y., & Dauchot, O. (2022). Linear instability of turbulent channel flow. *Physical Review Letters*, *129*(24), 244501.

[12] Kashyap, P. V., Duguet, Y., & Dauchot, O. (2024). Linear stability of turbulent channel flow with one-point closure. *Physical Review Fluids*, *9*(6), 063906.

The fluid dynamics of intrusions

H. Vu *, A. Slim †

We shall describe intrusions generated by a source into a linearly stratified ambient layer at the level of neutral buoyancy. Our analysis focuses on simulations of the Navier-Stokes equations under the Boussinesq approximation. We find that for a wide, lazy source, the intrusion profiles exhibit a remarkably clear self-similar collapse, although they do not match the solutions of existing shallow-water models. In contrast, we found that for a narrow, jet-like source, the intrusion profiles display a number of interesting features, including the formation of a vortex ring, varicose waves on the trailing jet, followed by the growth of sinusoidal instabilities and a transition to turbulence. The varicose waves generated differ from those of a pure jet in an unstratified ambient, but the sinuous modes are similar. To analyse this phenomenon, we conduct a stability analysis to understand how these instabilities are generated. This analysis will enhance our understanding of the nature of the waves and the role of stratification on the intrusion profiles.

*Monash University, Victoria, Australia
†Monash University, Victoria, Australia

Observation of nonaxisymmetric standard magneto-rotational instability induced by a free-shear layer

Yin Wang[1]*, Fatima Ebrahimi[1,2], Hongke Lu[3], Jeremy Goodman[2], Erik Gilson[1], Hantao Ji[1,2]

The standard magnetorotational instability (SMRI) with a magnetic field component parallel to the rotation axis is widely believed to be responsible for the fast accretion in astronomical disks. It is a linear instability triggered in the differentially rotating ionized disk flow by a magnetic field component parallel to the rotation axis. In conventional base flows with a Keplerian profile or an ideal Couette profile, most studies focus on axisymmetric SMRI, since excitation of nonaxisymmetric SMRI in such flows requires a magnetic Reynolds number Rm more than an order of magnitude larger. Here, we report that in a magnetized Taylor-Couette flow, nonaxisymmetric SMRI with an azimuthal mode number m=1 can be triggered by a free-shear layer in the base flow at Rm≳1 (Fig. 1), the same threshold as for axisymmetric SMRI[1]. Global linear analysis reveals that the free-shear layer reduces the required Rm, possibly by introducing an extremum in the vorticity of the base flow. Nonlinear simulations validate the results from linear analysis and confirm that a novel instability recently discovered experimentally is the nonaxisymmetric m=1 SMRI[2]. Our finding has astronomical implications as free-shear layers are ubiquitous in celestial systems, such as the disk-star boundary layer, the solar tachocline, and the edge of planet-opened gaps in protoplanetary disks.

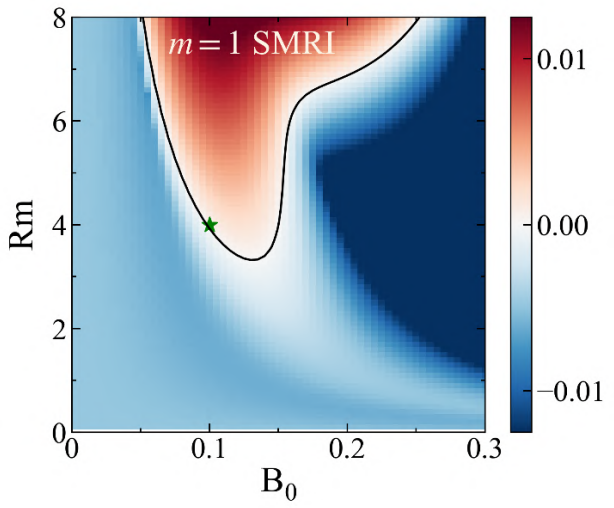

Figure 1: Dimensionless growth rate of the m=1 SMRI as a function of magnetic Reynolds number (Rm) and applied magnetic field strength (B_0).

References

[1] Wang, Y. et al. "Observation of nonaxisymmetric standard magnetorotationalInstability induced by a free-shear layer", *Phys. Rev. Lett.* 134, 135101 (2025).

[2] Wang, Y. et al. "Identification of a non-axisymmetric mode in laboratory experiments searching for standard magnetorotational instability", *Nat. Commun.* 13, 4679 (2022).

*Corresponding author: ywang3@pppl.gov
[1]Princeton Plasma Physics Laboratory, Princeton, USA
[2]Princeton University, Princeton, USA
[3]Dartmouth College, Hanover, USA

Self-sustained process in Couette-Poiseuille flow

T. Liu[1], M. Etchevest[2], B. Semin[1], P. Dimitruk[2], R. Godoy-Diana[1], J. E.Wesfreid[1,3]

Streamwise coherent vortices are well characterized as cellular structures that organize the flow in hydrodynamic instabilities such as Taylor-Couette, Dean, and Görtler flows. These structures arise as a consequence of linear centrifugal instability, and their nonlinear evolution typically corresponds to supercritical instabilities.
However, similar flow organization with longitudinal structures (aligned with the main or base flow direction x) is also observed in wall-bounded shear flows that have velocity gradients in the transverse y direction.
In these flows, the organization originates from a mechanism known as the lift-up process, where streamwise vorticity ("rolls") producing velocity fluctuations u_y generates high and low-speed modulations of the base flow $U(y)$, referred to streaks**.** This flow organization is a hallmark of the transition to turbulence in such flows, including plane Couette flow, Poiseuille flow in channels and pipes, and combinations such as Couette-Poiseuille flow. Most of these flows are linearly stable, and the transition to turbulence occurs via subcritical instabilities**.**

Our interest lies in the case where turbulence dynamics in these flows is governed by the nonlinear interaction between streaks and rolls, described by a self-sustaining process (SSP), initially modeled by Waleffe [1]. We investigate the dynamics of this process using a combination of experiments and numerical simulations.

The experiments are conducted in a plane Couette-Poiseuille channel, where streaks and rolls are quantified through the streamwise velocity fluctuation u_x and transverse velocity u_y respectively, measured using stereo-Particle Image Velocimetry (PIV). In parallel, Direct Numerical Simulations (DNS) of Couette-Poiseuille flow are performed using a pseudospectral code that employs the Fourier continuation method in the non-periodic direction, referred to as SPECTER [2].

Our focus is on the instability induced by streak waviness, which is a critical component of the SSP and has been extensively studied theoretically and numerically. However, experimental measurements of streak waviness remain rare. To analyze the transition of streaks from a straight to a wavy state, we apply a spatial filter that separates the straight and wavy components of the streak velocity [3].
A similar decomposition is also obtained from the DNS results (see figure). In both cases, we observe the relationship between the straight part of the streaks and the rolls—consistent with the laminar lift-up effect**.**

[1] Laboratoire PMMH, CNRS, ESPCI, Sorbone Université, Université Paris Cité, 7 quai Saint-Bernard, 75005 Paris (France),
[2] Universidad de Buenos Aires, FCEyN, Departamento de Física, Ciudad Universitaria, 1428 Buenos Aires (Argentina)
[3] Corresponding author: wesfreid@espci.fr

We introduce a new variable, $\langle|\omega_{y,wavy}|\rangle$, to quantify the waviness of the streaks**.** We then demonstrate that the average absolute value of the wall-normal velocity increases with $|\omega_{y,wavy}|$ in agreement with SSP theory.

This new SSP analysis approach is not specific to Couette-Poiseuille flow and can be applied to study similar mechanisms in other flow configurations.
Finally, we recall that the origin of wavy instabilities in Taylor-Couette flows was also a consequence of the SSP, although applied to structures formed from linear instabilities rather than subcritical ones [4] [5].

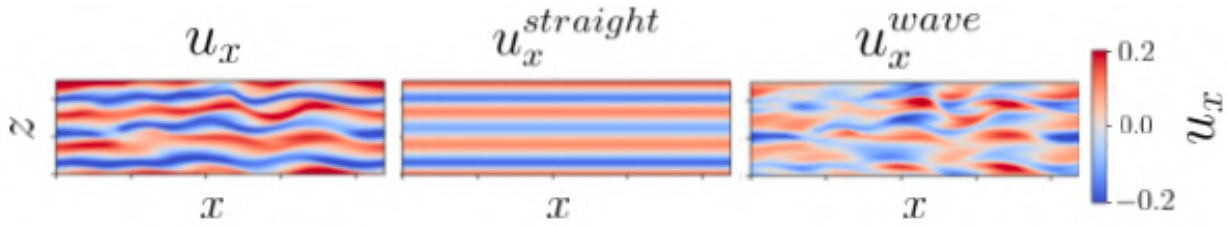

Figure 1: In the upper panels, the streamwise velocity field (left) and its decomposition into the straight part (middle) and wavy part (right) are displayed.

References

[1] Fabian Waleffe. *On a self-sustaining process in shear flows*. Physics of Fluids, 9(4):883–900, 1997.
[2] Mauro Fontana, Oscar P. Bruno, Pablo D. Mininni, and Pablo Dmitruk. *Fourier continuation method for incompressible fluids with boundaries*. Computer Physics Communications, 256:107482, 2020.
[3] Tao Liu, Benoît Semin, Ramiro Godoy-Diana, and José Eduardo Wesfreid. *Lift-up and streak waviness drive the self-sustained process in wall-bounded transition to turbulence*. Phys. Rev. Fluids,9:033901, 2024.
[4] Tommy Dessup, , Laurette S., Tuckerman, José Eduardo Wesfreid, , et al. *Self-sustaining process in Taylor-Couette flow*. Physical Review Fluids, 2018, vol. 3, no 12, p. 123902.
[5] D. Martinand, E. Serre, and R. M. Lueptow, *Mechanisms for the transition to waviness for Taylor vortices*, Phys. Fluids 26, 094102 (2014).

ICTW 2025 23rd INTERNATIONAL COUETTE-TAYLOR WORKSHOP 14th-16th JULY DURHAM, UK

Oblique modes & spatio-temporal linear stability of plane Couette flow

K. V. Wilhelm*†‡, J. Conrad†‡, S. Görtz†‡, M. Oberlack†‡, Y. Wang†

Plane Couette flow is known to be linearly stable at all Reynolds numbers for temporally evolving modes. Nevertheless, both experiments and DNS show transitial behavior and oblique laminar-turbulent structures at moderate Reynolds numbers. This research seeks to bridge this discrepancy by analyzing the linear stability of spatio-temporally evolving modes in plane Couette flow using Briggs' method.

Squire's theorem extended:

In linear stability theory, the Orr-Sommerfeld equation (OSE) governs the evolution of the amplitude $\tilde{v}$ of a wall-normal perturbation in parallel shear flows as

$$\left[(-i\omega + i\alpha U)\left(\frac{\mathrm{d}^2}{\mathrm{d}y^2} - (\alpha^2+\beta^2)\right) - i\alpha U'' - \frac{1}{Re}\left(\frac{\mathrm{d}^2}{\mathrm{d}y^2} - (\alpha^2+\beta^2)\right)^2\right]\tilde{v} = 0, \tag{1}$$

where the normal mode approach $v'(t,x,y,z) = \tilde{v}(y)exp[i(\alpha x + \beta z - \omega t)]$ has been employed to the wall-normal perturbation v', with wave frequency ω and streamwise and spanwise wave numbers α and β, and where $U = U(y)$ describes the laminar base flow and Re is the Reynolds number.

The key idea of Squire was that the OSE has a similar structure in 2D and 3D (Squire, 1933). This structural similarity means that the OSE has the same solution space in 2D and 3D, and allows an equivalence transformation between 2D and 3D perturbation modes. Introducing respective indices for 2D and 3D quantities and with the Reynolds number ratio $\phi := Re_{3D}/Re_{2D}$, the following relationships

$$Re_{3D} = \phi Re_{2D}, \quad \alpha_{3D} = \alpha_{2D}/\phi, \quad \omega_{3D} = \omega_{2D}/\phi, \quad \beta = \pm\sqrt{1-1/\phi^2}\alpha_{2D}, \tag{2}$$

can be derived.

In Squire's original analysis, he investigated temporally evolving modes, i.e. parameters in the number spaces $\omega \in \mathbb{C}, \alpha, \beta \in \mathbb{R}$ (Squire, 1933). He noticed that this parameter choice implies $\phi > 1$ to keep $\beta \in \mathbb{R}$ in (2), and thus he concluded $Re_{2D} < Re_{3D}$. If there is a 2D perturbation associated with a critical (2D) Reynolds number, the corresponding 3D perturbation will be at a higher (3D) Reynolds number.

When extending this to spatio-temporally evolving modes, $\omega, \alpha, \beta \in \mathbb{C}$, the equivalence transformation remains formally identical to (2), however, since complex roots of (2) are now admissible, the transformation admits two branches for β as

$$\beta = \begin{cases} \pm\sqrt{1-1/\phi^2}(\alpha_{2D,r} + i\alpha_{2D,i}) & \text{for } \phi > 1, \\ \pm\sqrt{1/\phi^2-1}(\alpha_{2D,i} - i\alpha_{2D,r}) & \text{for } \phi < 1. \end{cases} \tag{3}$$

Key results are: (i) critical Reynolds numbers may be smaller in 3D than in 2D for $\phi < 1$, i.e. if there is a 2D perturbation associated with a critical (2D) Reynolds number, the corresponding 3D perturbation may occur at a smaller, subcritical (3D) Reynolds number, and therefore, 3D modes may be spatio-temporally more unstable; (ii) the complex β gives rise to structures that can grow obliquely to the streamwise direction; (iii) the $\pm$-sign for β constitutes a symmetry breaking in the z-direction; (iv) the box width controls the critical 3D Reynolds number, since the box width limits the largest conceivable spanwise wavelength related to the wave number β_r, corresponding to a given growth factor $\alpha_{2D,i}$ by (3).

*Corresponding author: wilhelm@fdy.tu-darmstadt.de
†Chair of Fluid Dynamics, Technical University of Darmstadt, Darmstadt, Germany
‡Centre for Computational Engineering, Technical University of Darmstadt, Darmstadt, Germany

Oblique structures in plane Couette flow:

In the previous section, a 3D linear instability mechanism was presented. The idea for this was to some extent triggered by the experimental observation that transitional plane Couette flow forms oblique structures, i.e. at an angle in the plane of streamwise and spanwise directions.

In plane Couette flow, oblique stripes consisting of alternating turbulent and laminar regions were observed by Prigent et al. (2003) using Kalliroscope flakes in a moving belt channel apparatus. Similarly, numerical simulations by Barkley & Tuckerman (2005) also demonstrated the emergence of oblique patterns in transitional plane Couette flow. By employing a tilted computational domain aligned with the oblique structures, they were able to impose periodic boundary conditions, allowing these patterns to be sustained across a range of tilt angles and domain sizes.

Briggs' method:

Strictly speaking, the growth of individual spatial or spatio-temporal modes is unphysical, as perturbations become infinite in the domain due to the imaginary part of the wave numbers in positive or negative direction. Therefore, the perturbation energy is not meaningfully defined. An elegant resolution to this issue was introduced by Briggs (1964), originally developed in the context of wave propagation in plasma physics. Rather than considering individual modes, Briggs' approach solves an initial value problem based on a disturbance localized in both space and time over a whole distribution of frequencies and wave numbers

$$v'(t,x,y;y_0) = \frac{1}{2\pi}\int_{\mathcal{F}} \hat{v}(t,\alpha,y;y_0)e^{i\alpha x}\,\mathrm{d}\alpha, \qquad \hat{v}(t,\alpha,y;y_0) = \frac{1}{2\pi}\int_{\mathcal{L}} \tilde{v}(\omega,\alpha,y;y_0)e^{-i\omega t}\,\mathrm{d}\omega. \tag{4}$$

The temporal integration contour $\mathcal{L}$ has to lie above the highest singularity of $\tilde{v}$, i.e. zeros of the dispersion relation, in order to fulfill causality. The spatial integration contour $\mathcal{F}$ is initially along the real line. The integration contours produce trajectories of singularities in the respective other complex planes, i.e. a trajectory of ω-singularities $\omega(\mathcal{F})$ caused by the spatial integration contour $\mathcal{F}$ and trajectories of α-singularities $\alpha_l(\mathcal{L})$, $\alpha_u(\mathcal{L})$ caused by the temporal integration contour $\mathcal{L}$. These are exactly the temporal and spatial eigenvalues of the problem for a given α on $\mathcal{F}$ and a given ω on $\mathcal{L}$. The contours are closed in the complex planes by semicircles above and below the contours using Jordan's lemma, and are evaluated via the residuum theorem.

In Briggs' method, the integration contours are now continuously deformed, changing also the trajectories of singularities in the other respective complex planes. As long as all singularities stay in their original relative position, i.e. above or below the integration contours, the deformation is valid. The time-asymptotic behavior of the initial-value problem can be approximated using the method of steepest descent: when the integration contours pass through a saddle point, the contours cannot be lowered, since two singularities from different sides of the integration contour $\mathcal{F}$ merge. Perturbation modes with zero group velocity determine absolute or convective instability, whether the saddle point lies above or below the real ω-axis.

We propose an algorithm for the deformation of the integration contours: a potential function is assigned to each point on the integration contours as a measure of distance to the trajectories of singularities. The integration contours are moved in order to minimize the potential at every point, while the integration contours $\mathcal{L}$ is forced downwards and curvature terms ensure a smooth contour.

For plane Couette flow, since there are no unstable temporal eigenvalues in the first place, absolute instabilities are not possible. However, convective instabilities or instabilities due to a time-periodic forcing are conceivable.

References

Barkley, D., and Tuckerman, L. S. (2005), "Computational study of turbulent laminar patterns in Couette flow", *Physical Review Letters*, **94** 014502.

Briggs, R. J. (1964), "Electron-stream interaction with plasmas", The MIT Press.

Prigent, A., Grégoire, G., Chaté, H., and Dauchot, O. (2003), "Long-wavelength modulation of turbulent shear flows", *Physica D: Nonlinear Phenomena*, **174** 100–113.

Squire, H. B. (1933), "On the stability for three-dimensional disturbances of viscous fluid flow between parallel walls", *Proceedings of the Royal Society of London. Series A, Containing Papers of a Mathematical and Physical Character*, **142** 621–628.

Axially-aligned vortices in unsteady Taylor–Couette flow

A. P. Willis*†, M. J. Burin‡

It is 60 years since Donald Coles' (1965) landmark paper on "Transition in circular Couette flow". Towards the end of the work, there featured a surprising image, where structures in the flow were aligned with the axis, rather than wrapping around the cylinder, perpendicular to the usual manner of Taylor-vortex rolls, wavy rolls, and so on. Whilst the instability was observed upon a start-stop motion of the outer cylinder, confusingly, Coles only referred to this image when speculating that Tollmein instability was involved in his sudden-stop process for generating a multiplicity of wavy Taylor-vortex states.

At the last ICTW meeting in Barcelona, I presented a numerical study that isolated the instability, guided by Michael's more recent experimental observation of the instability following a start-stop of the outer cylinder (Figure 1). It was suggested that the instability be more likely related that of Stokes' oscillating boundary layer problem. In this presentation, we provide further evidence for this link, and examine why the instability has remained so elusive over the last 60 years. There are a number of factors contributing to this, but, now that PIV techniques are more prevalent, the instability is likely to be detected more frequently in future experiments.

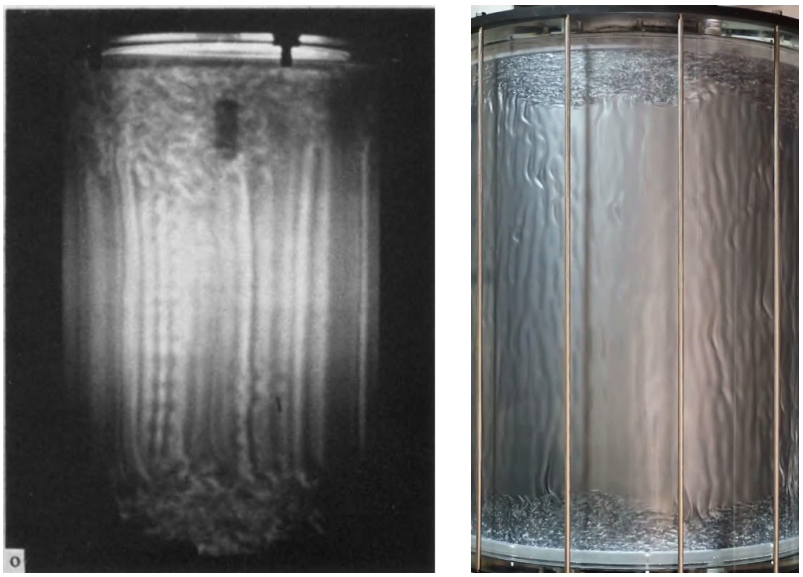

Figure 1: Instability following start-stop motion of the outer cylinder, observed (*left*) by Coles (1965) and (*right*) in the apparatus of Burin & Czarnocki (2012).

References

Coles, D. (1965). "Transition in circular Couette flow", *J. Fluid Mech.*, **21** 385–425.

Burin, M., & Czarnocki, C.J. (2012). "Subcritical transition and spiral turbulence in circular Couette flow", *J. Fluid Mech.*, **709** 106–122.

*Corresponding author: a.p.willis@sheffield.ac.uk
†University of Sheffield, Sheffield, UK
‡California State University, San Marcos, USA

Mutiple states and aspect ratios of rolls: An analogy between Taylor–Couette and Rayleigh–Bénard flows

Xiaojue Zhu*†

In turbulent Taylor–Couette (TC) flow, multiple statistically stationary states can emerge, each defined by a distinct aspect ratio (Γ_r) of Taylor vortices and associated with different transport properties. Using direct numerical simulations, we explore this multiplicity in axisymmetric TC flow with a large vertical extent, focusing on a radius ratio of $\eta = 0.714$ (where η_i and η_o are the inner and outer cylinder radii, respectively). For Taylor numbers $Ta > 10^{10}$, we observe a range of vortex aspect ratios, $2/3 \leq \Gamma_r \leq 4/3$, indicating the coexistence of multiple roll states in the turbulent regime. This behavior mirrors that seen in two-dimensional Rayleigh–Bénard (RB) convection (Wang et al., Phys. Rev. Lett., 125, 2020), where roll aspect ratios similarly vary across stable states. We attribute this correspondence to the elliptical deformation and viscous damping of vortices, reinforcing a deep analogy between TC and RB flows—two canonical systems of thermal and rotationally driven turbulence.

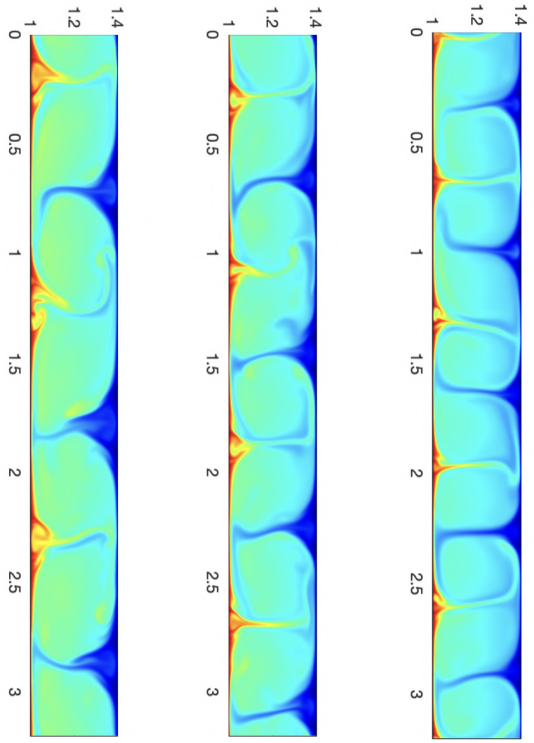

Figure 1: Multiple states arise in axisymmetric Taylor–Couette flow under identical initial conditions

*Corresponding author: zhux@mps.mpg.de
†Max Planck Institute for Solar System Research, 37077 Göttingen, Germany